SYNERGISTIC SURFACTANT INTERACTIONS AND THE CONSEQUENCES ON PHASE BEHAVIOR, INTERFACIAL TENSION REDUCTION AND HYDROPHOBIC SURFACE WETTING

BY

MAKONNEN MATEÓS PAYNE

A dissertation submitted to the Graduate Faculty in Chemical Engineering in partial fulfillment of the requirements for the degree of Doctor of Philosophy, The City University of New York

2008

This manuscript has been read and accepted for the
Graduate Faculty in Engineering in satisfaction of the
dissertation requirement for the degree of Doctor of Philosophy.

Alexander Couzis

Date — Chair of Examining Committee

Mumtaz Kassir

Date — Executive Officer

Charles Maldarelli

Morton Denn

Maribel Vazquez

Mohsen Yeganeh

Supervisory Committee

THE CITY UNIVERSITY OF NEW YORK

ABSTRACT

SYNERGISTIC SURFACTANT INTERACTIONS AND THE CONSEQUENCES ON PHASE BEHAVIOR, INTERFACIAL TENSION REDUCTION AND HYDROPHOBIC SURFACE WETTING

By

Makonnen Mateós Payne

Advisor: Professor Alexander Couzis

The ability for some of the nonionic trisiloxane surfactants to completely and rapidly wet a hydrophobic surface has been well documented for several years. However, to date, the behavior of the trisiloxane surfactants at the solid-liquid interface is not yet completely understood, leading to an incomplete understanding of the mechanism for complete wetting. In this work we report our findings with regard to the synergistic interactions between polyethylene oxide surfactants of the general structure C_iE_j and compare the behavior to a known super wetting surfactant. Pendant drop tensiometry experiments and sessile drop contact angle measurements on hydrophobic surfaces were conducted on combinations of C_iE_j surfactants with 1-dodecanol. We found that a number of combinations were capable of reducing significantly the air-liquid tension, however only systems that exhibited the propensity to form extended liquid crystalline phases, as shown by the combination of cross-polarized microscopy, cryo-TEM, and light scattering experiments, were able to improve on the wetting performance of the these systems. We have also conducted the parallel experiment focused on the surfactant adsorption at the

hydrophobic solid-liquid interface. Using in-situ infrared internal reflection spectroscopy and complimentary sum-frequency generation spectroscopy, we are able to dynamically interrogate the surfactant adsorption kinetics and interfacial water structure evolution at the hydrophobic solid-liquid interface. We will relate these findings to gain insight into the molecular requirements for superspreading.

ACKNOWLEDGEMENTS

To my advisors Alex and Charles, I thank you for the time spent discussing my project and asking the questions that helped me to think about the work in unique ways. Alex, I am infected your infinite curiosity about all things technical and childlike wonder when it comes to discovery. Charles, as I reintroduce myself to professional life and beyond, I will carry with me your quiet intensity and high standard of excellence.

I have had the opportunity to meet and work with quite a few brilliant people from whom I have learned a great deal and who subsequently had direct effect on the work presented here. From the ExxonMobil Research and Engineering Company, I would like to thank Dr. David Calabro and Dr. Benjamin McCool with whom I did my internship and as result met Dr. Mohsen Yeganeh with whom I spent many hours learning about and collecting SFG spectra and who subsequently sat on my dissertation review committee. From the New York Structural Biology Center, I would like to thank Dr. John Berriman and Ms. K.D. Derr for their hours of training and assistance with cryo-TEM imaging. I would also like to thank Dr. Paul Butler and Dr. Lionel Porcar for their hospitality during the trip to small angle neutron scattering facility at NIST and for their assistance with data gathering and analysis.

Completion of this work could not have been possible without the generous support of the National Aeronautics and Space Administration, the Sloan Foundation and the National Science Foundation, specifically the Nanotechnology IGERT, the Study of Multiscale Phenomena in Soft Materials IGERT and the AGEP (thank you Dr. Gail Smith).

Throughout this journey, I have come across people who I now call my friends. Whether it was studying together, blowing off steam by playing tennis, grabbing a cup of coffee or just sitting in the office and talking about our futures, they have helped make the long hours seem less daunting. Jimmy, Jon, Tieuvi, Kelly, Spyros, Nikhil, Lorraine, I am honored and proud to know you.

Thank you to Andy and Xu for teaching and allowing me to use the shop when I needed to make a new device or improve on an old one.

Thank you to Professors Morton Denn and Maribel Vazquez for the time taken to assist in the review of my work as part of my committee and for their infinite patience.

Finally, before I began this pursuit there were those that encouraged and supported my decision and during the process were constant sources guidance and influence; they are Dr. Ron Lewis, Dr. Paul Siracusa, Mr. Peter Bordonaro, Mr. Daniel Menelly, the entire Prep for Prep organization (particularly the students), my brothers of Kappa Alpha Psi

Fraternity, Inc., my lifelong friends, my family and last but by far not least, my wife Yolanda, who has put up with endless hours of my not being around and projects unfinished so that I could complete this one. I thank you all.

The process of earning a Doctorate degree often feels like a solitary process that no one can truly understand unless they have experienced it firsthand. However, to get to this point I have been lucky to have a full and very diverse support system to see me through to the end.

TABLE OF CONTENTS

CHAPTER 1 – Introduction …… **page 1**

References

CHAPTER 2 – Direction and Scope ……... **page 6**

2.1 – Scope of Research

2.2 – Direction of Research

2.2.1 – Analysis of Bulk Surfactant Behavior

2.2.2 – Analysis of the Air-Liquid Interface

2.2.3 – Analysis of the Solid-Liquid Interface

CHAPTER 3 – Synergistic Formation of Lamellar Surfactant Aggregates with Mixtures of Linear Poly(Ethylene Oxide) N-Alkylether Surfactants with 1-Dodecanol …. **page 13**

3.1 – Introduction

3.2 – Experimental

3.2.1 – Materials

3.2.2 – Methods

3.3 – Results

3.3.1 – Particle Size Analysis

3.3.2 – Cross Polarized Microscopy

3.3.3 – Small Angle Neutron Scattering

3.3.4 – Cyro-TEM

3.4 – Discussion

3.5 – Conclusion

3.6 - References

CHAPTER 4 – Synergistic Air-Liquid Interfacial Tension Reduction Initiated by Enhanced Liquid Crystalline Phase Behavior in Surfactant Mixtures …….. **page 61**

4.1 – Introduction

4.2 – Experimental

4.2.1 – Methods

4.3 – Results

4.3.1 Pendant Bubble Tensiometry

4.3.2 Langmuir-Blodgett Trough

4.4 – Discussion

4.5 – Conclusion

4.6 – References

CHAPTER 5 – Spectroscopic Study of the Solid-Liquid Interface …… **page 104**

5.1 – Introduction

5.2 – Experimantal

5.2.1 – Materials

5.2.2 – Methods

5.3 – Results

5.3.1 - Contact Angle Goniometry

5.3.2 - FTIR/ATR

5.3.3 - Sum Frequency Generation Spectroscopy

5.4 – Discussion

5.5 – Conclusion

5.6 - References

CHAPTER 6 – Summary and Future Work …… **page 145**

6.1 Summary

6.2 Future Work

LIST OF TABLES

Table 4.1: Equilibrium air-liquid interfacial tension for single component surfactant mixtures. …… **page 90**

Table 4.2: Equilibrium air-liquid interfacial tension for binary surfactant mixtures. Hydrocarbon chains are matched in length. ……..……...…… **page 91**

Table 4.3: Equilibrium air-liquid interfacial tension for binary surfactant mixtures. Hydrocarbon chains are mismatched in length, while keeping the glycol unit length constant. ……..……. **page 92**

Table 5.1: Equilibrium contact angle for solutions showing synergistic air-liquid interfacial tension reduction. ……..….. **page 127**

Table 5.2: Calculated solid-liquid interfacial tensions for water, dodecanol, $C_{12}E_8$ and the dodecanol/$C_{12}E_8$ mixture. …… **page 131**

LIST OF FIGURES

Figure 3.1 : Phase diagrams $C_{12}E_3$, $C_{12}E_4$, $C_{12}E_5$, $C_{12}E_6$, and $C_{12}E_8$. …… **page 40**

Figure 3.2: Sample cell for cross-polarized microscopy. …….…... **page 41**

Figure 3.3: The 30-meter long Small-Angle Neutron Scattering (SANS) instrument on neutron guide NG7 at the National Center for Neutron Research at NIST. ……... **page 42**

Figure 3.4: Demountable SANS cell used for to hold sample for SANS analysis. ……. **page 43**

Figure 3.5: $C_{12}E_3$ particle size analysis. ……. **page 44**

Figure 3.6: $C_{12}E_4$ particle size analysis. ……. **page 45**

Figure 3.7: Particle size analysis of mixtures of $C_{12}E_8$ with $C_{12}E_0$ in water. a) $C_{12}E_8$ at 0.7 mM CAC b) $C_{12}E_8$ at 0.7 mM with $C_{12}E_0$ at 0.37 mM c) $C_{12}E_8$ at 0.7 mM with $C_{12}E_0$ at 2.5 mM d) $C_{12}E_8$ at 1.4 mM with $C_{12}E_0$ at 5 mM. ……. **page 46**

Figure 3.8: Cross-polarized microscopy image of 1.4 mM $C_{12}E_8$/5 mM $C_{12}E_0$ mixture. The cloverleaf pattern in the lower left hand corner is the characteristic extinction pattern of L_α structures of surfactants. ……... **page 47**

Figure 3.9: CryoTEM image of 0.7 mM $C_{12}E_8$ solution. The arrows indicate the spherical micelles. The right side of the image shows the edge of the grid hole in which the surfactant solution is frozen. Capturing the grid hole's edge in the image increases the overall image contrast allowing, allowing imaging of the micelles which would otherwise be difficult to see. …….. **page 48**

Figure 3.10: A cryo-TEM image 0.7-mM $C_{12}E_8$/2.5mM $C_{12}E_0$ surfactant mixture. The aggregate structures appear to be single walled vesicles as evidenced by the core having the same contrast as the surrounding area (vitreous ice) and the dark ring, which is the hydrocarbon core of the vesicle. …… **page 49**

Figure 3.11: A $C_{14}E_8$/$C_{12}E_0$ mixture where primary structures on the order of 100 nm are present, but coexist with much smaller structures on the order of the size of a micelle. Also, the surface of the primary structures appears to be speckled of smaller scattering structures, which may be indicative of the formation of sponge-like structure in the bulk. …….. **page 50**

Figure 3.12: Cryo-TEM image of a 0.7-mM $C_{12}E_8$/2.5mM $C_{12}E_0$ surfactant mixture showing of inter-aggregate structuring in the system. Shows clearly the repeating ordered structure in the bulk aggregate formation. …… **page 51**

Figure 3.13: Fourier transform of circled region in Figure 3.7. …… **page 52**

Figure 3.14: I(q) versus q diagram for $C_{12}E_0$/$C_{12}E_8$. …….. **page 53**

Figure 3.15: I(q) versus q diagram for $C_{12}E_3$. …… **page 54**

Figure 3.16: Kratky-Porod plot of 0.7 mM $C_{12}E_8$ and 2.5 mM $C_{12}E_0$ in D_2O analyzed in 30-m SANS beam line. …….. **page 55**

Figure 3.17: Partial Zimm plot of 0.7 mM $C_{12}E_8$ and 2.5 mM $C_{12}E_0$ in D_2O analyzed in 30-m SANS beam line. …….. **page 56**

Figure 3.18: Partial Zimm plot of $C_{12}E_3$. ……... **page 57**

Figure 4.1: Pendant bubble setup used for air-liquid interfacial tension measurements. …….. **page 88**

Figure 4.2: Schematic of the L-B trough a) liquid expanded Langmuir monolayer, b) liquid condensed Langmuir monolayer, c) liquid expanded Gibbs monolayer with surfactant below the CMC, d) compressed Gibbs monolayer forcing surfactant back into the subphase to reestablish equilibrium. …… **page 89**

Figure 4.3: Surface tension of water from L-B trough showing that the subphase is clean before the addition of surfactant. ……... **page 93**

Figure 4.4: $C_{12}E_8$ injected to the water subphase of the L-B trough. The air-liquid interfacial tension reaches an equilibrium value of approximately 34 mN/m. ….. **page 94**

Figure 4.5: $C_{12}E_8$ tension remains stable for approximately 24 hours on the L-B trough. …….. **page 95**

Figure 4.6: Dynamic surface tension using L-B trough. Addition of dodecanol to the $C_{12}E_8$/water subphase on the L-B trough reduces the air-liquid interfacial tension of the system to approximately 21 mN/m. ……... **page 96**

Figure 4.7: Schematic of proposed model structure of the C_iE_j/dodeanol mixed monolayer. ……. **page 97**

Figure 4.8: Cryo TEM image of $C_{12}E_8$/dodecanol mixture discussed in Chapter 3. A) area of low monolayer density and high aggregate concentration, B) area of high monolayer density and low aggregate concentration. …… **page 98**

Figure 4.9: Cryo-TEM image of the $C_{12}E_0/C_{14}E_8$ demonstrating synergistic phase and air-liquid interfacial tension reduction. ……..…….... **page 99**

Figure 4.10: Electron diffraction pattern of region "B" of Figure 4.8. Outermost rings are representative of the structure of ice, however the diffuse centermost diffraction ring indicates the lattice spacing for hexagonally packed hydrocarbon chains. …..... **page 100**

Figure 5.1: Schematic of an SFG spectroscopic liquid cell with a quartz crystal. …… **page 125**

Figure 5.2: Schematic of ATR liquid cell with modified ATR crystal. ……... **page 126**

Figure 5.3: Dynamic adsorption profile via ATR/FTIR of dodecanol on an OTS monolayer. ……... **page 128**

Figure 5.4: Dynamic adsorption profile via ATR/FTIR of dodecanol on an OTS monolayer. Focus on the hydrocarbon stretching modes. ……... **page 129**

Figure 5.5: Dynamic adsorption profile via ATR/FTIR of dodecanol on an OTS monolayer. Focus on the $-CH_2$ bending modes. ……. **page 130**

Figure 5.6: SFG spectrum of pure water on an OTS modified quartz interface. …… **page 132**

Figure 5.7: SFG spectra comparing the adsorption behavior of pure water to that of a 7CMC $C_{12}E_8$ surfactant solution. ……. **page 133**

Figure 5.8: SFG spectra comparing the adsorption behavior of pure water to that of a saturated solution of dodecanol. …….. **page 134**

Figure 5.9: SFG spectra comparing the adsorption behavior of pure water to that of a dodecanol/$C_{12}E_8$ binary surfactant solution. …… **page 135**

Figure 5.10: SFG spectra comparing the adsorption behavior of pure water to that of a 7CMC $C_{12}E_8$ surfactant solution and the corresponding mixture containing dodecanol. The water removal is enhanced by using dodecanol with $C_{12}E_8$. …… **page 136**

Figure 5.11: SFG spectra of a deuterated dodecanol solution compared to that of clean water. …… **page 137**

Figure 5.12: Schematic of dodecanol adsorption of onto the OTS monolayer. Symmetry is induced at the interface between the two molecules making the interface SFG invisible. …… **page 138**

CHAPTER 1

INTRODUCTION

The study of wetting phenomena has been ubiquitous in fundamental research because of the infinite number of applications where the understanding of wetting phenomena is important. Biological systems[1-4], coatings[5] and the agricultural industry[6] are a few examples of such applications. A particular class of surfactants, referred to as ethylene glycol trisiloxane surfactants, has been dubbed "superspreaders" as a result of their ability to rapidly and completely wet a hydrophobic surface as demonstrated by drop impact studies and wetting rate experiments reported by Svitova[7] and Ward[8]. These surfactants have been in existence for decades, but their ability to wet surfaces has not yet been completely understood. This behavior has been attributed by some researchers to the unusual shape of these molecules[9], while others have focused on the liquid crystalline phase behavior[10-13].

In spite of their benefits, trisiloxane surfactants have structural shortcomings that must be addressed. The original trisiloxane surfactants were only effective at neutral pH and had a propensity to oxidize in acidic pH or in the presence of ultraviolet light. Given the industries where these materials were to be applied, the aforementioned shortcomings are severe. In addition, given the current trend of finding and using "green" chemistries, alternate systems of similar performance must be found. Currently there is no another

surfactant that on its own can have the same performance as the trisiloxane surfactants. Consequently, we must look to mixtures of aqueous soluble surfactants that, when adsorbed at the air-aqueous or aqueous-hydrophobic solid interface causes a very significant reduction in the tension of these interfaces and lead to enhanced wetting (near zero contact angle) on hydrophobic surfaces. The superspreading trisiloxane surfactants will serve as a baseline performance to which all other systems will be compared.

The linear polyethylene glycol alkyl ether (C_iE_j) surfactants are well understood with regard to their performance on hydrophobic surfaces. Structurally, the surfactants are similar to trisiloxanes in that the hydrophilic headgroups have the same structure. However, when in solution by themselves, the surfactants are incapable of matching the performance of the trisiloxane surfactant. As a result we must take advantage of the possible synergism that exists[14-17] when two surfactants are used in the same system. Rosen[18] has examined co-adsorbed surfactants at the air-liquid interface and has found systems that allow one to lower the air-liquid interfacial tension using a lower total surfactant concentration.

The binary systems being discussed in this work are the C_iE_j, linear nonionic surfactants, in combination with a linear medium chain alcohol. The addition of the alcohol becomes important because it has been previously shown that dodecanol, as an impurity during SDS production can and will contribute to synergistically reducing the air-liquid interfacial tension[19]. In addition, when compared to the siloxane moiety, the linear

twelve-carbon chain has the same hydrophobicity[20], but drastically different molecular volumes. The addition of dodecanol can lead to molecular aggregate structures close to those formed by the trisiloxane.

REFERENCES

(1) Chen, P.; Policova, Z.; Pace-Asciak, C. R.; Neumann, A. W. *Colloids and Surfaces B: Biointerfaces* **1999**, *15*, 313-324.

(2) Park, S. Y.; Hannemann, R. E.; Franses, E. I. *Colloids and Surfaces B: Biointerfaces* **1999**, *15*, 325-338.

(3) Sch¸rch, S.; Geiser, M.; Lee, M. M.; Gehr, P. *Colloids and Surfaces B: Biointerfaces* **1999**, *15*, 339-353.

(4) Mack, D. R.; Sherman, P. M. *Colloids and Surfaces B: Biointerfaces* **1999**, *15*, 355-363.

(5) Adams, J. W. *In Surface Phenomena and Additives in Water-Based Coatings and Printing Technology*; Plenum Press: New York, 1991.

(6) Stevens, P. J. G. *Pestic. Sci.* **1993**, *38*.

(7) He, M.; Hill, R. M.; Lin, Z.; Scrivens, L. E.; Davis, H. T. *Journal of Physical Chemistry* **1993**, *97*, 8820 - 8834.

(8) Dong, J.; Mao, G.; Hill, R. M. *Langmuir* **2004**, *20*, 2695-2700

(9) Kunieda, H.; Taoka, H.; Iwanaga, T.; Harashima, A. *Langmuir* **1998**, *14*, 5113-5120.

(10) Churaev, N. V.; Esipova, N. E.; Hill, R. M.; Sobolev, V. D.; Starov, V. M.; Zorin, Z. M. *Langmuir* **2001**, *17*, 1338-1348.

(11) Hill, R. M.; He, M.; Davis, H. T.; Scriven, L. E. *Langmuir* **1994**, *10*, 1724-1734.

(12) Svitova, T.; Hill, R. M.; Smirnova, Y.; Stuermer, A.; Yakubov, G. *Langmuir* **1998**, *14*, 5023-5031.

(13) Svitova, T.; Hoffmann, H.; Hill, R. M. *Langmuir* **1996**, *12*, 1712-1721.

(14) Bain, C. D.; Davies, P. B.; Ward, R. N. *Langmuir* **1994**, *10*, 2060 - 2063.

(15) Bain, C. D.; Ward, R. N.; Davies, P. B. *J. Phys. Chem. B* **1997**, *101*, 1594-1601.

(16) Rosen, M. J. *Langmuir* **1991**, *7*, 885 - 888.

(17) Rosen, M. J.; Zhou, Q. *Langmuir* **2001**, *17*, 3532 - 3537.

(18) Rosen, M. J. *Langmuir*, *7*, 885-888.

CHAPTER 2

DIRECTION AND SCOPE

2.1 Scope of Research

A pure water droplet, on a hydrophobic surface, subtends to a large contact angle ($\theta >$ 65°) as a result of the balance of three forces that are exerted on the drop that are a result of the interfaces that are created when two bulk phases come into contact with each other. In the case of water on a hydrophobic surface, the three phases are air (vapor), water (liquid), and the hydrophobic solid; the corresponding interfacial pairs are the vapor/solid, solid/liquid and liquid/vapor. This balance of forces is governed by Young's equation, $\gamma_{s/v} = \gamma_{s/l} + \gamma_{l/v}\cos\theta$, where, $\gamma_{s/l}$, and $\gamma_{l/v}$ are the vapor/solid, solid/liquid and liquid/vapor interfacial tensions respectively and θ is the contact angle of the drop on the surface. Given that $\gamma_{s/v}$ is constant and has a small value (~22 mN/m), the cause of the high contact angle of water is as result of higher values of the opposing forces of $\gamma_{s/l}$ (~52 mN/m) and the surface parallel component of $\gamma_{l/v}$, where $\gamma_{l/v}$ is 72.8 mN/m at 20° C.

An empirical analysis of Young's equation shows that in order to reduce the contact angle of water on a hydrophobic surface, the sum of $\gamma_{l/v} \cos \theta$ and $\gamma_{s/l}$ must be less than $\gamma_{s/v}$. Further analysis shows that both tensions in the sum must be reduced in order to get the water to wet the surface. If $\gamma_{l/v}$ is reduced, without a reduction in $\gamma_{s/l}$, the contact

angle will increase as the liquid-vapor tension is reduced, whereas the opposite is true when the liquid-vapor is held constant and the solid-vapor tension is reduced. Again, both tension must be reduced in order achieve wetting on a hydrophobic surface, but it is initially critical to reduce the solid-liquid interfacial tension until $\theta < 90°$ which can be thought of as a critical wetting angle.

Certain surfactants can be used to effectively reduce the air-liquid and solid-liquid interfacial tensions and consequently the contact angle of the water droplet on the hydrophobic surface. At equilibrium most surfactant will reach a finite contact angle on said surface. However, there is a class of surfactant call the polyoxyethylene glycol trisiloxane, which have the unique ability to, when added to water, cause a water droplet to completely and rapidly wet a hydrophobic surface forming a thin film of water with an immeasurable contact angle. This behavior is of great industrial importance. However, for all of their benefits, they have severe shortcomings as well, including their hydrolyzability under certain pH conditions, their wetting ability is dependant on the humidity conditions of the surrounding air and the surfactant are not considered to be environmentally friendly materials.

The purpose of this research is to determine systems of binary aqueous soluble surfactants that, when adsorbed at the air-aqueous or aqueous-solid interface cause a very significant reduction in the tension of these interfaces. In preliminary research, we have determined that the ability of a surfactant system to reduce considerably the air-aqueous

and air-hydrophobic solid interfacial tensions correlates with their ability to form extended (lamellar (L_α) or sponge (L_3)) phases in the bulk, structures which the trisiloxane surfactants are able to form spontaneously at concentrations on the order of 0.1 mM at room temperature. This behavior is unlike the majority of the surfactants that will be a part of this study, which only form these structures at temperatures and concentrations that are impractical for the majority of known wetting applications. The binary systems being discussed are polyoxyethylene glycol monoalkyl ether (C_iE_j) linear nonionic surfactants in combination with the linear medium chain alcohol n-dodecanol.

Our principal interest in these systems derives from their potential technological use as superior wetting agents in making water spread on hydrophobic surfaces, as, for example, in the wetting of agrochemical solutions on waxy leaf surfaces, the aqueous coating on hydrophobic surfaces and the impregnating of an aqueous phase through a nonwetting fabric. Surfactant systems that greatly reduce the air-aqueous or hydrophobic solid-aqueous interfacial tensions improve wetting because they reduce contact angles when aqueous drops are placed on hydrophobic surfaces. The ultimate goal being to get as close to a zero contact angle as possible, and to ultimately achieve complete wetting; similar to that achieved by the famous "superwetting" trisiloxane surfactants. In addition, surfactants, which reduce significantly the tension of the air-aqueous interface, have technological applications in promoting foaming and ink-jet printing where reduced tensions offer potential for smaller dots, thus enhancing the quality of the printed image.

2.2 Direction of Research

As one can see from the known behavior of the trisiloxanes, there are three main aspects of the surfactant mixtures that must be addressed in order to target systems that will potentially provide synergistically enhanced wetting or superwetting capabilities. The bulk aggregate structures of the surfactants predetermine the structure that surfactant mixtures will have at the air-liquid and solid-liquid interfaces. The predetermination can manifest it self as either the geometry of the adsorbed layer and/or the population density of the surfactants once adsorbed at the interfaces. One should note that the densities could potentially be different for the two interfaces. Understanding the behavior of the surfactant systems at the air-liquid interface serves three purposes. One, it serves as a targeting mechanism, which will predict the surfactant systems which have the potential to provide enhanced wetting on a hydrophobic surface. Two, it gives us information about the thermodynamic accessibility of the surfactant aggregate structures. Three, the analysis of the air-liquid interface gives information about the packing density of the surfactant molecules at the air-liquid interface. Finally, and most significantly, for the wetting we are trying to achieve the adsorption trends at the solid liquid interface must be examined. As was explained during the previous analysis of Young's equation, in order to wet a hydrophobic surface the solid-liquid interfacial tension must be reduced. A reduction in the solid-liquid tension implies a change in the solid surface that needs to be examined in order fully understand the posed problem.

2.2.1 Analysis of Bulk Surfactant Behavior

Above a certain concentration called the critical aggregate concentration (CAC), individual surfactant molecule will combine to form higher order structures, such as spherical micelles, lamellae, vesicles, and bi-continuous (spongy) phases. These phase are considered to be liquid crystalline in nature and the structure that the surfactants obtain is dependent on the equilibrium geometry on the monomer in the solvent, the overall surfactant concentration and the temperature of the system. The liquid crystalline phase of aqueous solution of the pure C_iE_j surfactants are very well known, however the phase behavior of surfactant mixtures is very complicated and is less well studied. Consequently we will use dynamic light scattering, cross-polarized light microscopy, cryogenic transmission electron microscopy (cryo-TEM), and small angle neutron scattering (SANS) to characterize the aqueous bulk aggregate structures that are formed when 1-dodecanol is added to aqueous solutions of $C_{12}E_4$, $C_{12}E_5$, $C_{12}E_6$, $C_{12}E_8$, $C_{14}E_8$, and $C_{10}E_8$.

2.2.2 Analysis of Air-Liquid Interface

The air-liquid interfacial tension of the superspreading polyethoxy trisiloxanes has values on the order of 20 mN/m[21] (add reference). The ability of these molecules to cause water to completely wet a hydrophobic surface has been partly attributed to their ability to reduce the air-liquid tension to such a low value. As a result the air-liquid interfacial

tension of the 1-dodecanol with aforementioned C_iE_j surfactants mixtures will be measured using pendant bubble tensiometry. The bulk aggregate structures that form in the surfactants mixtures predetermine the adsorption behavior at the interface, as described in the research scope. However, the aggregates formed by these mixtures can be thermodynamically unstable and will potentially phase separate. Monolayer penetration experiments, using a Langmuir-Blodgett trough, will performed to determine the effect of the addition of the co-surfactant to the monolayer and the dynamic behavior of the mixture at the interface. Finally, electron diffraction will be performed at the interface in order to examine the packing density of the surfactant at the air liquid interface; the results of which will be compared to the known adsorption behavior of 1-dodecanol and the C_iE_j surfactants.

2.2.3 Analysis of the Solid-Liquid Interface

Contact angle goniometry on a hydrophobically modified silicon wafer will act as a screening tool for the surfactant mixtures, several of which exhibit synergistic air-liquid interfacial tension reduction at the air-liquid interface. Once the appropriate mixtures have been identified, attenuated total internal reflection Fourier transform infrared (ATR/FTIR) will be used to explore the dynamic adsorption behavior of the dodecanol at the interface; $C_{12}E_8$ adsorption has been previously studied via ATR/FTIR. Sum frequency generation (SFG) spectroscopy, an interface specific technique, will also be used to obtain information regarding the equilibrium adsorption of individual surfactants

and their mixtures that exhibit synergistic wetting on the hydrophobic surface. The focus when using this technique will be how the adsorption of surfactant at the solid-liquid interface changes the structure of the water layer at the surface. The SFG structure of water is well known and has been studied for at least the last 20 years by Shen, Richmond and Yeganeh who have all examined how water structure changes with the addition of materials or with changes in the pH of the fluid.

CHAPTER 3

SYNERGISTIC FORMATION OF LAMELLAR SURFACTANT AGGREGATES WITH MIXTURES OF THE LINEAR POLY(ETHYLENE OXIDE) N-ALKYLETHER SURFACTANTS WITH 1-DODECANOL

3.1 INTRODUCTION

Surfactants, once they have reached their critical aggregate concentration (CAC), will self-assemble into organized three-dimensional structures of various geometries including, but not limited to spheres, lamellae, and bicontinuous (spongy) phases. These self-assembled structured, at high enough concentrations are liquid crystalline in nature and are capable of forming even higher order phases, such as a cubic phase. This surfactant behavior has been of interest for several decades because of applications in the pharmaceutical industry where the structures can be used for drug delivery, in catalysis where surfactant aggregates are used as structure directing agents as in the MCM class of catalysts and in membrane science as structure directing agents where surfactants can impart mesoporous structure and order to the membranes.

The three-dimensional shape adopted by the surfactants upon aggregation is dependent on several factors, including the hydrocarbon volume of the molecule (ν), the optimal headgroup area (α_0) and the critical chain length of the hydrocarbon (ℓ_c). Using these

values, Israelachvili[22] developed a parameter called the shape factor or packing parameter (P), where,

$$P = \frac{v}{a_o \ell_c}$$

The packing parameter can be can be used to predict the shape the surfactant aggregates will attain once above the surfactant are above their respective CACs. The value of the factor represents the shape that a single surfactant molecule would attain if it were to be rotated 360º along an axis that runs through both the hydrophilic and hydrophobic portion of the molecule. A shape factor of $P < 1/3$ is representative of a conical volume whose base is at the hydrophilic end; the cones will aggregate into a spherical micelle with the hydrocarbon chains forming a liquid-like hydrocarbon core. On the other end of the spectrum are values of $P > 1$, which represents a volume having the shape of truncated cone, where the orientation of the molecule in the cone is the reverse of the $P < 1/3$ case, consequently leading to the formation of a reverse micelle. The variable in P are readily accessible through experiment even when taking into account their sensitivity to temperature, alky chain configuration, pH, and ion concentration (in the case of ionic surfactants). However, currently, the use of this parameter is limited to single surfactant systems and cannot effectively predict the structure of mixed surfactant systems.

The poly(ethyleneglycol) alkylether class of nonionic surfactants of the general structure $CH_3(CH_2)_{i-1}$-$(OCH_2CH_2)_j$-OH and the shorthand structure C_iE_j, where C represents the

hydrocarbon based hydrophobe of the amphiphilic molecule, i is the number of carbon atoms in the hydrophobe, E represents the ethylene oxide unit on the hydrophilic portion of the molecule and j the number of ethylene oxide units, have bulk aggregate structures that are very well known and have been studied extensively. These surfactants are fairly ubiquitous in both academic and industrial research because of their detergency and the similarities to and inertness in biological systems. One of the first papers to comprehensively study the aqueous bulk behavior these surfactants was Mitchell and Tiddy (1983) [23], where liquid crystalline phase diagrams for the majority of the C_iE_j surfactants were developed. Since then, the bulk properties of aqueous solutions of the individual surfactants have been studied by Rosen[24], Schick[25], Laughlin[26], Strey[27] and Talmon[28], to name a few. Because the C_iE_j surfactants are nonionic they do not suffer from the complicating effects of pH and ion strength of the aqueous medium, leading to predictable phase behaviors when using Israelachvili's shape factor.

As one can see from Figure 3.1, $C_{10}E_8$, $C_{12}E_4$, $C_{12}E_5$, $C_{12}E_6$, $C_{12}E_8$ and $C_{14}E_8$, the surfactants included in this study, all have well understood behavior as evidenced by their fully developed phase diagrams[23,29,30]. All of these surfactants form spherical micelles at room temperature and at concentrations up to at least twenty times their respective CACs, with the exception of $C_{12}E_4$, which forms lamellae. Further analysis of the phase diagrams shows that as the number of the ethylene oxide units increases, the spherical micelle (L_1) region on the phase diagram increases, making the regions of lamellar (L_α), reverse micelle (L_2), isotropic immiscible surfactant (L_3), normal hexagonal (H_1), close

packed spherical micelle cubic phase (I_1) and normal bi-continuous cubic (V_1) phases smaller or nearly nonexistent. It should be noted that in all cases, there is monomer phase(W) present in the solution at in equilibrium with the aggregates. The change in presence of the different phases is explained by the shape and chemistry of the monomer and its resulting packing in an aqueous environment. Also of great significance to phase behavior is related to the systematic variations in the interfacial curvature as the size of the C_iE_j surfactants increase. As the length of the hydrophilic moiety of the surfactant molecule increases, the overall hydrophilicity of the surfactant molecule increases, leading to structures of greater curvature. Consequently this forces the surfactant molecules into highly curved surfactant structures like spherical or cylindrical micelles.

Medium chain length alcohols like 1-dodecanol ($C_{12}E_0$), although not a surfactant by definition, are of interest in this arena of study because of their propensity participate in micelle formation when used as an additive in surfactant mixtures. Unlike the C_iE_j surfactants, in aqueous solution, $C_{12}E_0$ has a limited solubility forming oily droplets or globules once above its solubility limit. However, in combination with other surfactants, synergistic behaviors begin to manifest themselves. The most famous example of this phenomenon is in the case of synthesis of sodium dodecylsulfate (SDS), where $C_{12}E_0$ a synthesis precursor, contaminates the final SDS product. Consequently, there are effects on the adsorption behavior of the surfactant and alcohol at the interface, enhanced foam stability and changes in surface viscosity[31]. The majority of the research surrounding dodecanol examines its behavior at concentration at or less than its solubility limit in

water. However, the focus of this study is to examine the synergistic liquid crystalline phase behavior that arises when $C_{12}E_0$ is added to micellar C_iE_j surfactant solutions at molar concentrations that are as high as thirty times its solubility limit in water. The behavior of dodecanol in combination with the C_iE_j surfactants at the air-liquid interface will be the topic of study for Chapter 4.

This apparent synergistic effect that alcohols have on surfactant aggregate phase behavior has been seen in other systems studied. There is evident synergistic behavior between C_8E_0 and C_8E_5[32] that creates the L_a and L_3 phases, which are not present in the phase diagram of the individual surfactants, but are present when the two are in optimal concentrations in water. Also important is the fact that the two phases occur at temperatures and concentrations lower than those seen in longer chain surfactants like $C_{12}E_5$[27]. The L_a and L_3 phases are induced by the addition of the alcohol to the C_iE_j-Water mixture. The thought is that the alcohol makes the C_iE_j structure more hydrophobic, forcing it out of solution, into surfactant-rich phases.

Constructed Gibbs triangles representing the phase diagrams of the system indicate that as the temperature of the system is less the 40 °C, the L_3 and L_a become increasingly apparent especially at the extremely dilute (< 2%) total surfactant concentration in water. This increase in the presence of the L_3 and L_α phases is at the expense of the $L_1^{|}$ and $L_1^{||}$ phases. In other phase diagrams, the L_3 and L_α phases are usually surrounded by multiple phase regions like $L_1^{|}$ and $L_1^{||}$, but addition of the alcohol stabilizes the L_3 and L_α phases.

Addition of C_8E_0 to H_2O-C_8E_5 increases the relative amount of C_8E_0 in the mixed film of C_8E_5 and C_8E_0, rendering it more hydrophobic. Accordingly, the presence of 1-octanol induces the formation of these bilayer phases, which suggests that the addition of 1-octanol might increase the rigidity of the mixed surfactant (C_8E_5 and C_8E_0) monolayer. The spontaneous curvature of the mixed film decreases and may at some point become zero, at which point the lamellar phase should form. Although a zero-spontaneous curvature forms the lamellar phase, the stability of the phase is not guaranteed, if the surfactant chains are too short. The synergism of the two short-chain molecules C_8E_5 and C_8E_0 is an interesting observation in so far as it permits generation of the analog phases observed in long-chain surfactant systems by choosing a certain C_8E_5/ C_8E_0 ratio. The synergistic effect of adding a co-surfactant was again seen in a water-$C_{12}E_5$-hexanol system. Addition of hexanol to the aqueous C_iE_j phase made available the L_3 and L_α phases at much lower temperatures and concentrations than are normally seen in a single component $C_{12}E_5$ aqueous solution. The present study gives us information on the dilute surfactant regime that allows us to explore the implications that these phases have the interfacial tension and the wetting ability of the system.

In a study performed by Jonströmer and Strey[27] where they analyzed the effect of additives on nonionic bilayers, the learned that the addition of alcohols to bilayer structures of $C_{12}E_5$, increases the flexibility of the bilayers and their projected area. They also provided two possible reasons for the increased solubility of the usually insoluble

alcohol: (i) the polar headgroup region is extended in C_iE_j systems making the polarity of this region less polar than pure water, consequently a higher solubility of the alcohols is reasonable, (ii) for the longer chain alcohols, the non-polar properties dominate the molecule, resulting in a low solubility in water but infinite in the oil. Thus, one can expect a larger fraction of the alcohol to be located with no preferred orientation within the interior of bilayer, thus partitioning between oriented and "solvent-like" alcohol molecules in the film may occur.

Our interest in obtaining these structures lies in the application to wetting behavior, which will be discussed in Chapter 5. To this end we explore the use of dodecanol to bring rise to synergistic behavior observed in the aforementioned studies for two reasons:

i. Although the studies have been able to access the lamellar structures with the addition of alcohols to their systems, these are added at concentration that are impractical for our proposed application
ii. Taking into account geometric considerations and its low water solubility, dodecanol should be quickly incorporated in to the core of the micelles, thus disrupting the structure of the micelle more readily when compared with hexanol and octanol.

3.2 EXPERIMENTAL

3.2.1 - Materials

$C_{10}E_8$, $C_{12}E_4$, $C_{12}E_5$, $C_{12}E_6$, $C_{12}E_8$ and $C_{14}E_8$ were obtained from Nikko Chemicals and were used without further purification. $C_{12}E_0$ and $C_{12}E_3$ were purchased from Fisher Scientific and were used as received.

Surfactant Solution Preparation

For the single component aqueous solutions of the C_iE_j surfactants, the required amount of the surfactant was measured on a balance accurate to 0.1-mg. The surfactant was place in a volumetric flask and the remaining volume was filled with deionized water. The mixture was allowed magnetically stirred for several hours or until it appeared homogeneous. The single component dodecanol solution was made using the method described by Franses[33]. In this method, dodecanol is added to water, the mixture is heated beyond the melting point of the alcohol and is maintained there for 90-minutes while being stirred. Once the mixture is stirred, the flask is allowed to cool to room temperature and then placed in a sonic bath for 3-4 hours. Once removed for the sonic bath, the solution is inspected for signs of non-dissolved alcohol: particulate matter floating in the bulk or oil droplets in the meniscus of the mixture in the neck of the flask.

It should be noted that it has been previously found that if dodecanol is placed in the flask beyond its solubility limit, removal of the non-dissolved alcohol will not disrupt the ability for the system to reach its minimum equilibrium interfacial tension.

For the binary solutions, two methods were used to make the solutions. The first method followed the same procedure described above where the dodecanol water mixture was first heated above the melting point of the alcohol. The mixture was allowed to cool while still on the magnetic stirrer and before it reached room temperature, the C_iE_j surfactant was added to the mixture. The binary mixture was allowed to cool to room temperature and the solution continued to stir for several hours while at room temperature. The second method reversed the order of addition of the two components where the C_iE_j was added to the flask first at room temperature and the warmed to approximately 40 °C, where the dodecanol was then added to the system. The binary mixture was stirred at temperature for 30-40 minutes and was then allowed to cool to room temperature while continuing to stir for 1-2 hours. It was determined that for high concentrations of dodecanol, the first procedure was preferable from the standpoint of the stability of the solution and the time it takes to make the solution.

3.2.2 Methods

Particle Size Analysis

The particle size analysis of the surfactant solution was performed using the Malvern Zetasizer Nano, which uses dynamic light scattering in order to measure the hydrodynamic diameter (D_H) of the surfactant aggregates in the mixtures to be studied. Using the Stokes-Einstein relation, $R_H = \frac{kT}{6\pi\eta D}$, where k is Boltzmann's constant, T is the temperature, η is the solvent viscosity and D is the translational diffusion coefficient, the Zetasizer is able to track the average change in position of the particle over time allowing the machine to develop a time dependant correlation function from which the D_H can be obtained. For a solution of monodisprese particle size, the correlation function will drop steeply for a particular time, however for polydisperse systems, there will several drop off points in the correlation function that will correspond to the different size ranges in the sample. The diameter obtained by this technique is that of a sphere that has the same translational diffusion coefficient as the particle being measured. For aggregates having a spherical geometry, the particle size will be accurate. For lamellar structures, more information will be needed to understand the detail of the structure. In the Zetasizer one can also change the temperature over time; consequently we will be able to test the thermal stability of the structures in solution. Approximately 1-ml of the desired sample was poured into a polystyrene cuvette which had been previously blown out with compressed nitrogen, unless a temperate ramp study was being performed, the particle size was measured at 23° C.

Cross-Polarized Microscopy

Cross-polarized microscopy was performed using a Nikon Eclipse E600 POL light microscope fitted with a Sony ExwaveHAD CCD color video camera. The temperature of the experiment was controlled using a Linkam LTS120 Peltier cooler using an EHEIM Professional II water bath as the heat sink.

A sample cell was constructed using ~6 mm sections of Tygon tubing with an inner diameter and wall thickness of 5-mm and a standard microscope slide. All of the cell components were sonicated in methanol prior to construction, and then rinsed with deionized water. After drying the materials, three of the Tygon tubing sections were placed on the on the microscope slide as shown in Figure 3.2. The entire assembly was placed on a hotplate and heated until the tubing softened enough to be pressed onto the slide. The assembly was then allowed to cool to room temperature and the cells were check for leakage. For the experiment, the surfactant solution was added to the cell using a glass Pasteur pipette and allowed to sit in the Peltier for at least ten minutes prior to viewing under the microscope.

Small Angle Neutron Scattering

Small Angle Neutron Scattering (SANS) was performed at the National Institute for Standards and Testing (NIST) Center for Neutron Research using the 30-meter beam line shown in Figure 3.3. This technique used a cold neutron source and takes advantage of

the fact that neutrons are scattered by nuclei in samples or by the magnetic moments associated with unpaired electron spins (dipoles) in magnetic samples. The nuclear scattering potential is short range so that most neutron scattering can be described by "s wave" scattering (zero orbital angular momentum) and the scattering cross section can be described by the first Born approximation. This covers structures from the near Ångstrom sizes to the near micrometer sizes. How small are the small angles? They are typically from 0.2° to 20° and cover two orders of magnitude in two steps. A low-Q configuration covers the first order of magnitude (0.2° to 2°) and a high-Q configuration covers the second one (2° to 20°). The scattering variable is defined as $Q = (4\pi/\lambda) \sin(\theta/2)$ where λ is the neutron wavelength and θ is the scattering angle. Within the small-angle approximation, Q simplifies to $Q = 2\pi\theta/\lambda$. The SANS scattering variable Q range is typically from 0.001 Å-1 to 0.45 Å-1. This corresponds to d-spacings from 6,300 Å down to 14 Å.

In order to obtain neutron scattering data, the surfactant solutions were prepared in D_2O instead of water; using the same procedure previously described for the surfactant solutions. A titanium demountable cell, whose parts are shown in Figure 3.4, was assembled in order to hold the surfactant solution. The cell consists of a cell body into which two quartz widows were placed, separated by a 1-mm spacer. A Viton o-ring sealed each window, which were then compressed by retaining rings that are held down by four screws. After assembling the cells, liquid samples can be inserted through the top using a syringe.

Cryogenic Transmission Electron Microscopy

Cryogenic Transmission Electron Microscopy (Cryo-TEM) was performed using either a FEI Tecnai TF20 with a 200kV tungsten filament field emission gun (FEG) fitted with standard side entry cryo-stage and a CCD camera with a 4k x 4k resolution Tecnai F20 or a JEOL 2100F with a 200kV FEG fitted with side entry cryo-stage and a CCD camera with 2k x 2k resolution. Both microscopes, located at the New York Structural Biology Center (NYSBC), were used to obtain images of the surfactant aggregate structures that were created by either the unary or binary surfactant systems when above their respective critical micelle concentrations (CMCs).

The samples were prepared on a Quantifoil R2/4 Copper, 200-mesh, holey carbon grids, with 2-μm holes on a 4-μm lattice spacing, which were purchased from Quantifoil Micro Tools GmbH and were used as received. In order to prepare the sample, a Plexiglas chamber with access openings, was humidified using a water pump until the chamber had a humidity of at least 80%. Placed inside the chamber was a vessel of liquid ethane, which was cooled using liquid nitrogen. A 4-μl drop was placed on the grid held by Dumont #5 tweezers, using an Eppendorf micropipet. The tweezers, with the grid, was then placed in the humidified chamber, in a holder designed specifically to hold the tweezers over the liquid ethane. A strip of Whatman filter paper was used to blot the excess fluid from grid. Once all of the excess solution was removed from the grid, it was

immediately plunged into the liquid ethane by stepping on a pedal that activated the plunger holding the tweezers. The freshly frozen sample was placed into a cryogenic holder until it was time to image the sample.

3.3 RESULTS

3.3.1 Particle Size Analysis

The particle sizes for the unary surfactant solutions at the seven times their respective critical micelle concentrations (CMC) exhibited the expected behavior, when measured at 23 ºC. With the exception of $C_{12}E_3$ and $C_{12}E_4$, all of the surfactants form micelles ranging from globular to spherical in shape, with unimodal distribution of particle sizes ranging from 6-nm to 10-nm. On the other end of the spectrum, $C_{12}E_3$ and $C_{12}E_4$ (Figure 3.5 and 3.6, respectively) had particle sizes ranging from 10-nm to 2-μm. This result for $C_{12}E_3$ is not surprising because its phase diagram indicates that the molecule aggregates into lamellae at all concentrations above the CAC. However, in the temperature and concentration regime in which we desire to work, it is unclear exactly what structure should be present in the $C_{12}E_4$ case, because the phase diagrams available only give a general idea as to where the phase boundaries exist. Also, differences in the compositions of what should be pure surfactants can have significant effects on the phase behavior; especially at dilute overall surfactant concentrations. To understand where we were in the phase diagram, the temperature of the analysis chamber was lowered to 4 °C and 10-nm micelles were formed. With an increase in temperature, the size of the particle increased until room temperature was reached and the particle size in Figure 3.6 was produced. The behavior exhibited by the unary systems serves as the baseline for the mixtures that were later formed.

Upon addition of dodecanol to each of the unary C_iE_j systems, structural changes occur only with some of the surfactants that form spherical micelles at the concentrations where the baseline was set (7 CAC). Initially, $C_{12}E_0/C_iE_j$ surfactant solutions were made using the procedure outlined in the previous section, with an initial attempt to solubilize $C_{12}E_0$ at ten times its solubility limit (0.023 mM) in water. The systems containing $C_{12}E_4$ and $C_{12}E_5$ were unable to accommodate the initial amount of $C_{12}E_0$, thus there was no further attempt to add more dodecanol. Large droplets of oil in the neck of the flask signaled the lack of complete incorporation of $C_{12}E_0$ into the $C_{12}E_4$ and $C_{12}E_5$ aggregate structures. In the case of $C_{12}E_4$, there was no significant change in the particle size profile of the mixture when compared to data of the pure aqueous $C_{12}E_4$ solution, but considering the broadness of the $C_{12}E_4$ profile, it would be difficult to discern if there was a difference in structure using particle size analysis unless there were changes in the overall proportions of the structures, which were not evident when doing particle size analysis. However, there were visual changes in the bulk $C_{12}E_5$ mixture, which became cloudy and appeared opalescent in nature, signaling a phase transition from the spherical micelle phase (L_1) to a phase(s) that scatters light; visually, a solution of spherical micelles appears optically clear.

The apparent synergistic appearance of lamellar phases in the $C_{12}E_0/C_{12}E_5$ system also occurred with $C_{12}E_6$ and $C_{12}E_8$, however it took far more $C_{12}E_0$ to cause the change when added to the latter two surfactants. The aqueous mixture of $C_{12}E_6$ was able to

accommodate the initial 0.23 mM of $C_{12}E_0$ into the system and up to 1.7 mM (74 times its solubility limit in water), with visible changes in the aggregate structure occurring. Octaethylene glycol dodecyl ether ($C_{12}E_8$) was capable of incorporating similar concentrations of dodecanol into its structure, reaching aqueous concentrations up to 5 mM. In the case of $C_{12}E_6$ and $C_{12}E_8$, the addition of more dodecanol may have been possible, however no further attempt was made to do so because of results that will be discussed in chapters 4 and 5. In both case, the solutions took on the appearance of having lamellar structures in the solution.

Figure 3.7 shows what the particle size analysis of several of the aqueous mixtures of $C_{12}E_8$ with $C_{12}E_0$, and compares it to the micellar solution of $C_{12}E_8$. With a 0.7 mM (7 CAC) concentration of $C_{12}E_8$ with 0.38 mM $C_{12}E_0$, we see that the vast majority of aggregates in the sample have sizes centered at approximately 20-nm with much smaller populations at 45–nm and 90-nm. In this case, the majority of the dodecanol has been incorporated in the core of the $C_{12}E_8$ micelles, thus swelling them in to globular micelles, similar to what $C_{12}E_5$ does at 7 CAC. With the addition of more $C_{12}E_0$ we can see that the micelles disappear from the solution and much larger surfactant aggregates develop in the mixture. Temperature studies show that changes in temperature drastically affect the sizes of the aggregates, however when returned to room temperature, the displayed profile is regained, indicating that the structures that are formed are equilibrium structures.

3.3.2 Cross Polarized Microscopy

Cross-polarized microscopy was attempted on the 0.7-mM $C_{12}E_8$/0.38-mM $C_{12}E_0$ and 0.7-mM $C_{12}E_8$/2.5mM $C_{12}E_0$, which showed birefringence and opalescence to the naked eye. The observed characteristic are generally associated with the L_α, L_3 or what has been dubbed the L_α^+ by Jonströmer and Strey[34], which consists of a dispersion of bilayers either in the form of multi-walled or single-walled vesicles or a two-phase region with a dilute aqueous solution in equilibrium with L_α. The L_α^+ phase is fully embedded in the L_α region of the phase diagram, but has the optical characteristics of the L_3 phase. However, the systems were too dilute for the light microscope to view the sample, alternately the overall surfactant concentration was doubled 1.4-mM $C_{12}E_8$/5-mM $C_{12}E_0$, with the assumption that the aggregate structure would be maintained as long as the surfactant ratio was maintained. What was observed was the appearance of the clover-leaf extinction pattern in Figure 3.8, indicative of L_α structures when viewed under crossed polarizers[35].

3.3.3 Small-Angle Neutron Scattering

Small-angle neutron scattering was used to do an in situ examination of the structures in the surfactant mixture. This technique was used for and aggregated $C_{12}E_3$ and the

solution containing 0.7 mM $C_{12}E_8$ and 2.5 mM $C_{12}E_0$ (see Figure 3.7 (c) for particle size analysis) with D_2O used as the solvent instead of water. Heavy water is used in place of normal deionized water because in order to provide contrast between the water and the surfactant structure. The SANS data in Figures 3.14 and 3.15 shows the scattering intensity data for the $C_{12}E_0/C_{12}E_8$ mixture and $C_{12}E_3$ (a known lamellar phase forming surfactant at 7 CMC).

The Kratky-Porod plot for the $C_{12}E_8/C_{12}E_0$ in Figure 16 indicates that the structures in the system have a platelet thickness of approximately 26 Å; about the length of the 12-carbon hydrocarbon chain. The associated Zimm plot for the same system is shown in Figure 3.17, which is used for a partial Zimm analysis because data for a single concentration was obtained (a full Zimm analysis requires at least four concentrations to be analyzed in order to obtain the radius of gyration, the molecular mass and the second virial coefficient). From the plot, the slope was determined to be approximately 79.2 nm, which represents the radius of gyration (R_g) of the structures in the sample. A similar analysis is done for $C_{12}E_3$ which gives a rod thickness of approximately 79 nm as shown in the inset in Figure 18 and the Zimm indicates a radius of gyration of approximately 362 nm.

3.3.4 Cryo-TEM

CryoTEM was used to characterize the other structures that may be in solution as it is well know that the lamellar structures often exist in equilibrium with each other[26,27,32,35]. The image in Figure 3.9 is a cryo-TEM image of 0.7-mM $C_{12}E_8$ in water, showing spherical micelles of approximately 6-nm, indicated by the arrows. The sizes are in good agreement with the particle size data previously mentioned. The image in Figures 3.10 is of the 0.7-mM $C_{12}E_8$/2.5mM $C_{12}E_0$ surfactant mixture. The aggregate structures appear to be single walled vesicles as evidenced by the core having the same contrast as the surrounding area (vitreous ice) and the dark ring, which is the hydrocarbon core of the vesicle.

3.4 DISCUSSION

The particle size analysis data obtained here for the individual surfactants systems correspond well with what should be expected[36-39] for the C_iE_j surfactants studied here. The addition of the alcohol to the systems structurally modifies the surfactant aggregates in such a way that lamellar structures become accessible. For the $C_{12}E_8$ system, with and without the alcohol, particle size analysis, cross-polarized microscopy and cryo-TEM confirm the transition for a purely micellar solution to one containing lamellar structures. This is system is of particular interest because the lamellar structures have been induced by the presence of the alcohol and have consequences on the ability to wet a hydrophobic surface, which will be the topic of discussion of subsequent chapters. The $C_{12}E_8$ micelles in the cryo-TEM image of Figure 3.9 are fairly monodisperse in size as should be expected. There are clear structural changes that occur as a result of the addition of $C_{12}E_0$ at several concentrations, culminating in the appearance of the L_α liquid crystalline phase as shown in Figure 3.8. This behavior was also readily visible when dodecanol was added to $C_{12}E_6$, and $C_{14}E_8$ (Figure 3.11). Additional phase formation is observed in the cryo-TEM image in Figure 3.11, where primary structures on the order of 100 nm are present, but coexist with much smaller structures on the order of the size of a micelle. Also, the surface of the primary structures appears to be speckled of smaller scattering structures, which may be indicative of the formation of sponge-like structure in the bulk.

Similar to the appearance of lamellar phases, with the introduction of dodecanol to aqueous mixtures of $C_{12}E_5$, $C_{12}E_6$, $C_{12}E_8$, $C_{10}E_8$ or $C_{14}E_8$ is the appearance of many of the same phases when the temperatures of the unary surfactant solutions are increased. In general, these surfactants, in the concentration range discussed here, are readily soluble in water. Generally, the solubility of a solute is directly proportional to the temperature of the system. However, the solubility of the surfactants is dependent on their ability to interact favorably with their solvent. In our case, the surfactant must be able to hydrogen bond with water and this ability is dependent on the relative to the sizes of the hydrophilic headgroup and the hydrophobic tail. The relationship between the size and interactions of the two moieties leads to a parameter commonly known as the hydrophilic-lipophilic balance (HLB) value.

In the case of the C_iE_j surfactants, the hydrogen bonding is key because it allows the polyethylene glycol moiety of the surfactants to obtain the low energy helical configuration[40,41] when the water molecules form bridges between the oxygen atoms on the PEG oligomer, as shown by SAXS and neutron reflectivity. This helical structure is the configuration of the headgroup, which in turn determines the aforementioned shape factor of the surfactant molecules. When the temperature of the system is increased, the thermal energy introduced to the system drives the water from the surfactant molecules. Consequently, the configuration of the headgroup must change to accommodate the loss of the bridging water molecules and combat the increase in conformational entropy. As a result of this change, the aggregates can no longer retain the shape of the spherical

micelle because the headgroup has changed configuration. What was once a solution of monomer and spherical micelles, must, as an adjustment to the new thermodynamics of the system, form structures that more easily accommodate the change on molecular configuration, such as lamellar structures. This behavior, as a result in the change in temperature, can be can be interpreted as the reduction in the solubility of the surfactants. Additionally, the structures formed can be classified as less soluble than the spherical micelles because they form as a result in the loss of solubility of the individual molecules and aggregates. The new structures that form are also one to several magnitudes larger that spherical micelles due to their ability to scatter visible light (at least 200 nm – 350 nm, half the wavelength of light), as show by the particle size analysis study shown in Figure 3.7. It is clear that these structures can be obtained simply by increasing the temperature of the system, but for a practical standpoint, elevated temperatures may not be acceptable, thus other methods of forming these phases are necessary.

Similar the formation of low solubility structures as a result of temperature in the case of the aqueous mixtures of the pure surfactants, similar structures form at room temperature are result of the addition of dodecanol to the system, a less soluble surface active molecule. It is clear the dodecanol molecules participate in the structure formation. From the particle size analysis data, the dodecanol molecules must be incorporated into the structure of the micelles of the pure surfactants. In order to accommodate the dodecanol, the micellar structures must open themselves up into structures with less curvature. From a purely geometric argument, the core of the micelles can accommodate

only so much dodecanol. Once the capacity of the core is reached the dodecanol molecules must then contribute to the formation of the new aggregate structures that will form as a result of their presence. The amount of dodecanol that can be accommodated in the final modified structure depends on the size of the original micelle created by the pure surfactant. Hence, at constant alkyl chain length of surfactant, $C_{12}E_8$ is able to solubilize the most dodecanol.

The particle size analysis data for the $C_{12}E_8/C_{12}E_0$ system having a monodisperse peak size at approximately 80 nm in Figure 3.7C in confirmed by the reported SANS data in Figure 3.17. In addition, the SANS data from Figure 3.16 suggest a lamellar cross-section of 2.6 nm. This leads us to believe that at this concentration, the structures exist as a sheet within which the hydrocarbon core is made up of intercalated hydrocarbon chains, as opposed to stacked chains, which would double the core thickness. In addition, the data also suggest that the ethoxylate contributes little to the thickness of the sheet leading one to believe that the characteristic helical coil of the ethoxylate is somehow disrupted by the synergistic formation of this lamellar phase.

As a direct comparison, $C_{12}E_3$ has also been examined via light scattering and SANS and the R_g of the structure is approximately 362 nm with a thickness of 7.9 nm. It is well known from the aforementioned Mitchell et al.[23] phase behavior paper that the concentration used here, $C_{12}E_3$ forms the L_α phase as shown in the phase diagram in Figure 3.1. The structural dimensions given by the partial Zimm and Guinier analysis of

$C_{12}E_3$ data leads us to believe that is has an overall structure similar that of the mixture, with some slight differences. Given the thickness of the sheet, it seems that the E_3 moiety contributes more strongly to the aggregate structure, since by comparison, both systems have the same hydrocarbon contribution to the lamellar thickness. Also worthy of comparison is the drastic difference in persistence length of the lamellar sheet, which could suggest that although in the $C_{12}E_8$ mixture, the lamellar structures are able to form, there may be limit to their stability in the bulk. This observation could be a possible explanation for vesicle type structures forming, as shown in cryo-TEM image in Figure 3.10. In that image, near the perimeter and in the field of the lighter gray region, there are vesicles that either appears to be breaking up or to be forming as a result of the sample preparation process.

As a final note for the $C_{12}E_8/C_{12}E_0$ system, there is inter-aggregate structure that forms in the system as shown in Figure 3.12. From this data, it is clear that there is repeating ordered structure in the bulk aggregate formation. The origin of this structure is questionable at this point as it only formed in the thick vitrified ice. Danino, Talmon and Zana[42] observed similar behavior with aqueous solutions of $C_{12}E_8$ where they investigated the structure by time-resolved fluorescence quenching (TRFQ) and cryo-TEM to obtain information on the size and shape of the surfactant aggregates and on the microstructure of the $C_{12}E_8$ mixtures. What they observed was that for $C_{12}E_8$ mixtures at either 21.8% or 27% by weight cubic and hexagonal phases, respectively were formed and images via cryo-TEM. The results that we obtain with the addition of dodecanol to

$C_{12}E_8$ is very similar in that not only have we formed a lamellar phase, under certain conditions, a hexagonal phase forms as well, which is done at concentrations at least three order of magnitude lower in total surfactant concentration. The Fourier transform of the circled region Figure 3.12 shows the two pairs of reflection points observed by Danino et al.[28], additionally showing crystalline ordering on smaller length scales as well. The difference in result between the mixed system and the Danino studied system is that similar to what was observed with the SANS data, the length scale of the order is much smaller than that of a pure high concentration $C_{12}E_8$ system and exists in discrete domains. In either case, the surfactant aggregates that form as a result of the presence of dodecanol in a $C_{12}E_8$ system is a result of a synergistic relationship between the two molecules.

3.5 CONCLUSION

The bulk surfactant behavior of the ethylene glycol n-alkyl ether surfactant is well known to be determined by concentration and temperature. We have shown here that at low concentrations and ambient temperature, lamellar aggregate structures are accessible by taking advantage of synergistic interaction between the surfactant and the analogous alcohol. The obtained data shown that the lamellar structures exist, but there are differences in the length scale of the structures themselves as well as in the length scale over which the inter-aggregate structures exist. The synergistic appearance of lamellar phases seems to be dependent on the initial structure of the pure surfactant micelle.

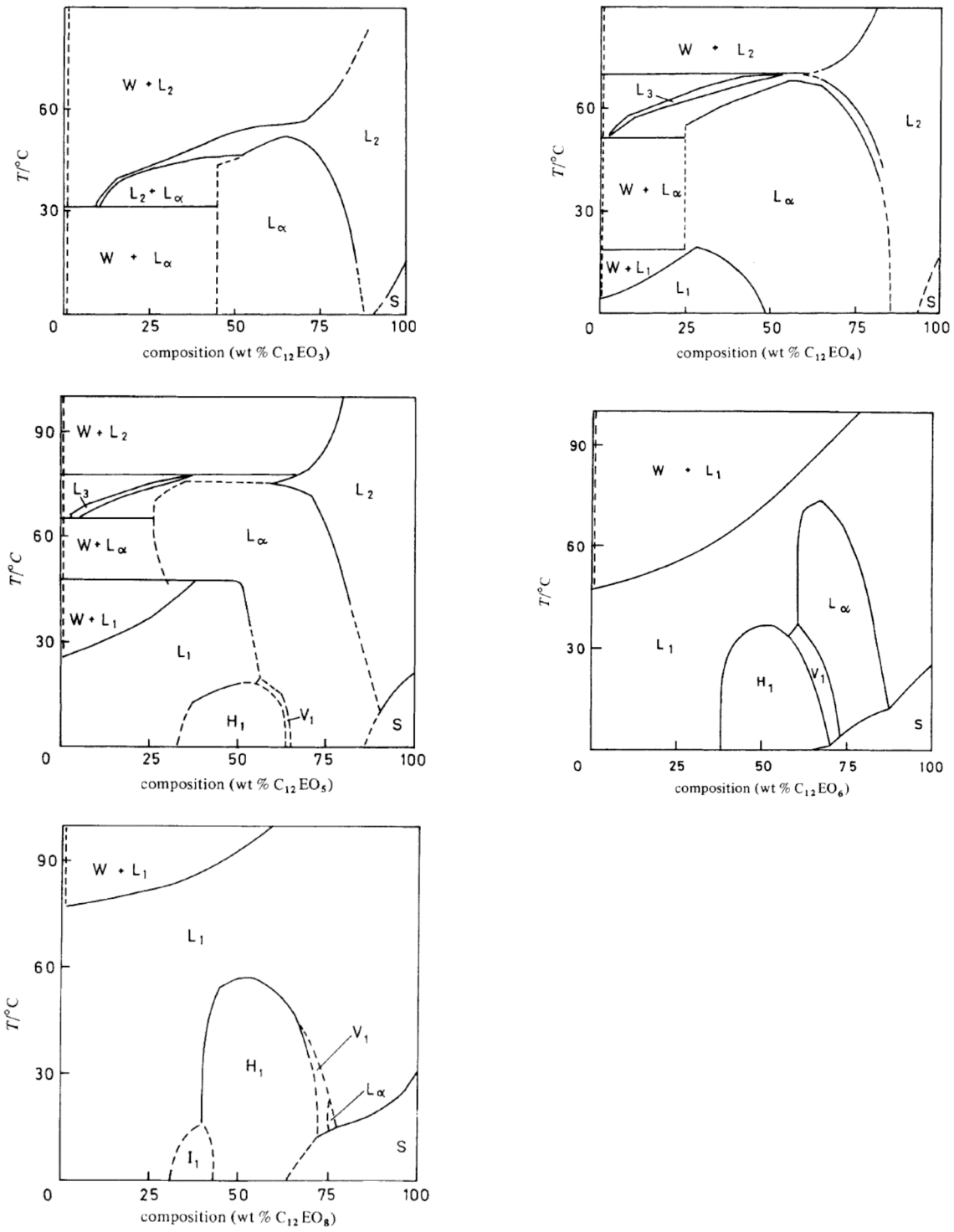

Figure 3.1 : Phase diagrams $C_{12}E_3$, $C_{12}E_4$, $C_{12}E_5$, $C_{12}E_6$, and $C_{12}E_8$

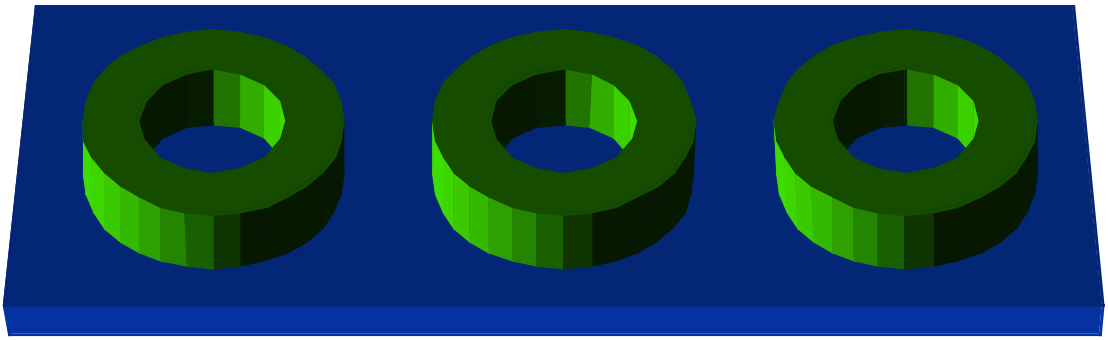

Figure 3.2: Sample cell for cross-polarized microscopy

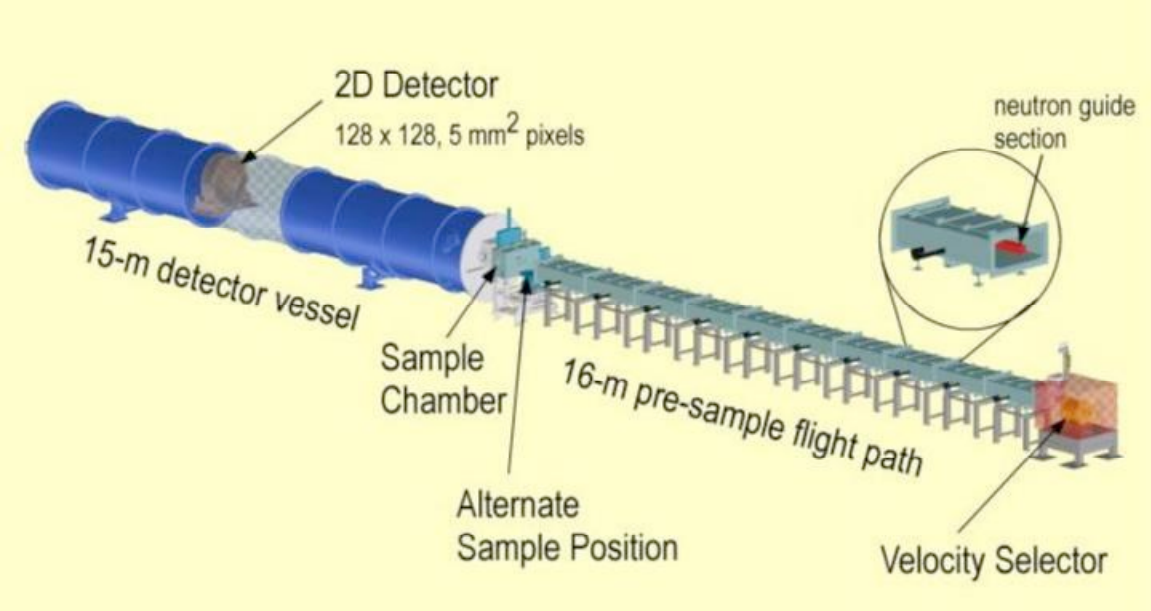

Figure 3.3: The 30-meter long Small-Angle Neutron Scattering (SANS) instrument on neutron guide NG7 at the National Center for Neutron Research at NIST.

- We acknowledge the support of the National Institute of Standards and Technology, U.S. Department of Commerce, in providing the neutron research facilities used in this work.

Figure 3.4: Demountable SANS cell used for to hold sample for SANS analysis. (reference: http://www.ncnr.nist.gov/programs/sans/equipment/dem_cell.html)

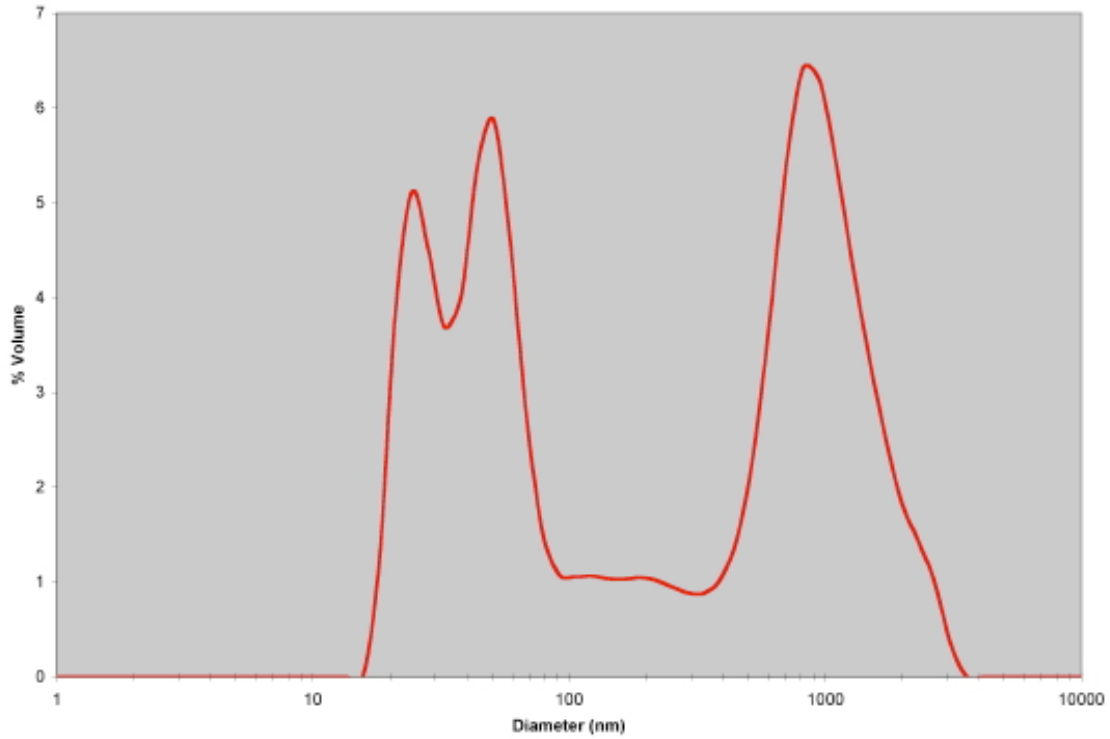

Figure 3.5: $C_{12}E_3$ particle size analysis.

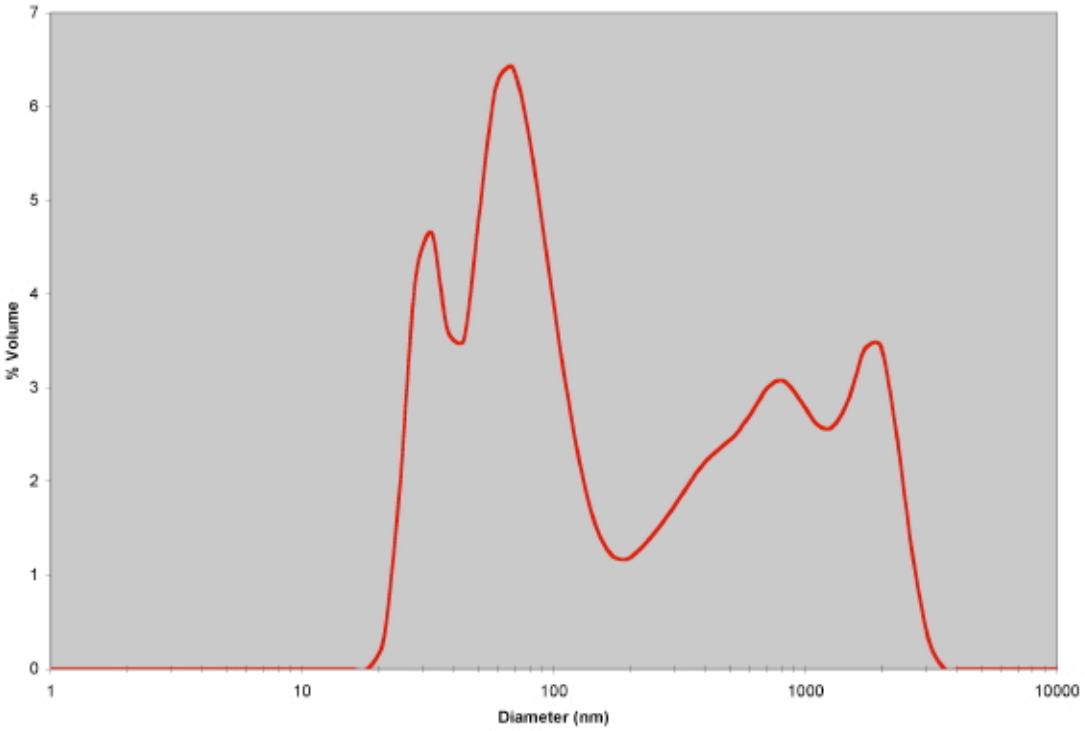

Figure 3.6: $C_{12}E_4$ particle size analysis

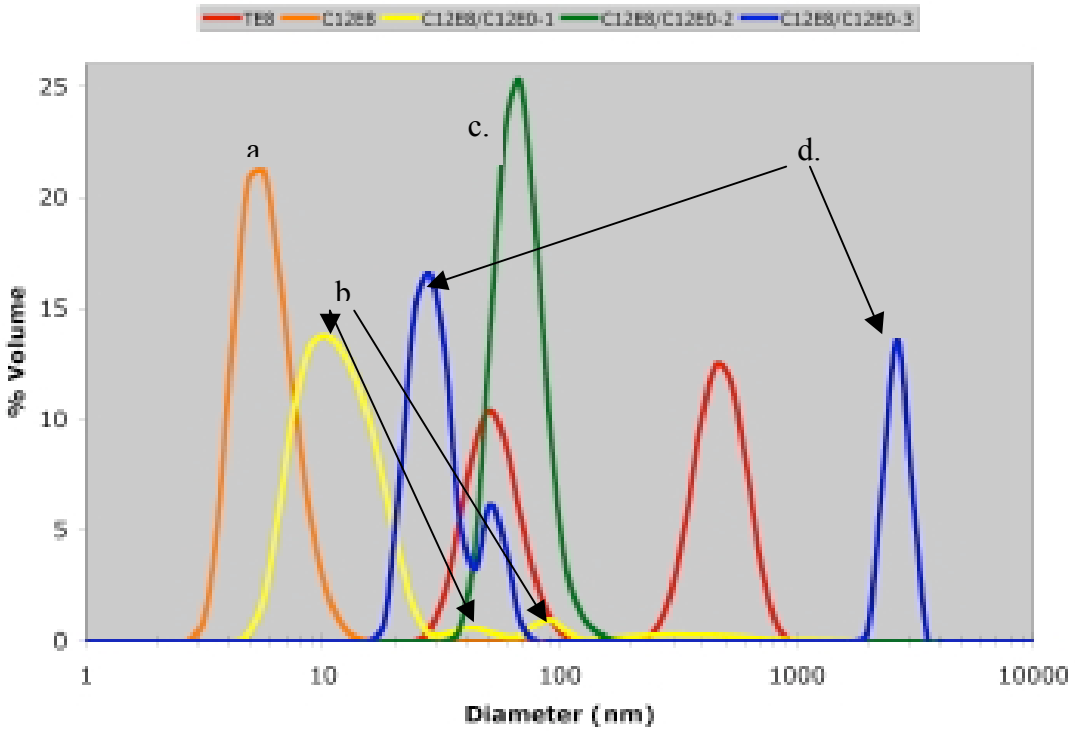

Figure 3.7: Particle size analysis of mixtures of $C_{12}E_8$ with $C_{12}E_0$ in water. a) $C_{12}E_8$ at 0.7 mM CAC b) $C_{12}E_8$ at 0.7 mM with $C_{12}E_0$ at 0.37 mM c) $C_{12}E_8$ at 0.7 mM with $C_{12}E_0$ at 2.5 mM d)) $C_{12}E_8$ at 1.4 mM with $C_{12}E_0$ at 5 mM

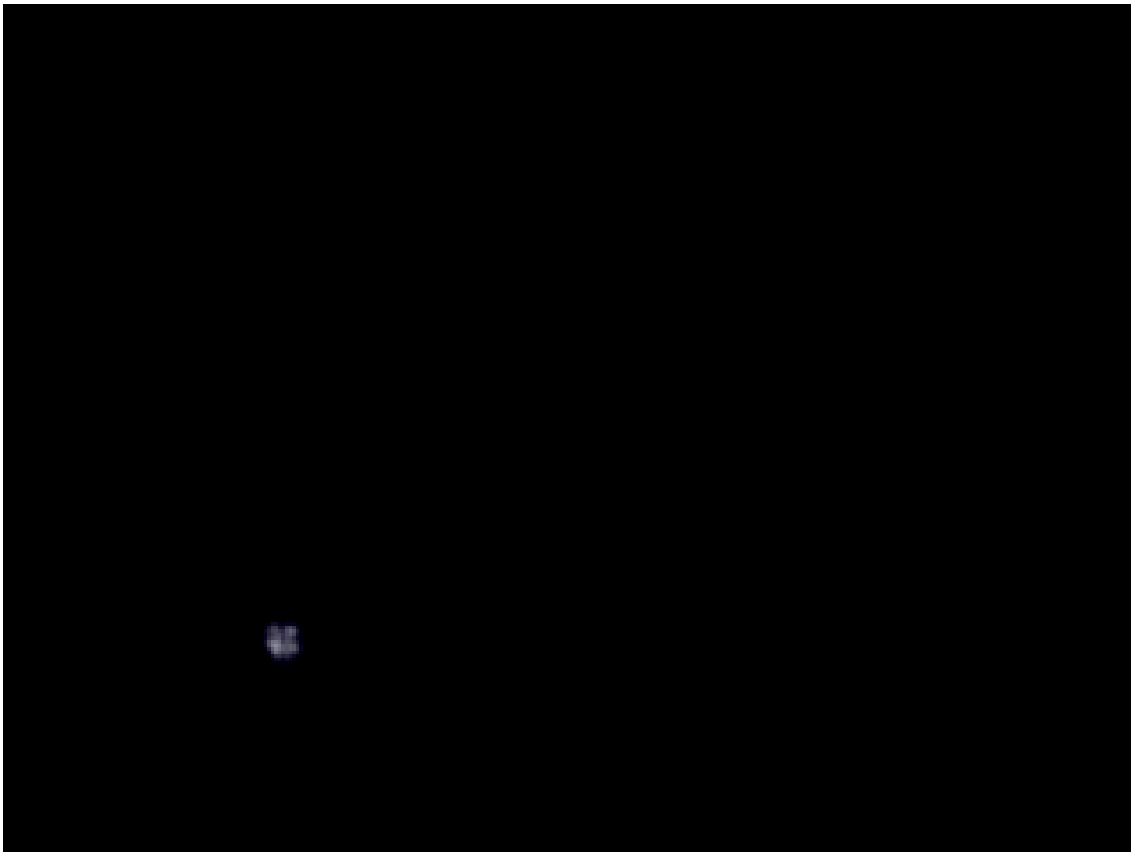

Figure 3.8: Cross-polarized microscopy image of 1.4 mM $C_{12}E_8$/5 mM $C_{12}E_0$ mixture. The cloverleaf pattern in the lower left hand corner is the characteristic extinction pattern of L_α structures of surfactants.

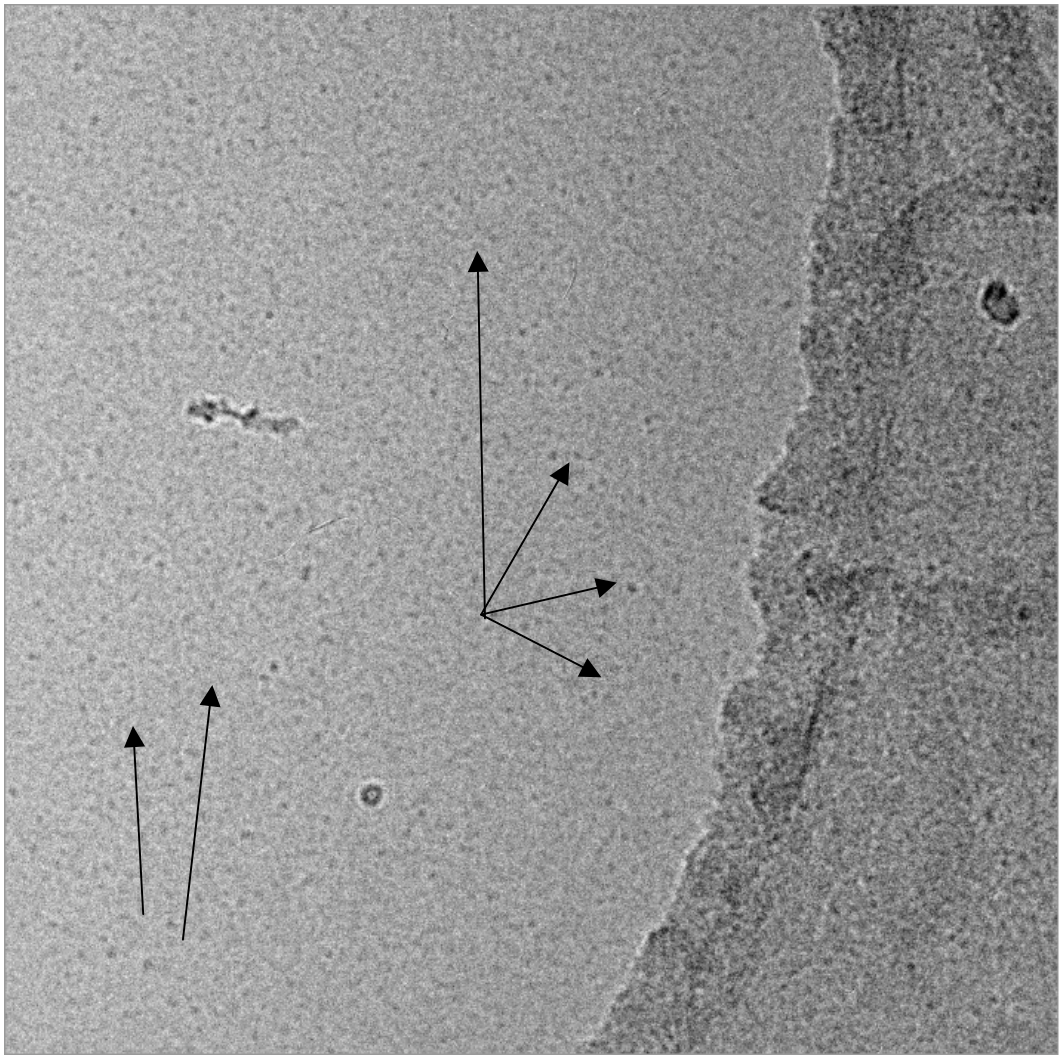

Figure 3.9: CryoTEM image of 0.7 mM $C_{12}E_8$ solution. The arrows indicate the spherical micelles. The right side of the image shows the edge of the grid hole in which the surfactant solution is frozen. Capturing the grid hole's edge in the image increases the overall image contrast allowing, allowing imaging of the micelles which would otherwise be difficult to see.

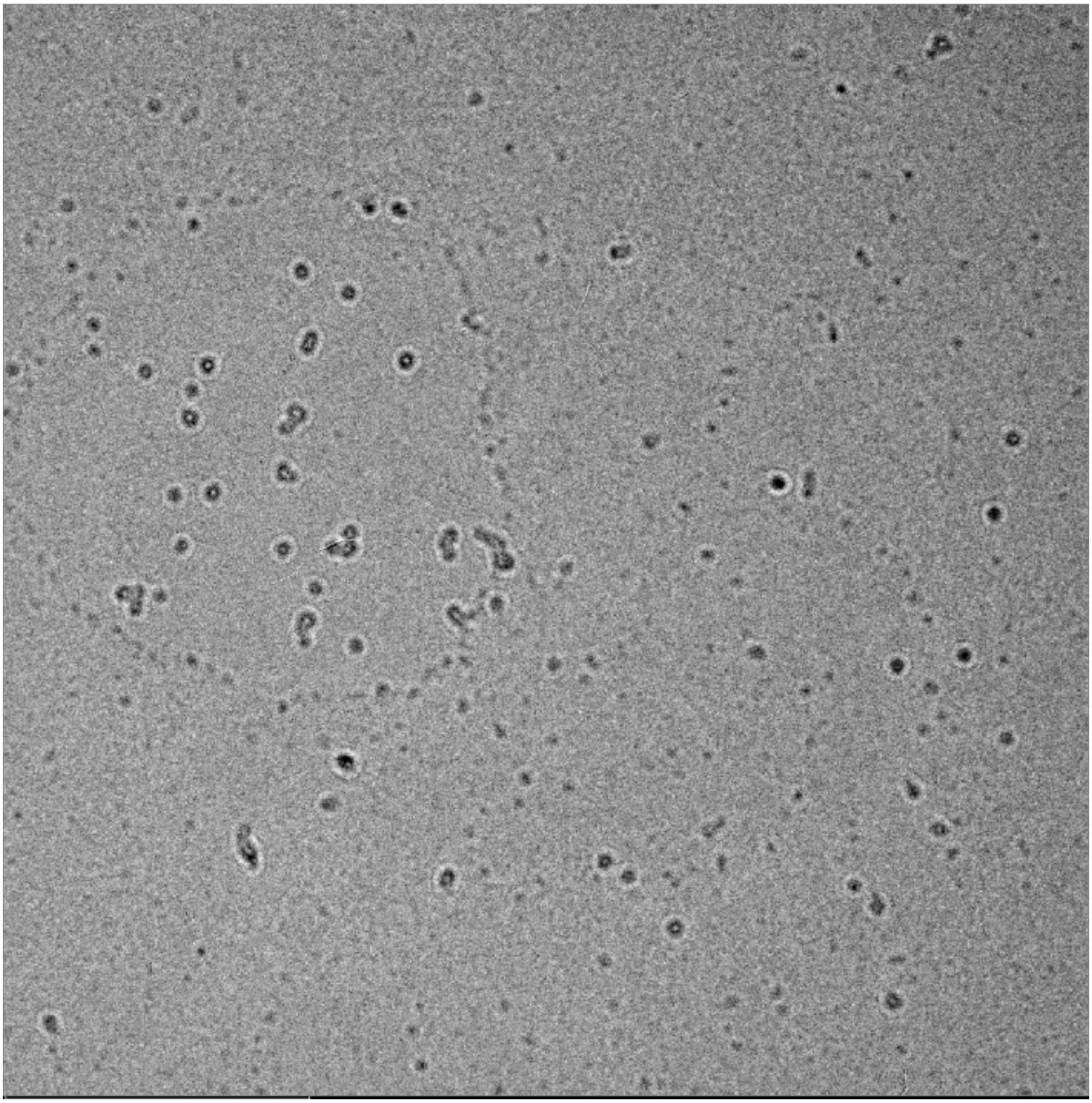

Figure 3.10: A cryo-TEM image 0.7-mM $C_{12}E_8$/2.5mM $C_{12}E_0$ surfactant mixture. The aggregate structures appear to be single walled vesicles as evidenced by the core having the same contrast as the surrounding area (vitreous ice) and the dark ring, which is the hydrocarbon core of the vesicle.

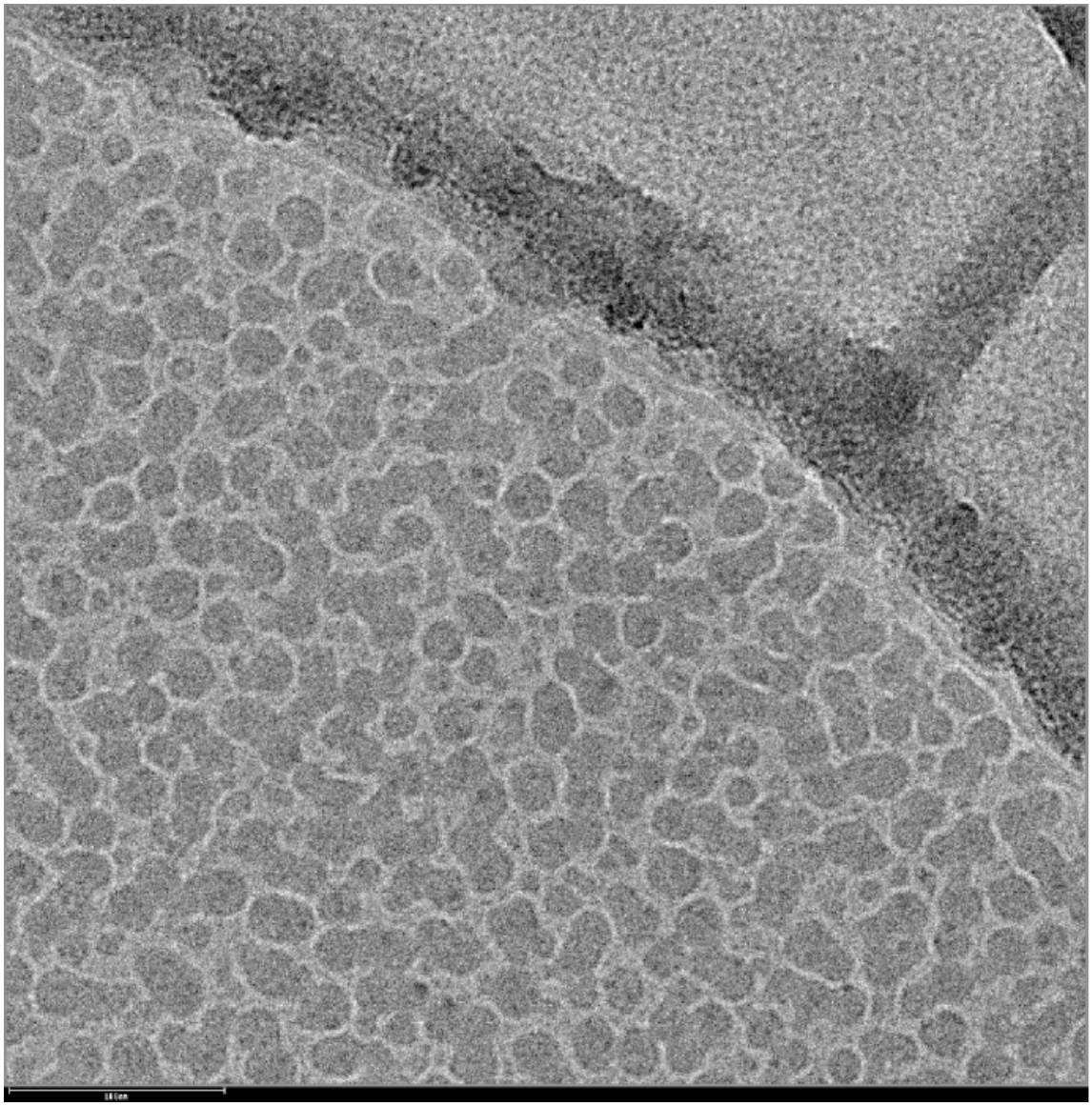

Figure 3.11: A $C_{14}E_8/C_{12}E_0$ mixture where primary structures on the order of 100 nm are present, but coexist with much smaller structures on the order of the size of a micelle. Also, the surface of the primary structures appears to be speckled of smaller scattering structures, which may be indicative of the formation of sponge-like structure in the bulk.

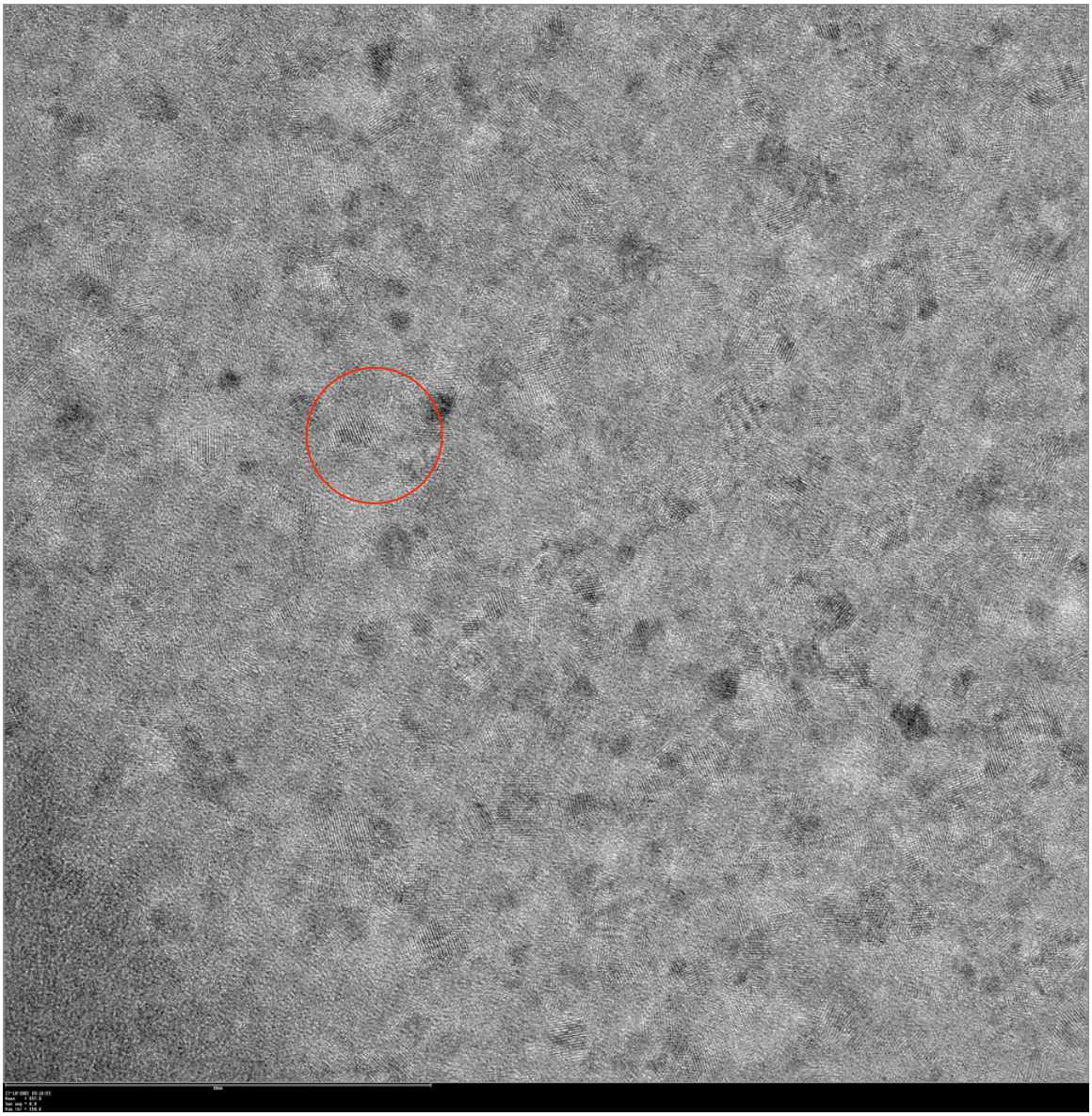

Figure 3.12: Cryo-TEM image of a 0.7-mM $C_{12}E_8$/2.5mM $C_{12}E_0$ surfactant mixture showing of inter-aggregate structuring in the system. Shows clearly the repeating ordered structure in the bulk aggregate formation.

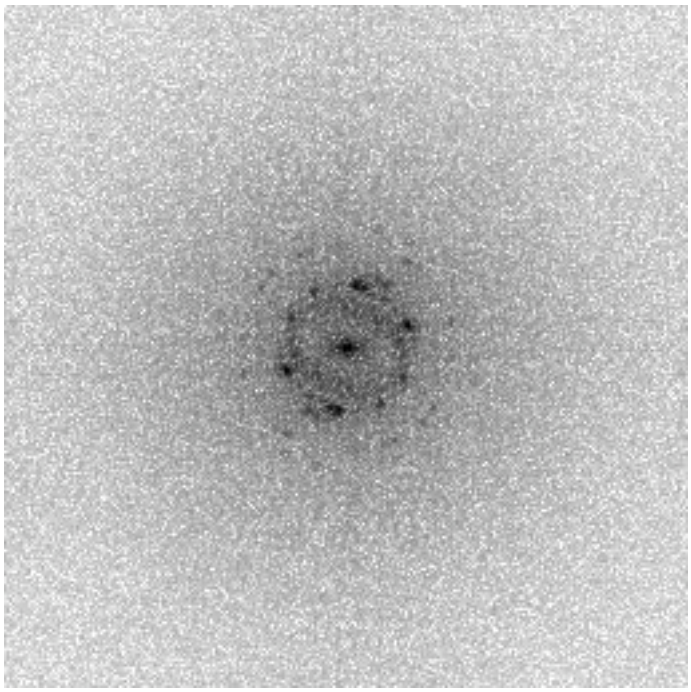

Figure 3.13: Fourier transform of circled region in Figure 3.12

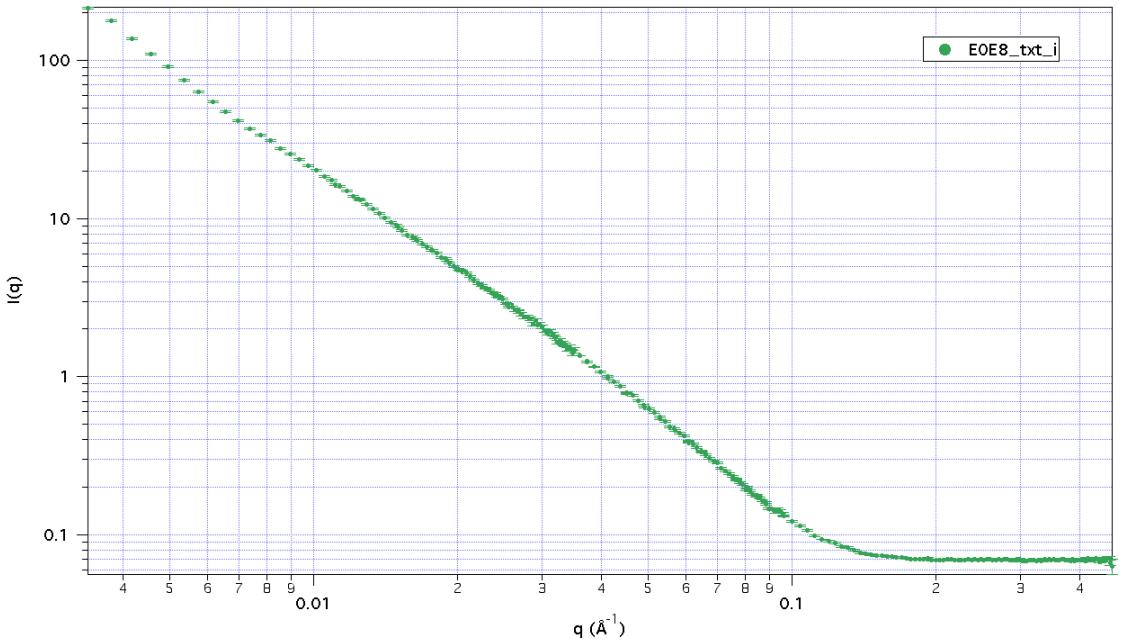

Figure 3.14: I(q) versus q diagram for $C_{12}E_0/C_{12}E_8$

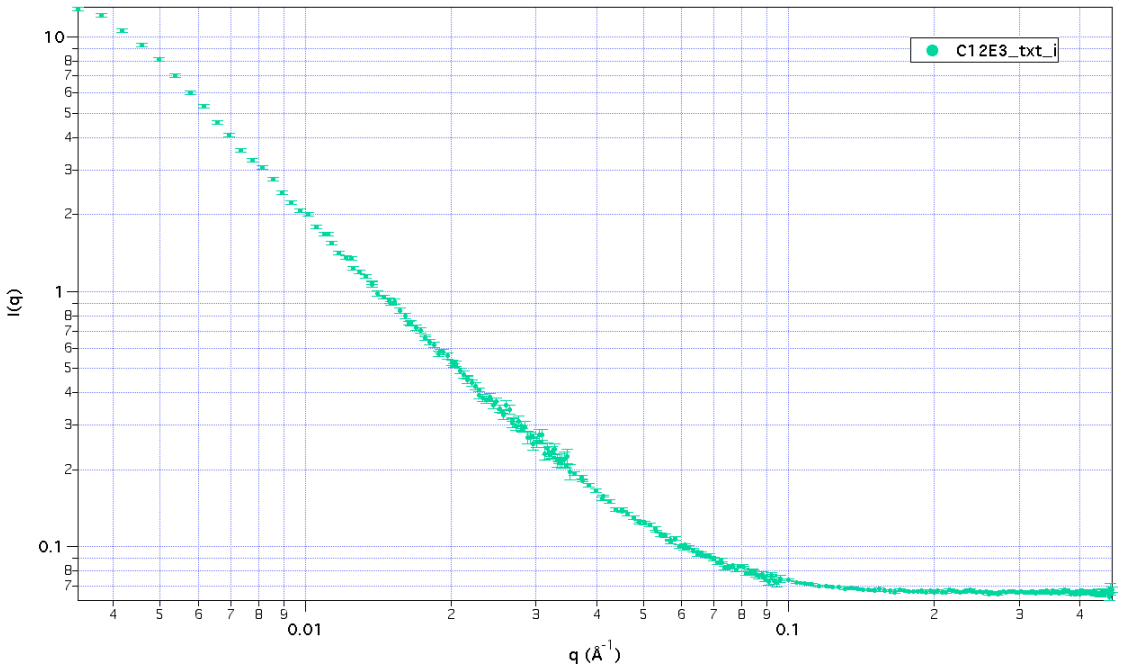

Figure 3.15: I(q) versus q diagram for $C_{12}E_3$

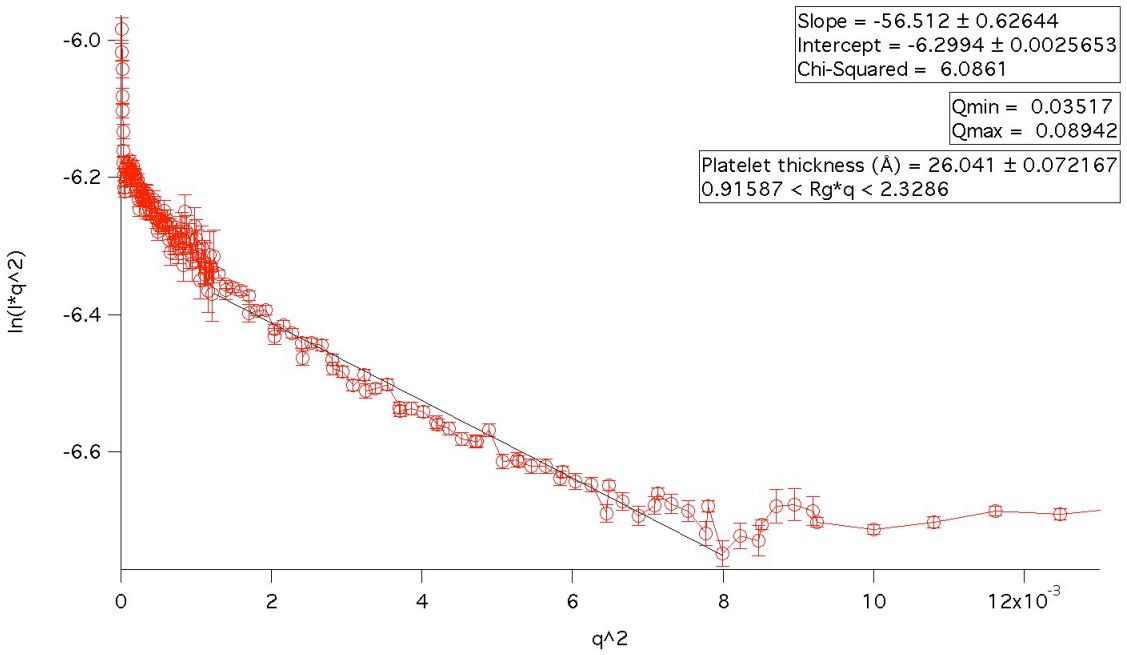

Figure 3.16: Kratky-Porod plot of 0.7 mM $C_{12}E_8$ and 2.5 mM $C_{12}E_0$ in D_2O analyzed in 30-m SANS beam line.

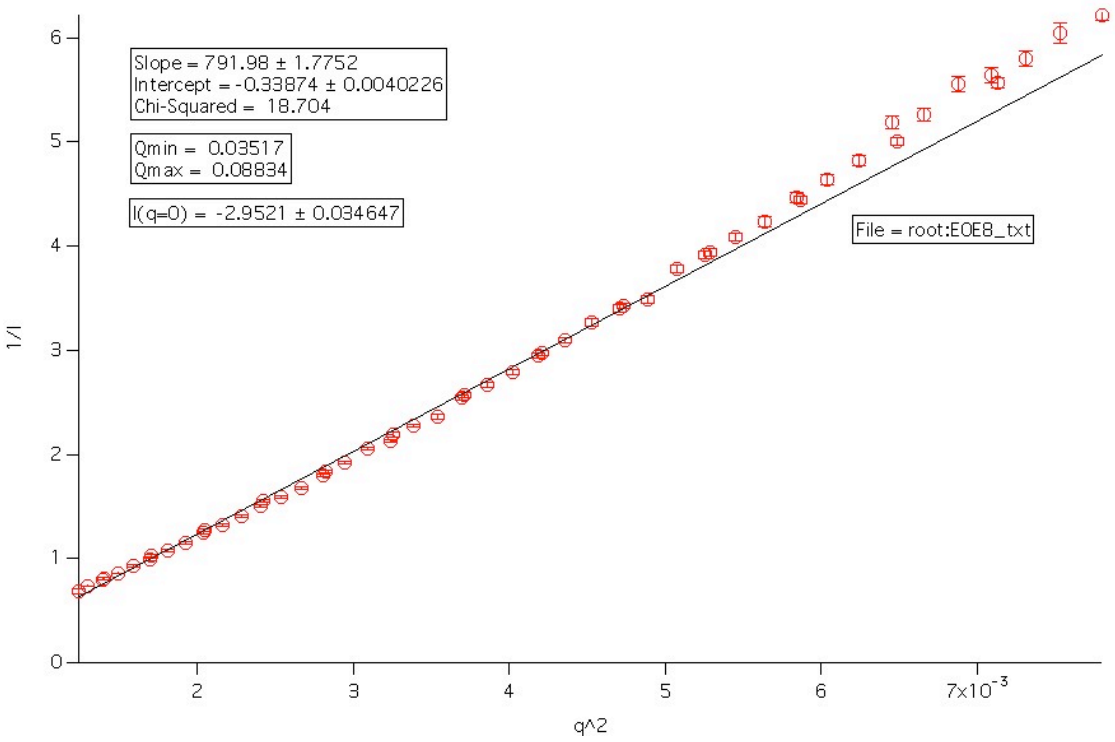

Figure 3.17: Partial Zimm plot of 0.7 mM $C_{12}E_8$ and 2.5 mM $C_{12}E_0$ in D_2O analyzed in 30-m SANS beam line.

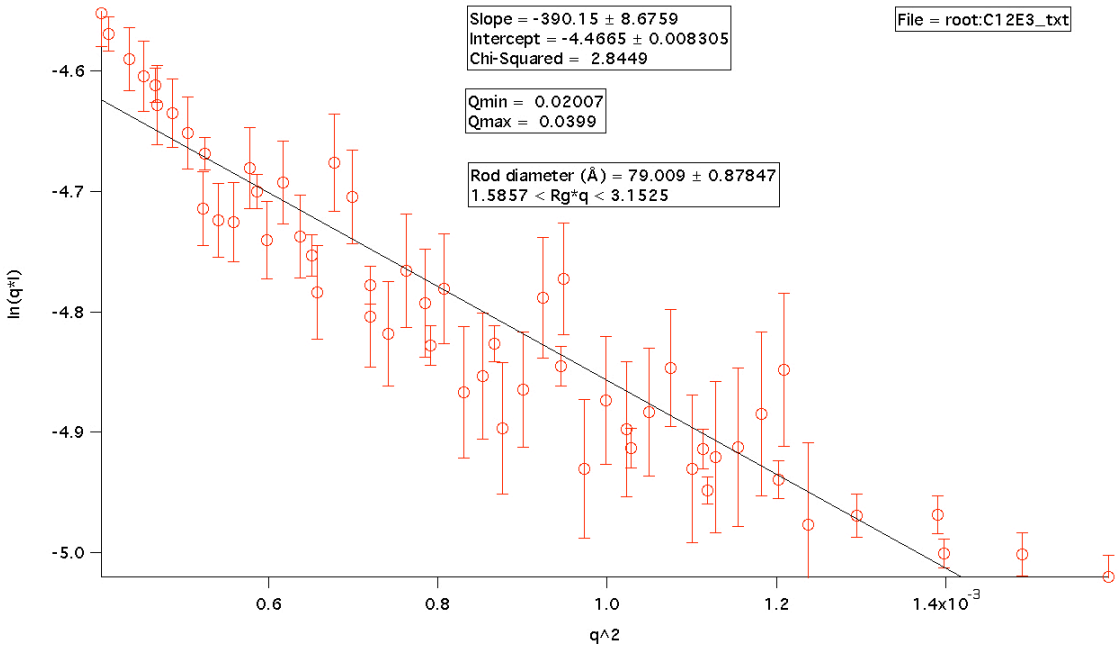

Figure 3.18: Slope of the Guinier region of the $C_{12}E_3$ system

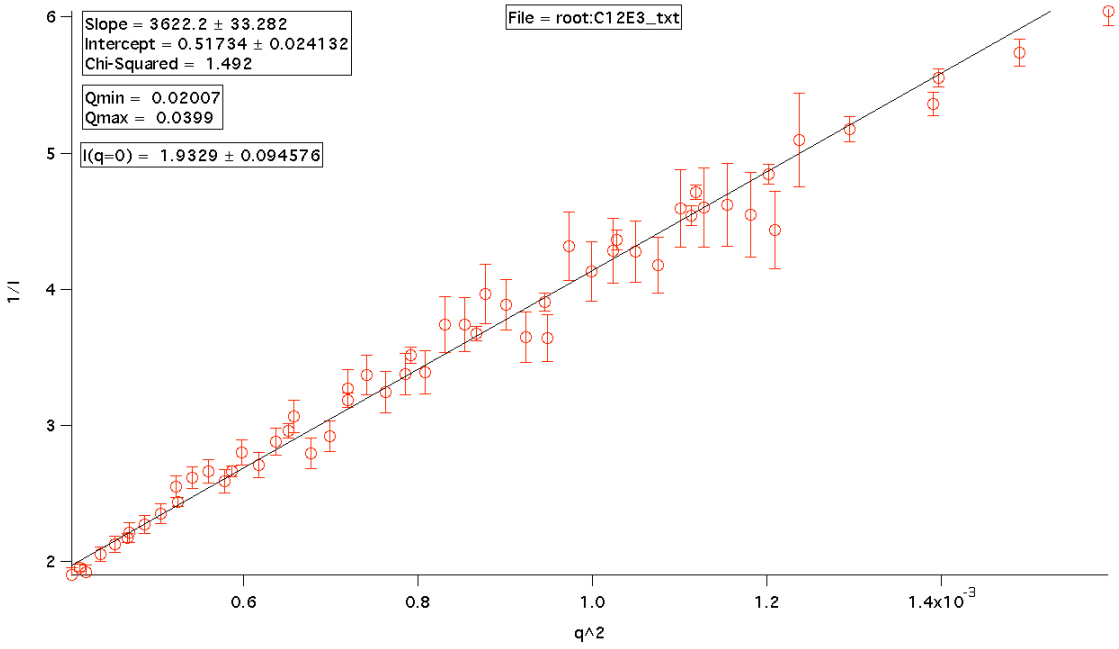

Figure 3.19: Partial Zimm plot of $C_{12}E_3$

REFERENCES

1. Israelachvili, J., *Intermolecular and Surface Forces*. Second ed. 1991, San Diego, CA: Academic Press Limited. 450.

2. Mitchell, D.J., et al., *Phase behaviour of polyoxyethylene surfactants with water.* J. Chem. Soc. Faraday Transactions, 1983. **79**: p. 975 - 1000.

3. Rosen, M.J., *Surfactants and Interfacial Phenomena*. 2nd ed. 1989, New York: Wiley-Interscience.

4. Schick, M.J., *Nonionic Surfactants*. Surfactant Scienc Series. Vol. 23. 1987, New York: Marcel Dekker, Inc. 1135.

5. Laughlin, R.G., *The Aqueous Phase Behavior of Surfactants*. 1994, Cincinatti: Academic Press - Harcourt Brace & Company. 558.

6. Jahns, E. and H. Finkelmann, *Lyotropic liquid crystalline phase behavior of a polymeric amphiphile polymerized via their hydrophilic ends.* Colloid & Polymer Science, 1987. **265**(4): p. 304-311.

7. Ning, H., S. Wiegand, and R. Kita, *Soret Effect in a Nonionic Surfactant System*, in *Smart Colloidal Materials*. 2006. p. 111-115.

8. Penders, M.H.G.M. and R. Strey, *Lamellar and L3 phases in the simple H20-C8E5-1-Octanol system: Evidence of Synergism.* Journal of Physical Chemistry, 1995. **99**: p. 6091 - 6095.

9. Strey, R. and R. Schomaker, *Dilute lamellar and L3 phases in the binary water-C12E5 system.* J. Chem. Soc. Faraday Transactions, 1990. **86**(12): p. 2253 - 2261.

10. Myrick, S.H. and E.I. Franses, *Effect of dispersed tetradecanol particles or droplets on the synamic surface tension of aqueous tetradecanol systems.* Langmuir, 1999. **15**: p. 1556 - 1561.

11. Jonstromer, M. and R. Strey, *Nonionic bilayers in dilute solutions: Effect of Additives.* Journal of Physical Chemistry, 1992. **96**: p. 5993 - 6000.

12. He, M., et al., *Phase-Behavior and Microstructure of Polyoxyethylene Trisiloxane Surfactants in Aqueous-Solution.* Journal of Physical Chemistry, 1993. **97**(34): p. 8820-8834.

13. Matsumoto, T. and H. Zenkoh, *Micelle structure in isotropic aqueous colloids of a poly(oxyethylene) amphiphile C12E8.* Colloid & Polymer Science, 1990. **268**(6): p. 536-543.

14. Tanford, C., Y. Nozeki, and M.F. Rohde, *Size and Shape of Globular Micelies Formed In Aqueous Solution by n-Alkyl Polyoxyethylene Ether.* The Journal of Physlcal Chemistry, 1977. **81**(16): p. 1555.

15. Trlolo, R., et al., *Small-Angle Neutron Scattering from Aqueous Mlcellar Solutions of a Nonionic Surfactant as a Function of Temperature.* The Journal of Physlcal Chemistry, 1982. **86**(19).

16. Nllsson, P.-G., H. Wennerstrom, and B. Llndman, *Structure of Micellar Solutions of Nonionic Surfactants. Nuclear Magnetic Resonance Self-Diffusion and Proton Relaxation Studies of Poly(ethy1ene oxide) Alkyl Ethers.* The Journal of Physlcal Chemistry, 1983. **87**(8).

17. Danino, D., Y. Talmon, and R. Zana, *Aggregation and Microstructure in Aqueous Solutions of the Nonionic Surfactant C12E8.* Journal of Colloid and Interface Science, 1997. **186**: p. 170.

CHAPTER 4

SYNERGISTIC AIR-INTERFACIAL TENSION REDUCTION INITIATED BY ENHANCED LIQUID CRYSTALLINE PHASE BEHAVIOR IN SURFACTANT MIXTURES

4.1 INTRODUCTION

A large number of studies have been reported that examine the air-liquid interfacial behavior of water with and without surfactant present. The structure of neat water at the air-water interface has been studied extensively using vibrational sum frequency generation spectroscopy (SFG). SFG is well suited for the study of interfaces because interfaces are generally asymmetric structures. Since SFG is a second-order process, it is not sensitive to molecular structures that possess inversion symmetry, under the dipole approximation[43,44]. In investigations of the structure of hydrogen bonding at the surface of water, performed originally by Shen et al[45,46] and then Gragson et al[47,48], it was determined that water at the neat interface does not have the same structure as water in the bulk. In general, a water molecule in the bulk is tetrahedrally hydrogen bonded to its neighboring water molecules. However, at the air-liquid interface only one of the hydrogens on the water molecules are hydrogen bonded to another water molecule. The SFG spectrum of water shows three different peaks centered at approximately 3700, 3400 and 3200 cm^{-1}. The peak at 3700 cm^{-1} is attributed to an OH stretch in which one

hydrogen atom of a water molecule is not hydrogen bonding with a water molecule (dangling OH), while the other one is bonded. The stretch of this dangling OH is energetically decoupled from the stretch of the adjoining hydrogen bonded OH bond. The appearance of the 3700 cm^{-1} peak in a spectrum indicates the presence of water molecules that straddle an interface between an aqueous phase and a non-hydrogen bonding phase such as air, a nonpolar liquid or a hydrophobic solid. The peak at 3200 cm^{-1} is assigned to the in-phase vibrations of the coupled OH symmetric stretching mode associated with high hydrogen bonding order where the water molecules are tetrahedrally coordinated, as in ice. The assignment of the peak at 3400 cm^{-1} has not been completely elucidated. There are some studies that assign this peak to the symmetric stretching of a water molecule that is asymmetrically hydrogen bonded (molecules with one H strongly hydrogen bonded while the other H weakly bonded to neighboring molecules) while others associate the peak with water molecules with bifurcating hydrogen bonds. Regardless of the exact description for the peak, it is the only one that is rendered in the FTIR spectrum of liquid water. Consequently, its appearance in an interfacial spectrum is indicative of "liquid-like" water molecules involved in an intermediate level of hydrogen bonding.

It has been shown that at least 20% [45] and up to 40% [47] of the surface molecules have one free –OH projecting into the vapor while the other is hydrogen bonded in the bulk. The presence of the pendant –OH groups multiplies the number of states[49] available to the water molecules at the interface, consequently increasing the entropy of the interface

relative to the bulk water. Ideally, we want to rid the interface of the pendant –OH group so that the surface energy can be lowered. In order to reduce the interfacial tension of water, an interface must be created that promotes the hydrogen bonding between water molecules and at the same time lowers the energy of the interface. Surfactants are the generally accepted means of achieving this reduction in tension.

A surfactant[26] is any molecule that has chimerical character in that one part of the molecule is hydrophobic while the remaining portion of the molecule is hydrophilic. A surfactant can be anionic, cationic, Zwitterionc, or nonionic. As the name suggest, an anionic surfactant is negatively charged while a cationic surfactant is positively charged. In both cases there is a complementary ion that is carried with the surfactant to help stabilize it when it is not in solution. For example, sodium dodecylsulfate is an anionic surfactant where sodium is the complementary ion and dodecylsulfate is the active part of the molecule, which is negatively charged. A Zwitterionic surfactant is electrically neutral and can therefore be classified as a nonionic surfactant, but what differentiates it from a true nonionic surfactant is that it contains formally charged substituent groups. This research will deal solely with true nonionic surfactants that contain no formal charge in any part of the molecule. In aqueous solution, surfactant molecules at concentrations below the critical micelle concentration (CMC) prefer to be at the air-aqueous interface with the hydrophobic portion of the molecule in the air while the hydrophilic moiety remains in the water. The hydrophilic portion of the surfactants that we are using are

capable of hydrogen bonding and as a result are capable of relieving the stress of pure water's interface.

The adsorption of surfactant from an aqueous phase onto an air/aqueous and aqueous/hydrophobic solid interface are a function of several factors[50], among them: (i) the affinity of the adsorbing surfactant to the aqueous phase (as measured for example by its solubility or critical aggregate or micelle concentration, CAC); the less the affinity the greater the adsorption; (ii) the energies of interaction of the adsorbing surfactant molecule with the water molecules in the vicinity of the surface, and (for the solid surface) the interaction of the surfactant with the solid surface molecules; and (iii) interactions between the adsorbing surfactant and surfactant already adsorbed at the surface. In the case of the C_iE_j surfactants, the affinity of the water phase is directly related to the ratio between the lengths of the hydrophobic alkyl moiety and the oligometric oxyethylene headgroup.

When surfactant is dissolved or dispersed in water and an interface is created with air, the surfactant will adsorb at the interface so that the hydrophobic tails are in the air while the headgroup stays in the water. The surfactant will continue to adsorb at the interface until energetic equilibrium is reached with the bulk. There is a phase behavior associated with surfactant adsorption at the air-liquid interface that is strongly dependent on temperature and surfactant geometry. For the surfactant systems used, temperature will remain constant so the effect of temperature will not come into play. However the geometries of

the surfactants used in this case are of different lengths (geometry), which have an effect on the manner in which they choose to aggregate in aqueous solutions[25,26,51]. As we are dealing with both the adsorption of a sparingly soluble alcohol and soluble C_iE_j surfactants, the phase behavior for each at the interface must be treated separately. Generally, when the surfactant initially adsorbs at the interface, it is in a gaseous state where the surface coverage is very low[52]. As adsorption of the surfactant progresses, the density of the monolayer at the interface increases until maximum packing is achieved. The maximum packing density of the interface is determined by the geometry of the surfactant adsorbing; the shorter the E_j portion of the surfactant, the greater the coverage of the interface. Ideally, the surfactant would pack tightly enough to reach a condensed state at the interface as long as the bulk concentration is above the CMC of the single component or the mixture. In this state, the hydrocarbon chains are in an all trans configuration, maximizing the dispersive van der Waals interactions between the hydrocarbon chains. When this occurs, the lowest energy state of the system can he achieved because there is maximum separation of the water from the air. Water is then able to obtain its fully hydrogen bonded, ice-like structure, which, as discussed previously, is the lowest energy state for water.

The spreading of a dodecanol monolayer on the surface of water allows water to configure itself into an ice-like structure that is not seen in the alcohol free water system[52,53]. For the experiments that we have run, dodecanol was used as the alcohol. SFG has been used in the analysis of the phase transitions of dodecanol at the air-liquid

interface do demonstrate its packing density[54]. An all-trans hydrocarbon chain has local inversion symmetry; the methylene modes separate into an IR-active and Raman-active set and are therefore inactive in SFG. The weak methylene features near 2845 and 2880 - 2920 cm^{-1} arise from conformational defects still present in the solid phase. The most common chain defects in dense monolayers are kinks and end-gauche conformation. Kinks are locally centrosymmetric, and therefore SFG-inactive, and the CH_2 group α to the OH appears at higher frequencies. The methylene peaks therefore probably arise from gauche defects at the methyl terminus. The SFG spectra of the other alcohols below their phase transition temperatures are similar to dodecanol. Although there are defects in the monolayer, the packing density is still on the order of ~20$Å^2$/molecule which is on the order of the cross-sectional area of the hydrocarbon chain. Since the chains cannot be packed any tighter than this, we know that we are getting maximum coverage of the interface using dodecanol. The key to dodecanol's ability to pack tightly at the interface is the size of its hydrophilic moiety, the terminal –OH group whose effective radius is smaller than that of the hydrocarbon chain. From our results, it has been shown that dodecanol is able to reduce the air-aqueous interfacial tension of water to 28 mN/m.

The packing of the C_iE_j surfactants at the air-liquid interface is drastically different from that of dodecanol; the packing is less dense and consequently less ordered [55-57]. The size of the hydrophilic ethoxylate chain contributes directly to the ability for the C_iE_j surfactant to pack at the air-liquid interface. Over the range of j (j = 4-6, 8) used, as the number of ethoxylate groups increases, the polarity of the surfactant also increases. This

decreases the efficiency of the packing of the surfactants, so more is needed to achieve the same reduction in interfacial tension when all of the surfactants are below their respective CMCs. In the same range in sizes of E_j, as j increases, the density of coverage of the interface also decreases, leading to lower maximum surface tension reduction. The notion of conformational disorder of the ethoxylate chain has been confirmed by SFG. The weak peak at approximately 2845 cm^{-1} in the IR spectrum for dodecanol is extremely prominent in the spectrum for $C_{12}E_3$[55]. The size of this peak is proportional to the number of gauche defects in the surfactant monolayer. Ultimately, these results indicate that within the range of E_j being discussed, these surfactant are not as surface active as dodecanol and as a results cannot reduce the air-liquid interfacial of water as low as dodecanol. This assertion is confirmed in the experiments performed in our research.

Synergism in the context of surfactants is defined as any interaction that enhances the properties of both surfactants to a degree greater than would be possible for either of the individual surfactants[24]. In the case of this research, the synergisms that will be discussed correspond to enhanced surface tension reduction and attainable surfactant phases. The solutions created will contain a mixture of surfactants that should have favorable interactions both in the bulk and at the interface, but in order to gain a complete understanding of the system one must take into account the structures that form. The individual surfactants do not form separate surfactant phases, but instead they cooperate to form single phases with a new structure resulting in modified CMC that incorporates properties of both surfactants[16,17,24,58-62]. The nature of the new structures that form and

the manner in which the surfactant system adsorbs at the interface will be governed by chemical interactions between species and the geometry of the two species. It should be noted that the influencing factor are the same as those for the single component mixtures discussed earlier.

One well-studied example of binary surfactant interaction is that of dodecanol with sodium dodecylsulfate (SDS). In the synthesis of SDS, dodecanol is a byproduct of the reaction, which is extremely difficult to remove from the final product. The trace amounts of dodecanol that are left behind in the production batches of SDS have significant effect on the surface tension, viscosity and foam stability of aqueous solutions. In a different system studied by Casson and Bain[54] using SFG, dodecanol and the alkyltrimethylammonium bromides (C_nTAB: $CH_3(CH_2)_{n-1}N(CH_3)_3Br$ with n = 12, 14, and 16) were allowed to adsorb at the air-liquid interface to examine the phase transition of the mixed monolayer. It was determined that when the two surfactants were allowed to adsorb at the air-liquid interface, the mixed monolayer took a conformation that was similar to that of the pure dodecanol. This was in spite of the C_nTAB's lack of order at the interface when it was at 2/3 its CMC in aqueous solution. Also noteworthy is that the C_nTAB monolayer in inherently disordered due to electrostatic repulsion interactions between headgroups of individual molecules. However, the addition of dodecanol allows the formation of crystalline phases at the interface. These results offer evidence for the ability for the mixed surfactant systems to reach maximum packing at the air-liquid interface and eliminating this property as the sole reason for synergistic reductions in

interfacial tension.

Rosen et al.[17,58] has been able to predict which surfactant mixtures will have synergism in surface tension reduction by determining the interaction parameters (β) of the surfactant at the air-liquid interface (β^{σ}) and in the mixed micelle (β^{M}). The β parameters are related to the surfactants' activity coefficients in the mixture and the more negative the value of the β parameter, the greater the attractive interaction between the two surfactants compared to the reference states of the individual surfactants by themselves. He has determined that in order for synergism in surface tension to occur, $\beta^{\sigma} - \beta^{M} < 0$ and $|\beta^{\sigma} - \beta^{M}| > |\ln(C_1^{0,cmc}C_2^{M}/C_2^{0,cmc}C_1^{M})|$, where $C_1^{0,cmc}$ and $C_2^{0,cmc}$ are the molar concentrations of surfactants 1 and 2, respectively, required to yield a surface tension equal to that of any mixture of surfactants 1 and 2 at its CMC; C_1^{M} and C_2^{M} are the CMC values for the individual surfactants 1 and 2, respectively. The strength of the interaction between surfactants in a mixed monolayer depends on the nature of the surface and the molecular environment (i.e. temperature and ionic strength of the solution phase). This criterion for synergism has predicted favorable interactions between mixtures containing Zwitterionic[16] surfactants as well as the lack thereof in anionic-nonionic systems. Although, charges on the Zwitterionic molecule will have an effect on the interaction between the molecules and as a result he governing parameters, the underlying principles should also define the interactions in the purely nonionic system.

Penfold et al.[60] measured specifically the adsorption of binary C_iE_j surfactants at the air-

liquid interface. Specular neutron reflection, in conjunction with isotopic labeling schemes, was used to determine the structure of a $C_{12}E_3/C_{12}E_8$ mixed monolayer at the air-water interface. It was determined that the alkyl chains in the mixed monolayer are more extended when compared to monolayers of either of the pure surfactants. Also the experiments showed that the E_3 was more extended and less hydrated that in the pure $C_{12}E_3$ monolayer and the E_8 was less extended and more hydrated than in the pure $C_{12}E_8$ monolayer. Because the E_8 is less extended, there is some frustration in the packing of the two surfactants, but this does not translate to a disruption in packing density of the two surfactants at the interface. In order to examine alkyl chain mismatch, Penfold[61] and coworkers examined the mixed monolayer of $C_{10}E_6$ and $C_{14}E_6$. What they found was that the in order to maximize dispersive interactions, the C_{10} surfactant moved itself farther from the solvent meaning that there is overlap between the ethoxylate and hydrocarbon chains and that some of the ethoxylate groups are no longer in the water. Nothing is said directly about the effect on surface tension in either of these cases, but it can be surmised that for the same surface coverage, a mismatch in alkyl chain length cases a more severe change to the surface of a mixed monolayer when compared to a mismatch in the ethoxylate chain lengths. This theory will be examined in the experiments to be performed.

In this research work we have used dodecanol ($C_{12}E_0$) as the cosurfactant paired with other C_iE_j surfactants in varying combinations and concentrations to determine which systems give the greatest reductions in interfacial tensions. In order for these systems to

have viable use in application, they must be able to reduce the interfacial quickly. It has been previously found through dynamic interfacial[63] tension results that the interfacial tension of the individual systems drops most rapidly when they are well above their respective CMCs in aqueous solution. Consequently, high concentrations of the binary surfactant will also be used to insure the same rapid reduction in interfacial tension. Use of the $C_{12}E_j$, as initial components in the systems, gives a good starting point because the 12-carbon chain has the same hydrophobicity as the trisiloxane moiety[64] of the nonionic trisiloxane surfactants. This is important because it give us a target for the reductions in interfacial tension as well as wetting ability because some of the trisiloxane molecules that have been found to completely wet a hydrophobic surface have the same oligomeric headgroup as the C_iE_j surfactants.

4.2 EXPERIMENTAL

4.2.1 Methods

Pendant Bubble Tensiometry

Pendant bubble tensiometry was used to measure the equilibrium air-liquid interfacial tensions of the surfactant solutions presented here. Dynamic surface tension were also attempted, however the solutions tested did not readily lend themselves to such analysis as they reached equilibrium far too quickly for the measurements to be effectively rendered.

In the pendant bubble setup shown in figure 2.1, white light is directed through a pinhole, then a series of lenses that collimate the light. The now collimated light illuminates a cuvette that contains the solution whose tension is to be measured. The light continues past the cuvette, through a focusing lens (in our case a microscope objective) and then onto the CCD chip of a camera, where anything in the path of the light is imaged. Using a syringe pump, air is pushed through poly(tetrafluoroehtylene) (PTFE) tubing that terminates in the cuvette. The image captured by the camera is the silhouette of the air bubble that forms at the end of the tubing, know as the pendant bubble. A macro in ScionImage (derived form NIH Image) converts the perimeter of the pendant bubble into x-y coordinates, which a FORTRAN program then uses to calculate the interfacial

tension, the Bond number (Bo), the volume, and the center of the bubble. The bond number of the bubble is calculated using the formula $Bo = (\rho-\rho_f)gR_o/\sigma$, where g is the gravitational acceleration constant, ρ and ρ_f are the densities of the bulk fluid and the bubble fluid respectively, R_o is the radius of curvature of the bubble at its apex and σ is the air-liquid interfacial tension of the system. Bo is the balance between the gravitational forces on the bubble and the surface forces, which ultimately controls the shape of the bubble.

In order to compare the surface tension of different bubbles directly, it is important that all bubbles have the same shape. Water will be used to insure that the pendant bubble system is functioning correctly and give a value of 0.34 for Bo, consequently each bubble of all systems examined will have to have a similar value before it is considered qualified for measure. It should also be noticed that at a constant Bo, as the σ decreases, R_o will have to decrease as the square root of σ, hence as the tension decreases, the size of the bubble will have to also decrease to maintain the balance of forces. The change in size offers visual cues as to whether or not the tension of the system is being reduced. A parameterized version of the Young-Laplace equation is used to calculate the interfacial tension of the bubble[51,65].

The pendant bubble apparatus was calibrated so that a sphere of known dimensions had the same radius, in units of pixels, at several positions on the monitor on which the bubble image is displayed. The final calibration step for the apparatus was to measure

the interfacial tension of purified water, which at 20 °C has a value of 72.8 mN/m. It should be noted that the surface tension for water decreases 0.15 mN/m for each °C of increased temperature. In addition, each bubble had to have a white center (the remaining area of the bubble appears black in the image), a fact that was used to regulate the focal plane for measurement. The white center is caused by the light moving directly through the center of the bubble where it is apparently planar, in spite of the difference in refractive index between the two fluids.

Langmuir-Blodgett Trough

A Nima Technology mini Langmuir-Blodgett (L-B) trough fitted with a paper Wilhemy plate was modified and used to analyze the dynamic surface tension of single and mixed soluble surfactant monolayers at the air-water interface. The L-B trough consists of two motorized belt driven PTFE barriers that skim across the surface of the liquid that will serve as the subphase of the system that is contained by a PTFE trough, as shown in the series of images in Figure 2.2. Traditionally, the L-B trough is used for examine the adsorption and interfacial phase behavior of insoluble surfactant at the air-liquid interface. To do so, the surfactant to be examined is first dissolved in a volatile, subphase insoluble solvent such as chloroform, if water is used as the subphase. The surfactant is then deposited in the area between the two barriers (active area), as in Figure 2.2(A), by micro syringe on the air-liquid interface in small enough droplets that the solvent is allowed to spread at the interface, and then evaporate leaving behind the surfactant.

Although initially chosen to be dilute in what is called a gaseous state, the surfactant monolayer can be compressed between the barriers until it reaches a liquid-condensed (LC) or in some cases, a liquid-solid (LS) state at the interface as in Figure 2.2 (B). The data generated is referred to as the pressure-area (Π-A) isotherm and provides information about the packing and the phase behavior for insoluble surfactants at the air-liquid interface.

In the case of the soluble surfactants Gibbs monolayers are formed, which are structurally identical to Langmuir monolayer. The difference being that for Gibbs monolayers, Π-A curves cannot be effectively generated as increased pressure on the surfactant at the interface (increased chemical potential of the surfactant at the interface) because of equilibrium requirements causes the surfactant to redissolve into the subphase and then adsorb at the inactive area of the interface as shown in Figure 2.2 (C) and (D) where (C) represents a solution below the CMC and (D) a solution above the CMC. In spite of the inability to directly measure the P-A isotherm, the curve can however be generated using the Gibbs adsorption equation.

In our case, a circular PTFE trough with an interfacial area of 2874.76 mm^2 and a depth of 1 cm, is filled with water to create a clean air water interface to be measured using the Wilhemy plate for the L-B trough. The L-B trough was allowed to sit in a semi-closed chamber filled with water to prevent evaporation from the active interface. A concentrated solution of $C_{12}E_8$ is then injected in the subphase so that the final

concentration is solution is 1.4 mM; the volume of solution injected was in the 10^{-6} liter to avoid a large change in volume of the subphase. After equilibrium was reached and maintained, a supersaturated dispersion of $C_{12}E_0$ was injected into the subphase such that the overall $C_{12}E_0$ concentration was at 5 mM. A surface tension versus time plot was generated to examine the stability of the surface tension reduction.

4.3 RESULTS

4.3.1 Pendant Bubble Tensiometry

Using pendant bubble tensiometry, the air-liquid interfacial tension of the single surfactant solutions as well as those of the mixed surfactant solutions were measured and the results are shown on Tables 4.1 through 4.3. The measured tensions for, $C_{12}E_0$ (28.3 mN/m), $C_{12}E_4$ (28.2 mN/m), $C_{12}E_5$ (30.4 mN/m), $C_{12}E_6$ (31.6 mN/m), $C_{12}E_8$ (34.4 mN/m), $C_{10}E_8$ (35.2 mN/m) and $C_{14}E_8$ (35.4 mN/m), were all in excellent agreement with the published values[63,66-75]. The tension of water was also measured as a system check and on average gave a value of 72.4 mN/m when measured at 23 ºC. The concentrations of the surfactant were well above there respective critical micelle concentrations[76] except for $C_{12}E_0$ which was at its solubility limit in water, therefore the tensions reported are the lowest possible equilibrium tension for the respective systems at 23 °C. Based on these surface tension values, binary solutions were made in order to determine whether or not synergism was possible between the C_iE_j surfactants and $C_{12}E_0$.

As can be seen in table 4.2, for binary surfactant mixtures where the hydrocarbon chain lengths are matched at 12 carbons per surfactant tail while varying the ethoxylate length, the most significant tension reduction was observed in the $C_{12}E_8/C_{12}E_0$. In all cases, the C_iE_j surfactant was in solution at seven times their respective critical micelle concentrations. The CMC was used as the concentration measurement, as opposed to

absolute molar concentration, due the adsorption kinetics associated with the CMC for each surfactant, which will be discussed further in the next section. Dodecanol was added to each system in an initial aliquot of ten times its solubility limit (0.023 mM) in water. In the case of $C_{12}E_4$ and $C_{12}E_5$, no further dodecanol could be accommodated and the equilibrium air-liquid interracial tensions were 26.3 mM/m and 26.8 mN/m respectively. However, the initial aliquot for $C_{12}E_6$ and $C_{12}E_8$ gave tensions of 27.0 mN/m and 28.7 mN/m, respectively. The two surfactants were capable accommodating more dodecanol than the initial aliquot with a final concentration of 1.3 mM for $C_{12}E_6$ giving a surface tension of 22.3 mN/m and 2.5 mM for $C_{12}E_8$ giving a final surface tension of 22.0 mN/m.

To confirm assertions made by Penfold *et al*[60-62], solutions were made with $C_{10}E_8$ and $C_{14}E_8$, where the length of the alkyl chain of the C_iE_j mismatched that of dodecanol and was compared to the $C_{12}E_8/C_{12}E_0$ solution, because the ethoxylate unit number was matched. The first solution, $C_{14}E_8$ at 7 times its CMC and dodecanol at 10 times reached an equilibrium surface tension of 23.3 mN/m. The $C_{10}E_8/C_{12}E_0$, was mad in a manner different than all of the previous solutions. Instead of using $C_{10}E_8$ at seven times the CMC it was decided that instead of maintaining the CMC for each mixture, the molar concentration of the $C_{10}E_8$ was matched to that of $C_{12}E_8$. The reason being that the number of micelles that would be present in a 7 CMC $C_{10}E_8$ solution would be far greater than that of $C_{14}E_8$ and $C_{12}E_8$ by orders of magnitude. Sum frequency generation spectroscopy based dodecanol studies by Bain et al.[14] show that above the CMC

dodecanol is adsorbed into the micelle, which ahs been confirmed by phase behavior studies in the previous chapter of this thesis. With the number of micelles that are being formed by $C_{10}E_8$ relative to the concentration of $C_{12}E_0$, it is reasonable to believe that Bain's assertion would hold true in this case, thus there should be little to no reduction in the air-liquid interfacial tension. Instead, the $C_{10}E_8/C_{12}E_0$ solution had $C_{10}E_8$ in solution at 0.75 it CMC with $C_{12}E_0$ at ten times its solubility limit and obtained a equilibrium surface tension of 21.8 mN/m.

4.3.2 Langmuir-Blodgett Trough

To determine structure the of the molecules at the air-liquid interface when the surfactant is in the bulk at concentrations above their respective CMC., the surface tension of a clean water interface was measured to insure that it was devoid of surfactant. A known volume of water was removed, having the effect of reducing the air-liquid interfacial tension from 72.6 mN/m to zero as a result of the interface breaking contact with the Wilhemy plate as shown in Figure 4.3. The removed volume was replaced by injecting a concentrated $C_{12}E_8$ solution at several points below the clean interface to allow the surfactant to adsorb naturally to the clean interface and so that the final concentration in the entire volume (28.7 mL) was 0.7 mM (7CMC).

The graph in Figure 4.4 shows the effect of the addition of $C_{12}E_8$ to the subphase. For the first ~100 seconds the dynamics of the surfactant adsorbing at the interface can be

observed, however after that point the system reaches an equilibrium tension of 34.4 mN/m which was maintained for a little over 24 hours (Figure 5). A small volume of a supersaturated solution of $C_{12}E_0$ was injected as a single shot into the subphase of the $C_{12}E_8$ solution, such that the final concentration of $C_{12}E_0$ was 2.5 mM. Almost instantaneously, as shown by the step-function behavior with respect to time in Figure 4.6, the air-liquid interfacial tension drops from the 34.4 mN/m for the neat $C_{12}E_8$ to approximately 21 mN/m eventually settling at 21.6 mN/m. Over approximately 24 hours, the tension was maintained at an average of 21.3 mN/m as shown in the graph in Figure 4.6.

4.4 DISCUSSION

The initial concentration of 7 CMC, for most of the C_iE_j surfactants studied here, was chosen such that the micelle-free zone[77] at the air-liquid interface did not exist and would not appear as a result of loss of surfactant from the bulk due to adsorption. This choice eliminates the diffusion limit for surfactant adsorption leaving only the kinetic dependence, which is the faster of the two adsorption mechanisms. A study by Song et al.[77], studied the concentration dependent adsorption of $C_{14}E_6$ at the air-liquid interface and found that the micelle-free zone disappears at 4.75 CMC. The consequence of this is that the entire micelles adsorb the break up at the interface as opposed having the micelle break up and having monomer diffuse through the micelle–free zone to the air-liquid interface. The rate of adsorption, and consequently the rate of tension reduction, is potentially enhanced by the presence of dodecanol in the system.

In surfactant solutions with concentrations above their respectiveCMCs and at equilibrium at the air-liquid interface, it is well established that the surfactant will form a monolayer whose density is directly dependent on the molecular area of the molecule. A number of studies have determined that $C_{12}E_0$, $C_{12}E_4$, $C_{12}E_5$, $C_{12}E_6$, $C_{12}E_8$ have an molecular interfacial area of 20 $Å^2$, 38 $Å^2$, 49 $Å^2$, 54 $Å^2$, 65 $Å^2$, respectively[78,79]. As previously mentioned, the air-liquid interfacial tension is directly related to the interfacial area of the molecules at the air-liquid interface when the surfactant is in the bulk at concentrations above their respective CMC. This can be though of in terms of a monolayer's ability to segregate the air from the water. Bain et al. [80] and Penfold et al. [60-

[62] have studied the orientation of the surfactants at the interface and almost universally, in this class of surfactants studied here, as hydrophilic headgroup get larger the surfactants larger tilt angle relative to the surface normal. This has the effect of creating an oil and air layer at the interface; the denser the oily layer, the lower the air liquid interfacial tension. From these results, it is clear why $C_{12}E_0$ is most effective at lowering the air-liquid interfacial tension when compared within the homologous series. Also, of importance is the determination that the headgroup determines the interfacial area and as a result the equilibrium interfacial tension. When comparing the series E_8 series of surfactant chosen for this study, the molecular interfacial area of the $C_{10}E_8$, $C_{12}E_8$ and $C_{14}E_8$ are all 65Å^2, with air-liquid interfacial tensions of 35.3 mN/m, 34.4 mN/m and 35.2 mN/m, respectively; all within the same range of tensions.

The addition of $C_{12}E_0$ to the individual surfactant systems in al cases reduces that the air-liquid interfacial tension. However, in the case of $C_{12}E_4$, $C_{12}E_5$ and at the lowest concentration in $C_{12}E_8$, the reduction only brings the tension down to what $C_{12}E_0$ is capable of achieving on its own. The desired synergism is apparent in the $C_{12}E_6$, the high concentration $C_{12}E_8$, $C_{10}E_8$ and $C_{14}E_8$ systems, where the reported air-liquid interfacial tension were far below the values that either surfactant in the mixture are capable of achieving themselves.

The data obtained here, as well as spectroscopic studies of surfactant laden interfaces, the achieved synergism can attributed to the interfacial structure of the mononlayer at the

water side of the air-liquid interface and the bulk intermolecular structure achieved by the surfactant, as discussed in the previous chapter. Looking at the schematic in Figure 4.7, it is reasonable assume that the air side of the interface cannot achieve a packing density greater that $C_{12}E_0$, as the molecular interfacial area of 20 $Å^2$ is approximately the cross sectional area of the of the all-trans hydrocarbon chain. Given this fact, the synergistic reduction in air-liquid interfacial tension observed must be caused by the replacement of some of the $C_{12}E_0$ molecules by C_iE_j molecules. Techniques to directly analyze the water-side of the air-liquid interface are not readily available, however indirect analysis is possible by isotopically labeling the hydrocarbon on the C_iE_j to determine it quantity in the adsorbed monolayer. Although possible, this experiment was outside of the scope of this study.

Our work clearly suggests that it is not enough that the two surfactant exist in the solution, It appears that not only must the $C_{12}E_0$ be in the mixture as the major component, but, in the case where the hydrocarbon chain lengths are matched, dodecanol must exist at a molar concentration of at least three times that of the C_iE_j concentration. In addition, lamellar surfactant phases must exist in the mixture as well. The liquid-crystalline structure observed in the cryo-TEM image of the $C_{12}E_0/C_{12}E_8$ system in Figure 4.8, shows that the structures are directly adsorbing at the interface to supply said interface with surfactant. A consequence of the technique required to effectively analyze a cryo-TEM sample it that a fresh air-liquid interface is created and the ultimately frozen in that state. The time between creation of the interface and cryogenically freezing the

sample is on the order of tenths of a second, and to the naked eye appears instantaneous. The image in Figure 4.8 appear to have captured the surfactant structures in mid adsorption, where the area in the image with the higher population of intact structures is in the "lighter" field (indicated by the letter A), as opposed to the structure free area (as indicated by the letter B). Examination of the darker region in Figure 4.8 by electron diffraction, produces the image in Figure 4.10. Theoretically, cubic ice (which can form during the cryoTEM sample vitrification process) has a lattice spacing of 0.366 nm for the (111) face and 0.224 nm for the (220) face. The rings in the diffraction pattern are at 0.370 nm 0.214 nm, which is reasonable agreement with the theoretical values. The diffuse ring inside the 0.370 nm ring is representative of the hexagonal lattice spacing of hydrocarbon chains of the C_{12} moieties adsorbed at the air liquid interface. The diffraction rings are diffuse, indicating that the adsorption lack long-range order, similar to the aggregate structures discussed in the previous chapter, but there is ordering there. This observation leads on to believe the bulk aggregate structure predetermines the binary surfactant arrangement necessary for synergistic air-liquid interfacial tension reduction.

This behavior is also confirmed by assertions made by Song et al, that whole surfactant aggregate adsorb at the interface as opposed to the structures first breaking up in the sublayer then supplying the interface with individual molecules. If the second adsorption mechanism were true, the dynamics of the adsorption would be drastically different and one could reasonable assume that this mechanism could lead to adsorption patterns that resemble the systems that do not show synergism. The $C_{12}E_0/C_{14}E_8$ (Figure 4.9) and the

$C_{12}E_0/C_{12}E_6$ system showed similar structural behavior in the bulk, and thus can be reasonably linked to the observed synergism seen in the air-liquid interfacial tension reduction in spite not being able to capture the structures while adsorbing.

The synergism that exists in the $C_{10}E_8/C_{12}E_0$ system is interesting because unlike the other systems that had the C_iE_j surfactant in the system at multiples of their CMC, $C_{10}E_8$ was only in the solution at 0.75 CMC, but was able to significantly reduce the air-liquid interfacial tension. Given that the individual surfactants are not forming micelles in the solution, if micelles do exist in this system, it is as a result of cooperative aggregation. In addition, analysis of the air-liquid interface should show an abundance of dodecanol because when comparing the solubility the E_8 series of surfactants and dodecanol, $C_{10}E_8$ is the most soluble (the reason why the CMC is so high) of the group. Thus when in an aqueous system together with $C_{12}E_0$, the alcohol should dominate in interfacial adsorption giving a surface tension very near that of pure dodecanol. However, the result of 21.8 mN/m indicates that there is cooperative adsorption at the air-liquid interface between the two surfactants. Many studies have been done that examine the cooperative dynamics of surfactant mixtures at concentrations less than the CMC for example Casson who examines dodecanol adsorption in the presence of cetyl trimethyammonium bromide[54], but they do not effectively explain the synergism observed in this particular system; further studies will be necessary.

It was believed that the mismatched hydrocarbon chain lengths should not reduce the tensions as well as the matched chain lengths, but the data obtained for this system disagreed with our thinking. The aforementioned studies by Penfold et al. made the observation that there is frustrated packing at the air-liquid interface in the mixed system of $C_{12}E_3$ and $C_{12}E_8$ as well as in the mismatched hydrocarbon chain length system, which should lead to not maximizing the surface coverage, consequently not lowering the air-liquid interfacial tension. In both of these cases, there is competition for space between the two headgroups. It is possible that the mismatched systems studied here do not suffer for the same interfacial conformation problems because the headgroup of the dodecanol (-OH group) is of the same order in interfacial area as the hydrocarbon chain, if not smaller. Consequently, the –OH group is not competing for space with the E_8 headgroups. One can think of the monolayer having two domains, on where the E_8 are as tightly pack as possible and the $C_{12}E_0$ molecule filling in the spaces, as shown in the schematic in Figure 7, as structure that has been proposed by several studies [54,81,82]

4.4 CONCLUSION

We were able to synergistically obtain low air-liquid interfacial tensions by adding dodecanol to an aqueous C_iE_j surfactant system. It is apparent that the tension reduction is achieved. In addition the observed structures adsorbed directly to the interface thus predetermining the interfacial molecular distribution at the interface. The interfacial behavior appear to be dynamically stable for at very least minutes, but up days at a time.

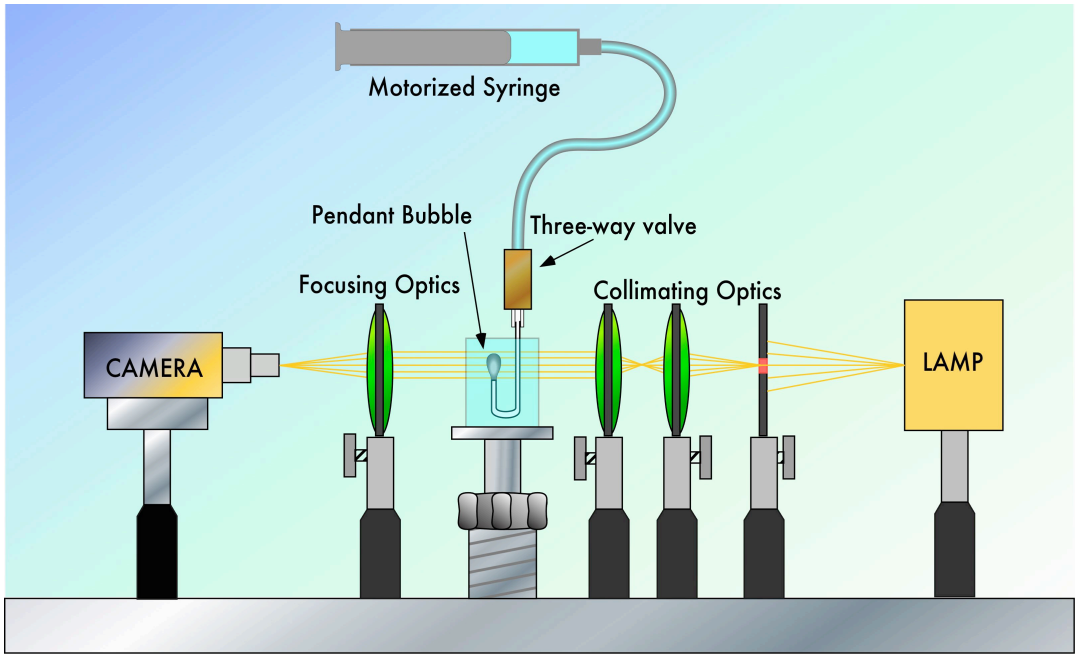

Figure 4.1: Pendant bubble setup used for air-liquid interfacial tension measurements.

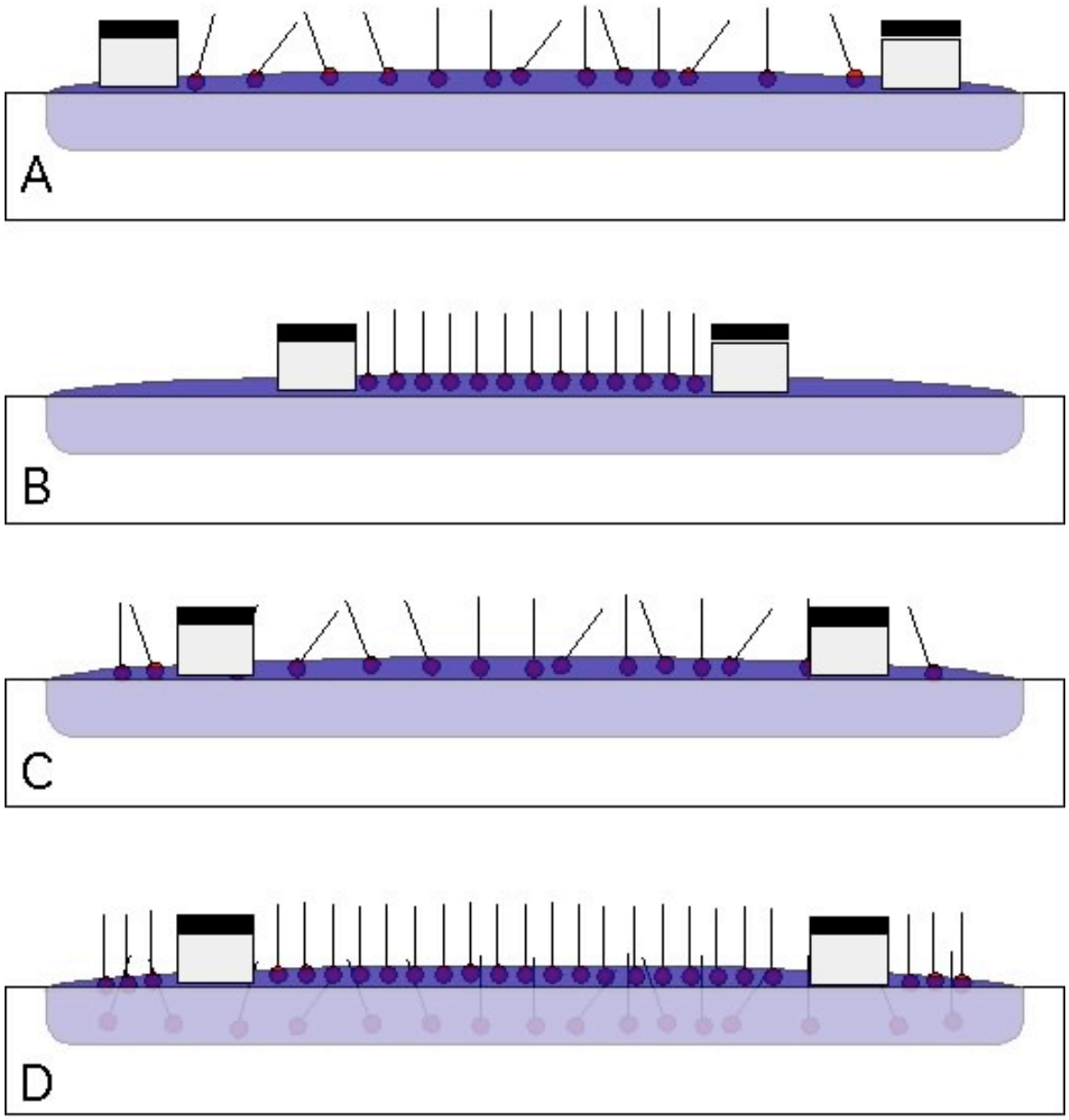

Figure 4.2: Schematic of the L-B trough a) liquid expanded Langmuir monolayer, b) liquid condensed Langmuir monolayer, c) liquid expanded Gibbs monolayer with surfactant below the CMC, d) compressed Gibbs monolayer forcing surfactant back into the subphase to reestablish equilibrium.

Solution	Equilibrium Surface Tension (mN/m), 23 ºC
Water	72.2
$C_{12}E_0$	28.3
$C_{12}E_4$	28.2
$C_{12}E_5$	30.4
$C_{12}E_6$	31.6
$C_{12}E_8$	34.4
$C_{10}E_8$	35.2
$C_{14}E_8$	35.4

Table 4.1: Equilibrium air-liquid interfacial tension for single component surfactant mixtures.

Binary Mixture **i = 12; j = 4, 5, 6, 8**	**Equilibrium Surface Tension (mN/m), 23 ºC**
$C_{12}E_4$/ $C_{12}E_0$ 7 cmc/0.23 mM	26.3
$C_{12}E_5$/ $C_{12}E_0$ 7 cmc/0.23 mM	26.8
$C_{12}E_6$/ $C_{12}E_0$ 7 cmc/0.23 mM	27.0
$C_{12}E_6$/ $C_{12}E_0$ 7 cmc/1.3 mM	22.3
$C_{12}E_8$/ $C_{12}E_0$ 7 cmc/0.23 mM	28.7
$C_{12}E_8$/ $C_{12}E_0$ 7 cmc/2.5 mM	22.0

Table 4.2: Equilibrium air-liquid interfacial tension for binary surfactant mixtures. Hydrocarbon chains are matched in length.

Binary Mixture **i = 10, 12, 14; j = 8**	**Equilibrium Surface Tension (mN/m), 23 ºC**
$C_{10}E_8$/ $C_{12}E_0$ 0.75 cmc/0.23 mM	21.8
$C_{12}E_8$/ $C_{12}E_0$ 7 cmc/0.23 mM	28.7
$C_{14}E_8$/ $C_{12}E_0$ 7 cmc/0.23 mM	23.3

Table 4.3: Equilibrium air-liquid interfacial tension for binary surfactant mixtures. Hydrocarbon chains are matched in length.

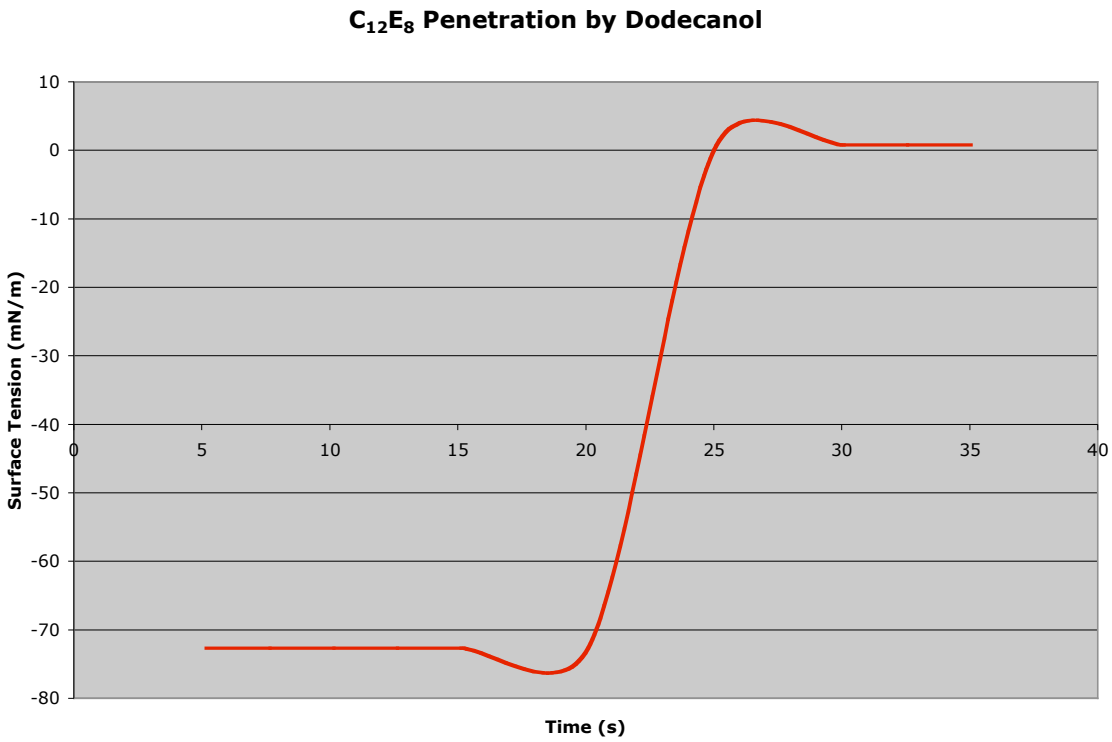

Figure 4.3: Surface tension of water from L-B trough showing that the subphase is clean before the addition of surfactant.

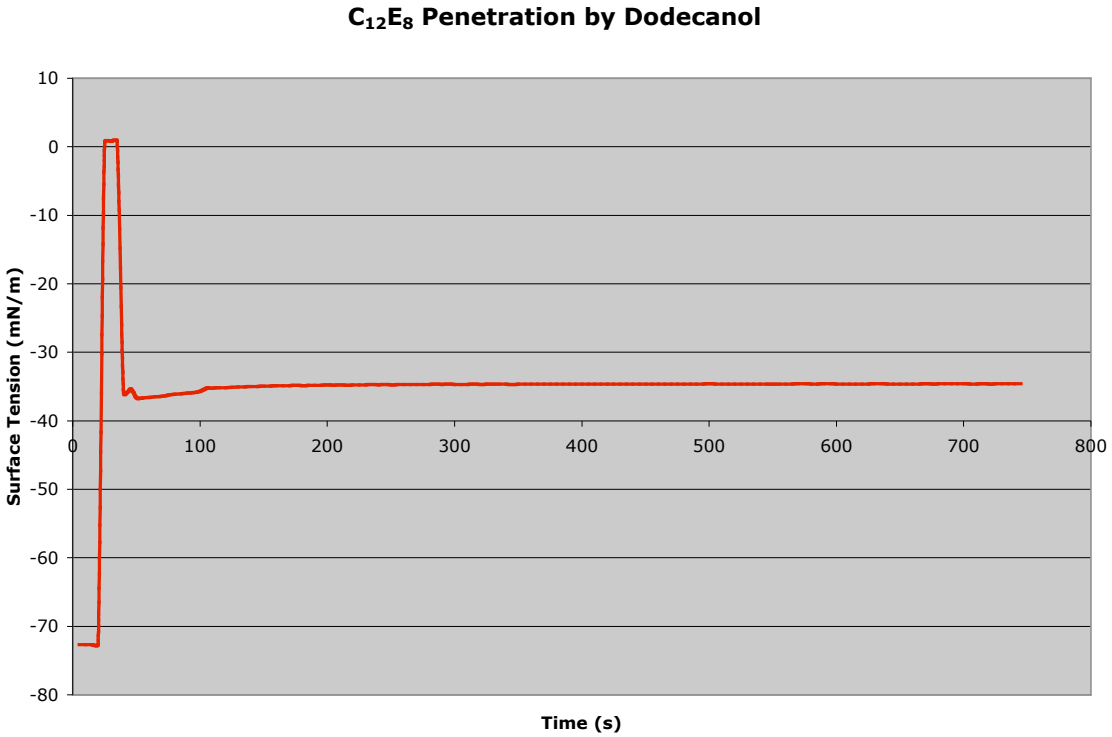

Figure 4.4: $C_{12}E_8$ injected to the water subphase of the L-B trough. The air-liquid interfacial tension reaches an equilibrium value of approximately 34 mN/m.

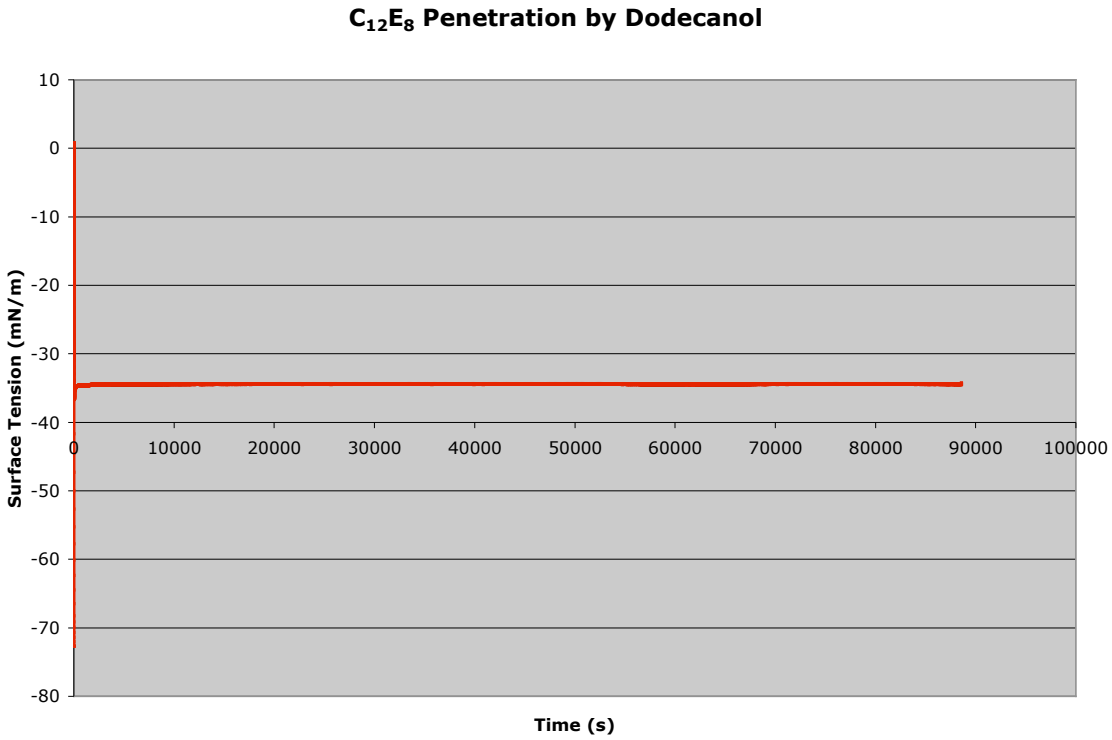

Figure 4.5: $C_{12}E_8$ tension remains stable for approximately 24 hours on the L-B trough.

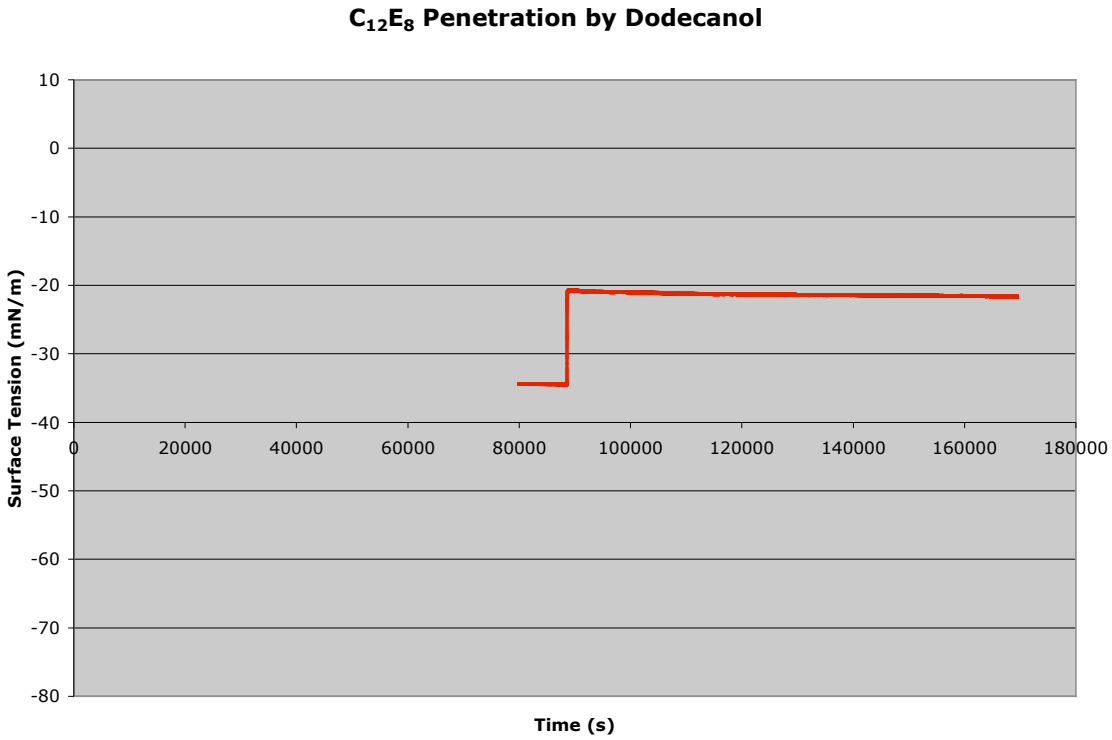

Figure 4.6: Dynamic surface tension using L-B trough. Addition of dodecanol to the $C_{12}E_8$/water subphase on the L-B trough reduces the air-liquid interfacial tension of the system to approximately 21 mN/m.

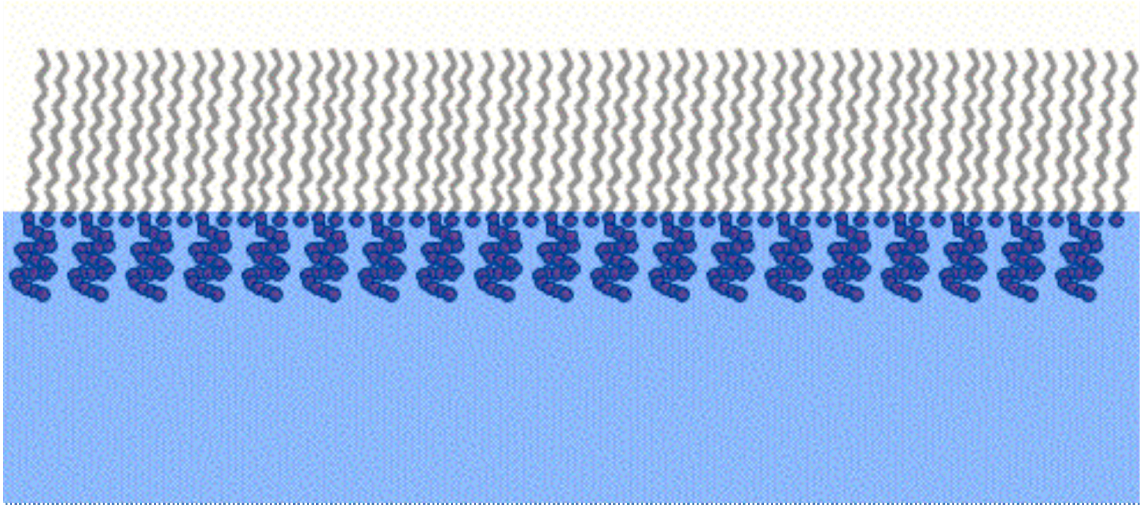

Figure 4.7: Schematic of proposed model structure of the C_iE_j/dodeanol mixed monolayer.

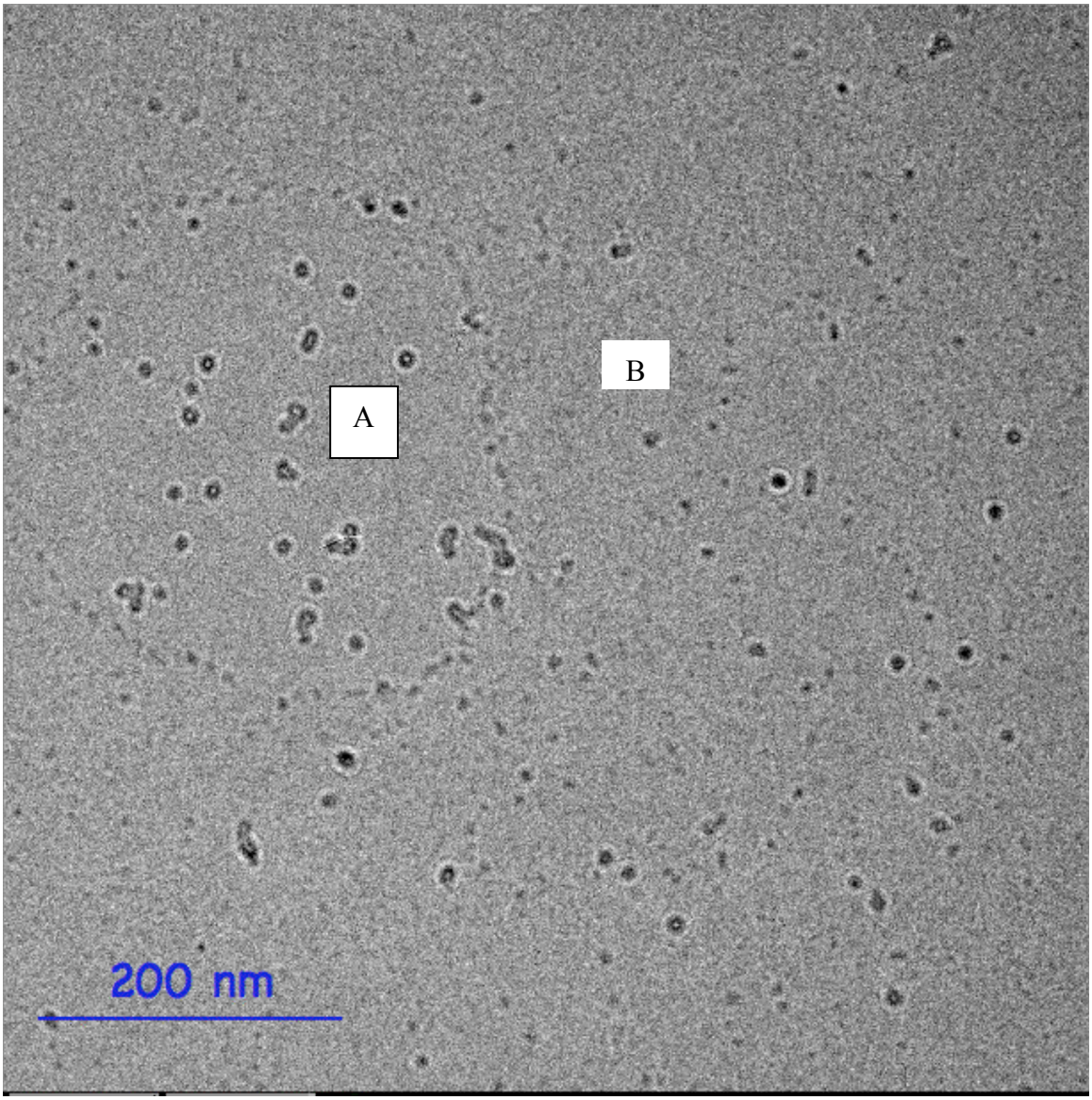

Figure 4.8: Cryo TEM image of $C_{12}E_8$/dodecanol mixture discussed in Chapter 3. A) area of low monolayer density and high aggregate concentration, B) area of high monolayer density and low aggregate concentration.

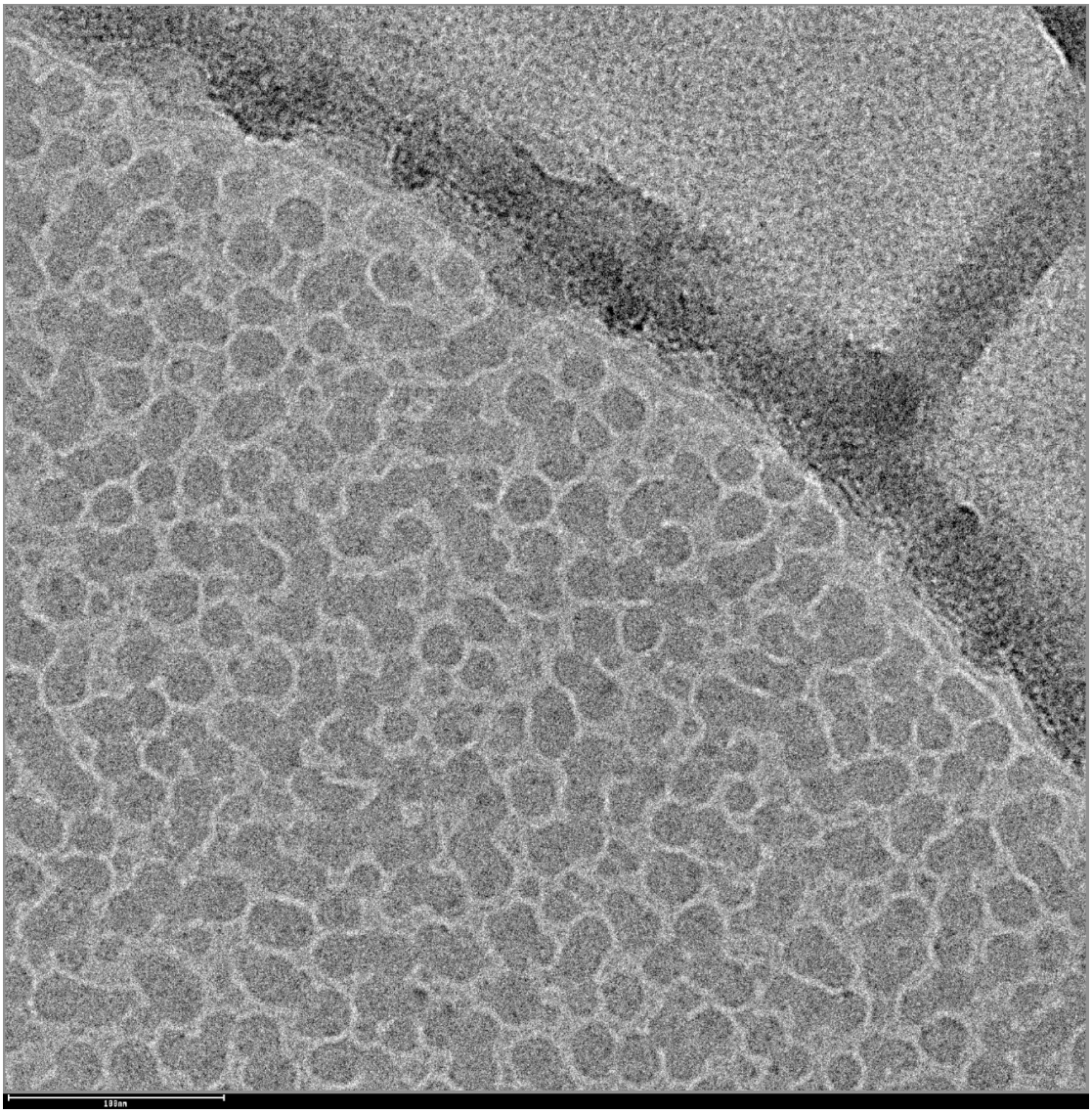

Figure 4.9: Cryo-TEM image of the $C_{12}E_0/C_{14}E_8$ demonstrating synergistic phase and air-liquid interfacial tension reduction.

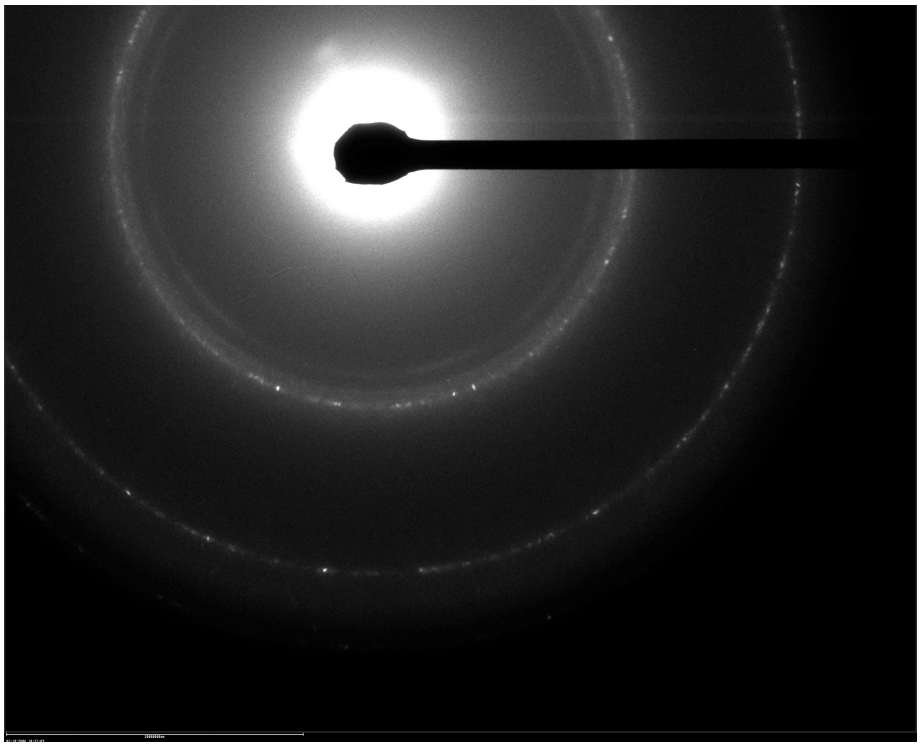

Figure 4.10: Electron diffraction pattern of region "B" of Figure 4.8. Outermost rings are representative of the structure of ice, however the diffuse centermost diffraction ring indicates the lattice spacing for hexagonally packed hydrocarbon chains.

REFERENCES

(1) Shen, Y. R. *Surface Science* **1994**, *299/300*, 551 - 562.

(2) Shen, Y. R. *Nature* **1989**, *337*, 519 - 524.

(3) Du, Q.; Superfine, R.; Freyesz, E.; Shen, Y. R. *Physical Review Letters* **1993**, *70*, 2313 - 2316.

(4) Shen, Y. R.; Du, Q.; Superfine, R.; Freyesz, E. *Physical Review Letters* **1993**, *70*, 2313 - 2316.

(5) Gragson, D. E.; Richmond, G. L. *The Journal of Physical Chemistry B* **1998**, *102*, 3847 - 3861.

(6) Gragson, D. E.; Richmond, G. L. *J. Phys. Chem. B* **1998**, *102*, 3847 - 3861.

(7) McQuarrie, D. A. *Statistical Mechanics*; 1 ed.; University Science Books: Sausalito, CA, 2000.

(8) Laughlin, R. G. *The Aqueous Phase Behavior of Surfactants*; Academic Press - Harcourt Brace & Company: Cincinatti, 1994.

(9) Kumar, N.; Maldarelli, C.; Couzis, A. *Colloids and Surfaces A: Physicochemical and Engineering Aspects* **2006**, *277*, 98-106.

(10) Hiemenz, P. C.; Rajagopalan, R. *Principles of Colloid and Surface Chemistry*; 3rd ed.; Marcel Dekker, Inc: New York, 1997.

(11) Schick, M. J. *Nonionic Surfactants*; Marcel Dekker, Inc.: New York, 1987; Vol. 23.

(12) Casson, B. D.; Braun, R.; Bain, C. D. *Faraday Discussions* **1996**, *104*, 209 - 229.

(13) Richmond, G. L. *Chem. Rev.* **2002**, *102*, 2693 - 2724.

(14) Casson, B. D.; Bain, C. D. *Journal of Physical Chemistry B* **1999**, *103*, 4678 - 4686.

(15) Goates, S. R.; Schofield, D. A.; Bain, C. D. *Langmuir* **1999**, *15*, 1400 - 1409.

(16) Lu, J. R.; Lee, E. M.; Thomas, R. K.; Penfold, J.; Flitach, S. L. *Langmuir* **1993**, *9*, 1352 - 1360.

(17) Lu, J. R.; Li, Z. X.; Su, T. J.; Thomas, R. K. *Langmuir* **1993**, *9*, 2408 - 2416.

(18) Rosen, M. J. *Surfactants and Interfacial Phenomena*; 2nd ed.; Wiley-Interscience: New York, 1989.

(19) Rosen, M. J. *Langmuir* **1991**, *7*, 885 - 888.

(20) Rosen, M. J.; Zhou, Q. *Langmuir* **2001**, *17*, 3532 - 3537.

(21) Zhou, Q.; Rosen, M. J. *Langmuir* **2003**, *19*, 4555 - 4562.

(22) Zhou, Q.; Wu, Y.; Rosen, M. J. *Langmuir* **2003**, *19*, 7955 - 7962.

(23) Penfold, J.; Staples, E.; Tucker, I.; Thomas, R. K. *Journal of Colloid and Interface Science* **1998**, *201*, 223 - 232.

(24) Penfold, J.; Staples, E.; Tucker, I.; Thomas, R. K.; Woodling, R.; Dong, C. C. *Journal of Colloid and Interface Science* **2003**, *262*, 235 - 242.

(25) Penfold, J.; Staples, E. J.; Tucker, I.; Thomas, R. K. *Colloids and Surfaces A: Physicochemical and Engineering Aspects* **1999**, *155*, 11 - 26.

(26) Subramanyam, R. Ph.D., City University of New York, 1999.
(27) Kumar, N. Ph.D., City University of New York, 2001.

(28) Lin, S.-Y.; chen, L.-J.; Xyu, J.-W.; Wang, W.-J. *Langmuir* **1995**, *11*, 4159 - 4166.

(29) B.P., B.; Fletcher, P. D. I.; Paunov, V. N.; D., S. *Langmuir* **2000**, *16*, 8926 - 8931.

(30) Casson, B. D.; Bain, C. D. *Journal of the American Chemical Society* **1999**, *121*, 2615 - 2616.

(31) Hsu, C.-T.; Chang, C.-H.; Lin, S.-Y. *Langmuir* **2000**, *16*, 1211 - 1215.

(32) Hsu, C.-T.; Shao, M.-J.; Lin, S.-Y. *Langmuir* **2000**, *16*, 3187 - 3194.

(33) Lee, Y.-C.; Liu, H.-S.; Lin, S.-Y. *Colloids and Surfaces A: Physicochemical and Engineering Aspects* **2003**, *212*, 123 - 134.

(34) Pollard, M. L.; Pan, R.; Steiner, C.; Maldarelli, C. *Langmuir* **1998**, *14*, 7222 - 7234.

(35) Raymond, E. A.; Tarbuck, T. L.; Brown, M. G.; Richmond, G. L. *J. Phys. Chem. B* **2003**, *107*, 546 - 556.

(36) Raymond, E. A.; Tarbuck, T. L.; Brown, M. G.; Richmond, G. L. *J. Phys. Chem. B* **2003**, *107*, 546 - 556.

(37) Vollhardt, D.; Fainerman, V. B.; Emrich, G. *J. Phys. Chem. B* **2000**, *104*, 8536 - 8543.

(38) Zhmud, B. V.; Tiberg, F.; Kizling, J. *Langmuir* **2000**, *16*, 2557 - 2565.

(39) Huibers, P. D. T.; Lobanov, V. S.; Katritzky, A. R.; Shah, D. O.; Karelson, M. *Langmuir* **1996**, *12*, 1462 - 1470.

(40) Bain, C. D.; Davies, P. B.; Ward, R. N. *Langmuir* **1994**, *10*, 2060 - 2063.

(41) Song, Q.; Couzis, A.; Somasundaran, P.; Maldarelli, C. *Colloids and Surfaces A: Physicochem. Eng. Aspects* **2006**, *282-283*, 162 - 182.

(42) Lu, J. R.; Li, Z. X.; Thomas, R. K.; Binks, B. P.; Crichton, D.; Fletcher, P. D. I.; McNab, J. R.; Penfold, J. *J. Phys. Chem. B* **1998**, *102*, 5785 - 5793.

(43) Kumar, N.; Couzis, A.; Maldarelli, C. *Journal of Colloid and Interface Science* **2003**, *267*, 272 - 285.

(44) Matsubsara, H.; Nakano, T.; Matsuda, T.; T.Takiue; M.Aratono *Langmuir* **2006**, *22*.

(45) Zhou, Q.; Rosen, M. J. *Langmuir*, *19*, 4555-4562.

CHAPTER 5

SPECTROSCOPIC STUDY OF THE SOLID-LIQUID INTERFACE

5.1 INTRODUCTION

In order to effectively characterize the wetting behavior of a surfactant or surfactants their behavior at the solid-liquid interface must be examined. Our previous examination of Young's equation shows the importance of the reduction of the solid-liquid interfacial tension in order to achieve wetting on a hydrophobic surface. The arrangement of the molecules at the solid-liquid interface, as well as the interaction with the surface, influences the eventual reduction of the interfacial tension. The study of surfactant behavior at the hydrophobic solid-liquid interface is ubiquitous in the field of interfacial phenomena as a result of the significant role this interface plays on the wetting behavior of water.

As we are trying to obtain a system that lowers the interfacial tension at both the air-aqueous and solid-aqueous interfaces, it is necessary to have an understanding of how pure water behaves on hydrophobic solid surfaces so that we know what issues need to be combated. SFG studies by Shen[83] *et al* and Ye *et al* have obtained spectra for the structure of neat water at the hydrophobic solid-aqueous interface. The model hydrophobic surface used consists of an octadecyltrichlorosilane (OTS/

$CH_3(CH2)_{17}SiCl_3$) monolayer self-assembled onto the native oxide surface of silicon (an OTS SAM surface). The silane adsorbs to the silicon surface, which leaves its methyl termination exposed. A water droplet placed on this surface subtends to an angle of 108^0 or greater; a characteristic angle for water on a hydrophobic surface. The SFG spectra obtained by Shen *et al* on these model surfaces shows a sharp peak at 3680 cm^{-1} (free OH) and a broad one at 3200 cm^{-1} (ice-like water) with a shoulder at 3400 cm^{-1} (liquid-like water); these are the same values observed for water at the air-liquid interface. Shen *et al* argue that this spectrum suggests that water re-structures itself in the molecular layers next to the methyl-terminated surface of the OTS monolayer. Specifically, in the water layers nearest the surface, an ice-like hexagonal packing replaces the liquid arrangement found in bulk water leaving dangling OH bonds protruding into the hydrophobic layer. This orients the water layer in such a way that the dipole moments point toward the hydrophobic surface. This packing, although leaving dangling OH bonds, minimizes the overall surface energy by maximizing the number and strength of hydrogen bonds of the water molecules that do not have a dangling OH and explains the peaks at 3200 cm^{-1} and 3680 cm^{-1} as well as the weak shoulder at 3400 cm^{-1}. As mentioned previously, Shen *et al* and Richmond[84] and coworkers have reported that similar structuring has also been observed at the interfaces between air and water and apolar liquid and water. Ye *et al* more carefully considered water structuring at the silicon oxide - OTS/water interface, studying both the water at the methyl terminated solution interface, and in the "underlayer" beneath the chains and between the siloxane linkages and the silicon oxide surface.

In general, the mechanism by which surfactants reduce the equilibrium contact angle of water on a hydrophobic surface is by adsorbing onto the air/water and water/hydrophobic solid interfaces at the three phase contact line. The adsorption reduces the tensions on the surfaces, affecting the balance of forces at the contact line, which determines the equilibrium angle. The balance of forces is given by the Young-Dupree[51,63] equation $\gamma_{a/s} = \gamma\cos\theta + \gamma_{s/\ell}$(where $\gamma_{s/l}$ and $\gamma_{a/s}$ are the aqueous/hydrophobic and air/hydrophobic solid tensions and γ the air/aqueous tension). In the case of a very hydrophobic surface, $\gamma_{a/s} < \gamma_{s/\ell}$ and $\theta > 90^{o}$ must be true in order to effectively reduce the contact angle. At constant temperature, the reduction in the interfacial tension is related to the surfactant adsorption by the Gibbs-Duhem equation: $\frac{d\gamma_{s/\ell}}{d\ell n\, C} = -RT\Gamma^{s/\ell}$ and $\frac{d\gamma}{d\ell n\, C} = -RT\Gamma$where $\Gamma^{s/\ell}$ and Γ are the (excess) surface concentrations on the aqueous/hydrophobic solid and air/aqueous interfaces, respectively, and RT is the thermal energy. Thus the reductions in surface tension from the clean values are related to the adsorption isotherms, $\gamma_{s/\ell}(C) = \gamma^{o}_{s/\ell} - RT\int_0^C \Gamma^{s/\ell}(C)\, d\ell nC$ and $\gamma_{a/s}(C) = \gamma^{o}_{a/s} - RT\int_0^C \Gamma(C)\, d\ell nC$ and the binary surfactant systems must, therefore, have larger integrated adsorption compared to the single component systems, i.e. $\int_0^C (\Gamma_{binary}(C) - \Gamma_{unary.}(C))d\ell nC > 0$. The theories discussed here have not yet been validated for the systems that are in the scope of this study. However, this conclusion has been verified experimentally by Rosen and Wu[59] in a comparative study of the adsorption of non-superspreading alkyl pyrrolidinones and a commercial trisiloxane on an aqueous/ polyethylene surface) and Kumar *et al*. in a study

of M(D'E_4OH)M and M(D'E_8OH)M and the non-superspreading $C_{12}E_4$ and $C_{12}E_8$ on the air/aqueous interface.

Woglemuth, Worknman and Manne examine the adsorption of $C_{12}E_8$[85] on what he calls an amorphous hydrophobic silicon wafer. His motivation for using trimethylchlorosilane to hydrophobically the silicon wafer was to improve on similar experiments performed by Ducker et al,[86] where the surface is modified with diethyloctylchlorosilane. It was Manne's belief that using the shorter hydrocarbon chain would keep the interface smooth, leaving only dispersive interactions possible for the surfactants as they adsorb, as opposed to the Ducker case where intercalation of the monolayer is possible. In spite of Manne desire to improve on the experimental condition, he reports that his static water contact angles for the surfaces are ~80° the surface, consequently it is conceivable that the surface is hydrophilic enough for the adsorption of hemi-micelles on the surface as observed by Ducker[87] in similar experiments on hydrophilic surfaces.

In addition to the importance of the Young-Dupré and the reduction of tensions is an understanding of the hydrophobic solid-aqueous spreading coefficient ($S_{S/L}$)[88], which is quantitatively defined as $S_{S/L} = \gamma_{A/S} - (\gamma_{S/L} + \gamma)$[24]. A negative spreading coefficient is associated with a system that does not spread because it is energetically unfavorable while a positive coefficient means that the drop can spread spontaneously. The more positive the spreading coefficient is, the greater the possible final coverage area of the drop. Zhou, Wu and Rosen[59] have demonstrated enhanced spreading of aqueous drops

on a polyethylene (PE) film using a mixed nonionic surfactant system of C_8-pyrrolidone and Igepal CA-520. It was determined that the Igepal had greater adsorption from the mixed system as compared to the pure Igepal solution and the total surfactant adsorption was greater that was calculated to be the ideal. Of greater importance was that the binary system was able to synergistically lower the contact angle of a water drop on the PE film. Ideally, the binary surfactant systems would be able to mimic the superspreading ability of the trisiloxanes. The ability for the system to wet will be determined by both the reduction of the air-liquid interfacial tension as well as the solid-liquid interfacial tension. The balance of the tension vectors at the three phase contact line will determine the ability for the system to wet a hydrophobic surface.

5.2 EXPERIMENTAL

5.2.1 Materials

The surfactants used in this case were the same as those in chapter three and four. Deuterated dodecanol (95%, $CD_3(CD_2)_{11}OH$) was purchased from Cambridge Isotopes and used as obtained. Double polished boron doped <100> silicon wafers were purchased from Montco Silicon Technologies. Polishing slurries from Buehler International and Mager Scientific to modify the silicon wafer to the desired configuration to be used for the FTIR/ATR.

5.2.2 Methods

Contact Angle Goniometry

The contact angle for sessile drops of the surfactant solutions on an OTS modified silicon wafer fragment was measured using a Ramé-Hart contact angle goniometer. Using a syringe capable of measuring microliter sized drops, the measured solution was deposited onto the hydrophobic surface to be measured. The drops reported here had volumes that were 4-6 ml.

Vibrational Sum Frequency Generation Spectroscopy

Vibrational sum frequency generation spectroscopy (SFG) is a second-order process involving the input of two pulsed laser beams, one in the visible regime of frequency ω_{vis} and the other in the infrared regime of frequency ω_{IR}. The two beams are overlapped at an interface of interest producing beam having the sum frequency ω_{SF}, where $\omega_{vis} + \omega_{IR} = \omega_{SF}$. Second-order processes are forbidden in the bulk of centrosymmetric non-chiral media, consequently SFG is ideal for examining the behavior of surfactants adsorbed at the interface.

The SFG experiments were conducted at ExxonMobil Research and Engineering Co. on the SFG II setup[89]. A visible (532 nm, 7 ns duration pulse) and tunable infrared (7 ns) were overlapped on the major face of a trapezoidal fused quartz prism coated with an octadecyltrichlorosilane (OTS) monolayer. A uniform monolayer were prepared using a procedure previously described[90]. In short, a trapezoidal fused quartz prism was immersed in a 2-mM (OTS) solution prepared in an 80:12:8 (by volume) mixture of hexadecane, carbon tetrachloride and chloroform. Prior to immersion in the OTS solution, the prism as cleaned by first sonicating it for 40 minutes in a concentrated sulfuric acid/Nochromix solution. The crystal was rinsed by subjecting it to three cycles of sonicating in deionized water for 15 minutes during each cycle. The crystal was then dried with nitrogen and then placed in a UV/O_3 stripper for 5 minutes at 80 °C. Water contact angle measurements were performed on the prism to insure that a dense

monolayer was obtained. If the prism had a contact angle less than 108°, it was not used for the experiment. In addition to using water contact angle to characterize the surface, ellipsometric measurements were taken using an Elli2000 imaging ellipsometer on an OTS modified silicon wafer that was made in parallel with the quartz prism, under the same conditions. The prepared prism was placed in a stainless steel, liquid flow cell as shown in Figure 5.1. In order to clean the cell, it was flushed with a series of solvents in decreasing order of polarity, ending with heptane. The cell was dried with air then baked at 350 °C for 30 minutes. After the baking cycle, the cell was blown with nitrogen and subject to plasma cleaning for several minutes while under vacuum.

Water was first pumped into the cell through one of the Luer lock input ports on the fluid cell. Water was flushed through the system several times to make sure that air-bubbles were not present in the system. During the flushing cycles, the SFG intensity was measured and tuned at 3200 cm^{-1} in order to maximize the sum frequency signal. Once certain of the maximized signal measurements were taken with water on the OTS monolayer (Figure 5.1). The flushing cycles and water measurement procedures were repeated between each surfactant laden solution experiments. With each flush between experiments, the original clean water spectrum was obtained prior to analysis of each surfactant solution.

ATR/FTIR

Attenuated total reflectance (ATR) is a sampling technique used in conjunction with infrared spectroscopy which enables samples to be examined directly in the solid or liquid state without further preparation[91]. ATR uses a property of total internal reflection called the evanescent wave. A beam of infrared light is passed through the ATR crystal in such a way that it reflects at least once off the internal surface in contact with the sample. This reflection forms the evanescent wave, which extends into the sample, typically by a few microns. The beam is then collected by a detector as it exits the crystal.

This evanescent effect works best if the crystal is made of an optical material with a higher refractive index than the sample being studied. In the case of a liquid sample, pouring a shallow amount over the surface of the crystal is sufficient. In the case of a solid sample, it is pressed into direct contact with the crystal. Because the evanescent wave into the solid sample is improved with a more intimate contact, solid samples are usually firmly clamped against the ATR crystal, so that trapped air is not the medium through which the evanescent wave travels, as that would distort the results.

In conjunction with ATR, Fourier transform infrared spectroscopy (FTIR) is a technique that takes advantage of total internal reflection property of a metallic single crystal. The infrared beam enters one face of the crystal, reflects off of the internal faces of the crystal a certain number (N) of times, where N is simple function of the length and thickness of the crystal, then exits into an MCT detector. Because magnetic and electrical field cannot be discontinuous at a boundary, an evanescent field is generated which carries the

information about the surface to the detector. The ATR/FTIR experiments were performed on a Bio-Rad FTS 175, using the ATR fixture, which can be adjusted to maximize the detected signal. A schematic of the system used is shown in Figure 5.2.

A standard 50 mm x 10 mm x 4 mm single crystal silicon prism allows for 12 internal reflections. As the strength of signal obtained from ATR is linearly additive, it was decide that a thinner crystal was necessary in order to obtained the desired adsorption information. To this end, a 500 micron silicon wafer was cleaved such that it had the approximate width and length of the standard crystal. In addition, the faces, onto which the IR beam would be hitting, were polished to a 45° relative to the crystal face normal. The polishing was done in two steps, the first being a gross material removal using Buehler 5 micron alumina slurry, then a finishing step using a Mager 1 micron diamond suspension. Both steps were performed on a Mager 8 inch Chemox cloth on a low speed polishing wheel. To clean the crystal of any residual slurry, the newly polished crystals were sonicated in methanol, then cleaned in a Nochromix®/H_2SO_4 bath, finally rinsing in deionized water. This newly fashioned ATR crystal provides an eight-fold increase in the number of internal reflections leading to more interfacial data.

The method used for tracking the adsorption has been previously desribed[64] and will only be described her in short. Once assembled, the fluid cell in Figure 5.2 is flushed with water that is introduced to the system via syringe. The system is flushed while taking scans of the cell. Once the cell is deemed clean, the surfactant solution to be analyzed is

introduced immediately to the system. The two syringes are connected simultaneously to the cell by a flow T, thus the transition from water to surfactant solution is interrupted.

5.3 RESULTS

5.3.1 Contact Angle Goniometry

The contact angle data for select surfactant solutions from the previous chapter on air-liquid interfacial tension reduction are shown on table Table 5.1. The $C_{12}E_8$ and $C_{12}E_6$ system reach equilibrium contact angle of 15° and 18°, respectively. The $C_{12}E_5$ system reached a contact angle of 33° and the $C_{14}E_8$ system a contact angle of 41°. Water was used as the check for the system to insure that the surface was hydrophobic. Water had an equilibrium contact angle of 106°.

5.3.2 FTIR/ATR

Dynamic adsorption of a supersaturated solution of dodecanol onto and OTS modified silicon ATR crystal is shown in Figure 5.3. The characteristic peaks for the hydrocarbon region are shown in the region between 2960 cm^{-1} and 2850 cm^{-1} as shown in the magnified spectra in Figure 5.4. Also worthy of note are the negative peaks between 1525 cm^{-1} and 1350 cm-1. This region is representative of the $–CH_2$ bending modes of the OTS monolayer. Overall, the timescale represented in spectra presented here is 100 minutes.

5.3.3 Sum Frequency Generation Spectroscopy

The frequency dependent ppp equilibrium adsorption profiles for water, a 7 cmc $C_{12}E_8$ solution, a saturated $C_{12}E_0$ solution a $C_{12}E_8$/ $C_{12}E_0$ 7 cmc/2.5 mM mixture and a saturated deuterated $C_{12}E_0$ (d-$C_{12}E_0$) solution a shown in Figures 6-11. The ppp polarization pattern was used because it exhibited the greatest sensitivity to changes in both the hydrocarbon and water regions of the spectra. The water on OTS spectrum in Figure 6 shows the characteristic peaks at 2870 cm^{-1}, 2930 cm^{-1} and 2960 cm^{-1}, representative of the CH_3 symmetric stretch (CH_3-S), the CH_3 Fermi resonance (CH_3-F) and the CH_3 asymmetric stretch (CH_3-A), respectively[47,92-94]. In addition to the sharp and strong hydrocarbon peaks, clearly visible are broad peaks centered at 3200 cm^{-1} and 3450 cm^{-1} are seen and are generally attributed to the ice-like and liquid structures of water and the peak attributed to free –OH[45,46] centered at ~3700 cm^{-1}.

5.4 DISCUSSION

As the goal of this study is to find alternate superspreading systems, the solutions that exhibited some of the characteristics of superspreading systems (low air-liquid interfacial tension and turbidity) were examined in order to determine the effect that the observed synergism has on the wetting behavior on a hydrophobic surface. The $C_{12}E_6$ and $C_{12}E_8$ systems on Table 1 exhibit similar behavior with regard to their ability to synergistically lower the contact angle on a hydrophobic surface, when compared to the contact angle of the individual components[63]. The $C_{12}E_5$ system, although it does not at exhibit synergism at the air-liquid interface, it does synergistically lower the contact angle to ~33°. In these three cases, the solutions all have apparent lamellar phases in the solution. The $C_{14}E_8$ mixture, on the other hand, does not exhibit synergistic contact angle reduction in spite of the extremely low air—liquid interfacial tension obtained. The trend observed here leads one to believe and confirms that it is not enough to lower the air-liquid interfacial tension in order to wet a hydrophobic surface. There is an additional requirement that must be fulfilled in the bulk and at the solid-liquid interface. Although, the appearance lamellar phases in the solution are indicative of solutions that may have the ability to superspread, it is not an absolute characteristic. Stoebe et al.[20] found that superspreading is not limited to turbid solutions and may be a more general phenomenon.

To understand why the mixtures were able synergistically lower the contact angle, the surfactant adsorption at the solid-liquid interface was examined by ATR/ FTIR. A

previous study by Kumar et al.[64,95] examined the adsorption behavior of $C_{12}E_8$ at the hydrophobic surface. What was concluded from this study was that $C_{12}E_8$ removes bulk water from the interface as the surfactant is adsorbing. As a parallel study, we examined dodecanol adsorption onto an OTS modified crystal, the results of which are in Figure 5.3. In Figure 5.4, we are focused on the hydrocarbon region, which shows the adsorption of $C_{12}E_0$ onto the surface. Over time, the peaks at 2860 cm^{-1} and 2930 cm^{-1} grows signifying and increase in the density of dodecanol at the interface. However, there is a disruption in the order of the OTS monolayer as signified by the peak at 2965 cm^{-1} that becomes negative. The 2965 cm^{-1} peak represent the highly order $–CH_3$ monolayer that is formed as a result of the chemisorbed OTS monolayer onto silicon. The almost crystalline order of the monolayer is very well known[96] and the fact that 2965 cm^{-1} speaks to the disruption of the monolayer. This is further confirmed by the peaks centered at 1450 cm^{-1} and 1375 cm^{-1}. The $–CH_2$ bending modes are not visible to IR when the OTS monolayer is tightly packed, however the appearance of the peaks points to intercalation of the $C_{12}E_0$ molecules in to the OTS monolayer.

An understanding of the behavior of the individual components of the $C_{12}E_8/C_{12}E_0$ mixture has been gained using ATR/FTIR, however characterization of the mixture proved to be difficult, as it was not possible properly resolve the adsorption profile. ATR/FTIR is a powerful technique for examining interfaces, however the evanescent wave that carries all of the information about the sample also carries information about the bulk. As mentioned previously, the evanescent waved penetrates and decays on

length scales of microns. However the monolayer thickness is on the order of nanometers, thus the majority of the information received is about the bulk. Care was taken to measure a background reading for the system however, the surface specific spectra could not be resolved, hence to use of SFG, which is surface specific.

The spectrum for water on OTS in Figure 5.6 shows the peaks related to $-CH_3$ stretches of the OTS monolayer, as described in the previous section. Also of importance are the peaks corresponding to adsorbed water, which should be most affected by the presence of surfactant. Free –OH, centered at ~3700 cm^{-1}, has been studied a great deal at the air-liquid interface and it has been suggested that a consequence of the presence of the free -OH is the high air-liquid interfacial tension of water[45,97]. This would also suggest that the presence of the free –OH at the hydrophobic solid-liquid interface explains the high contact angle to which water subtends. In turn, the reduction of free -OH at either or both the air-liquid and hydrophobic solid-liquid interfaces should lead to reduced interfacial tensions, consequently leading to enhanced wetting on a hydrophobic surface. The presence of free –OH at the hydrophobic surface has been debated to certain degree because it is unclear whether or not water would exhibit the same behavior at both the air-liquid and the hydrophobic solid-liquid interfaces. However, the existence of the free –OH comes as a result of interfacial water not being able to bond with another water molecule or the interface. Since some of the water molecule would also not be able to bond with any of the material at the solid-liquid interface, unlike the behavior at a

hydrophilic solid surface, it stands to reason that there would be free –OH at a hydrocarbon based hydrophobic solid surface as well.

With the addition of an aqueous solution of $C_{12}E_8$ at 7 CMC to the SFG cell, we see in Figure 5.7 that there are minor changes to the hydrocarbon region of the spectrum. However, more significantly, a reduction in all of the vibrational modes of water are observed, including what appears to be a complete removal of the free –OH at the solid interface. The removal of bulk water is in agreement with the observation made by Kumar et al.[64] where bulk water was removed for the solid-liquid interface. In addition the ratio of ice-like to liquid water is reduced. This result signifies that $C_{12}E_8$ removed some of the water and rearranges what is left behind at the interface.

After several flushing cycles, a saturated $C_{12}E_0$ solution was pushed into the cell, with the resulting spectrum in Figure 5.8. Unlike $C_{12}E_8$, the hydrocarbon region appears to be heavily modified in the presence of the alcohol. At first glance, it appears that the alcohol completely destroys the monolayer, however when the system is flushed the original water signal is regained. SFG is able to resolve structures whose ensemble average of their dipole points in a single direction, leading to asymmetry. If a peak disappears, it is a result destruction of the system being analyzed or symmetry being imparted to the system, causing it to be SFG invisible. Since we know that the monolayer has not been destroyed, then the reason for the disappearance of the $–CH_3$ peaks must be the latter reason. The schematic in Figure 5.12 shows how dodecanol may

adsorb on the OTS monolayer. We know that the $C_{12}E_0$ will have a dense packing at the solid-liquid interface from Bain's work[14,54] as well as the ATR/FTIR work reported here. We also know that when it adsorbs, it will do so with the $–CH_3$ of the alcohol in contact with the $–CH_3$ of the OTS monolayer. Looking at the adsorption schematic in Figure 12, one can see that symmetry is imparted in the system as the $–CH_3$ of the interface and alcohols meet. To test this, $C_{12}E_0$ was replaced with d-$C_{12}E_0$ at the same concentration. Because deuterium if heavier than hydrogen, $-CD_3$ will oscillate at a lower frequency than $–CH_3$. As shown in Figure 11, when d-$C_{12}E_0$ adsorbs on the OTS monolayer, the $–CH_3$ peaks on the OTS monolayer are fully resolved. Because of this result, any system studied where the $–CH_3$ peaks are unresolved will be attributed to interference effects due to $C_{12}E_0$ if the system contains it.

The $C_{12}E_0$ spectrum also shows that significantly more water is removed from the surface when compared to $C_{12}E_8$. Again, the ice like and liquid-like water seem to rearrange themselves in the presence of the alcohol, as seen by the change in ratio between the related peaks. The free –OH peak virtually disappears as well. In the spectrum for C12E0 shown here, it seems that there is a small amount free –OH as well, but it is difficult to quantify whether of not the peaks are real or an artifact of the fitting.

The synergism observed in the $C_{12}E_0/C_{12}E_8$ systems with regard to the air-liquid interfacial tension reduction and the liquid crystalline phase behavior is also present in the SFG spectrum in Figure 5.9. The combination of the two surfactants appears to

virtually remove all water from the interface. The liquid-like and ice-like structure of water have completely disappeared and the free –OH has done the same. The SFG results points to requirements needed in order to obtain enhanced wetting on a hydrophobic surface. It seems that the ability to remove water for the interface is a key component in bring able to synergistically wet a surface, at least for the hydrocarbon hydrophobic tail. However, this is not an absolute requirement as will be show in the next chapter.

From a macroscopic perspective[98], the behavior of the surfactants can be predicted using Young's Equation (1). Knowing the contact angle (θ) of a drop on the surface, the air-liquid interfacial tension ($\gamma_{l/v}$) and the solid-vapor interfacial tension ($\gamma_{s/v}$), one can readily calculate the solid-liquid interfacial tension ($\gamma_{s/l}$), which would give insight into how readily a surfactant or surfactant system will adsorb on a solid surface of a particular energy. However, although a constant for a given surface in air, $\gamma_{s/v}$ cannot be directly measured. For a hydrophobic surface, like the OTS modified silicon wafer, where all of the interactions are dispersive in nature, $\gamma_{s/l}$ can be estimated using (2), which when substituted into (1), where (3) is then obtained. The solid vapor interfacial tension can now be estimated for an OTS surface in air using $\gamma_{l/v}$, θ and $\gamma_{l/v}^{d}$ for water, where $\gamma_{l/v}^{d}$ is the dispersive component of $\gamma_{l/v}$, where $\gamma_{l/v} = \gamma_{l/v}^{e} + \gamma_{l/v}^{d}$ and $\gamma_{l/v}^{e}$ is the electrostatic component of the air-liquid interfacial tension. Table 1 lists the calculated values for $\gamma_{s/l}$ for water, $C_{12}E_0$, $C_{12}E_8$ and their specified mixture, where the values for $\gamma_{l/v}^{d}$, q, $\gamma_{l/v}$, and

the calculated $\gamma_{s/v}$, were 21.7 mN/m, 109.9°, 72.8 mN/m and 26.5 mN/m, respectively. From the data shown in Table 3, we can see that of the two surfactants in the mixture, $C_{12}E_0$ has a stronger affinity for the surface as evidenced by its lower solid–liquid interfacial tension. However, there is a clear synergistic effect when the mixture is applied to the OTS surface where the solid-liquid interfacial tension to nearly zero. This data gives us a macroscopic view of the surfactant adsorption behavior, but does not give enough information about what is happening at the molecular level to cause the observed synergism in the mixtures.

$$(1)\ \gamma_{s/v} = \gamma_{s/l} + \gamma_{l/v}\cos\theta$$

$$(2)\ \gamma_{s/l} = \gamma_{s/v} + \gamma_{l/v} - 2\sqrt{\gamma_{s/v}\gamma_{lv}^{d}}$$

$$(3)\ \gamma_{s/v} = \frac{\gamma_{l/v}^{2}(1+\cos\theta)^{2}}{4\gamma_{l/v}^{d}}$$

5.5 CONCLUSION

The synergism that is observed in the $C_{12}E_0/C_{12}E_8$ system that exhibits enhanced phase behavior and air-liquid interfacial tension reduction is also observed at the solid-liquid interface by SFG. The behavior of this surfactant system offers insight to what systems would obtain enhance wetting of a hydrophobic surface, but may not lead to universal requirements for surfactants of alternate chemistries. Both dodecanol and $C_{12}E_8$ are present at the solid-liquid interface, however of the two surfactants in the mixture, dodecanol has the higher surface density. The surfactant mixture synergistically reduces the solid-liquid interfacial tension, and as a result the contact angle on a hydrophobic surface. In the surfactant mixtures, dodecanol is responsible for the removal of the majority of the ice-like and liquid water at the solid interface, but in not capable of removing all of the free -OH. The observed synergism of the surfactant mixtures has a direct effect on the reorganization or removal of water at the solid-liquid interface, including a complete removal of the free -OH.

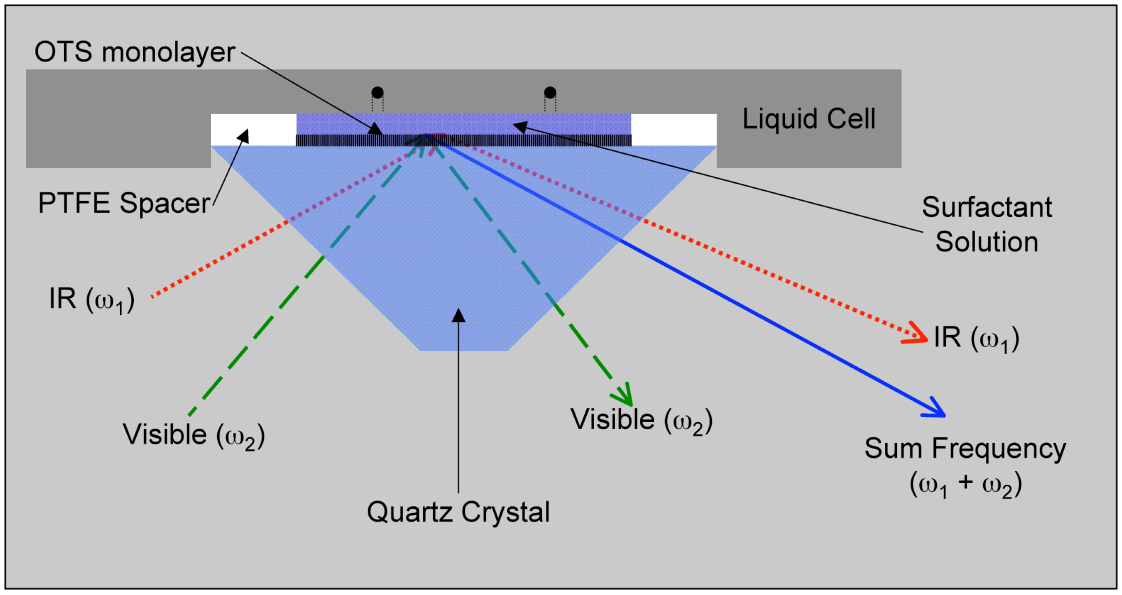

Figure 5.1: Schematic of an SFG spectroscopic liquid cell with a quartz crystal.

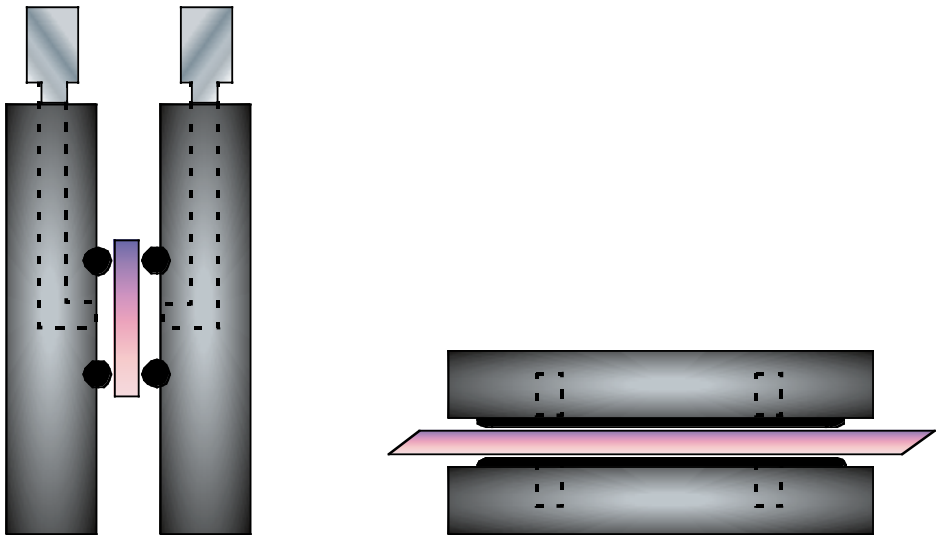

Figure 5.2: Schematic of ATR liquid cell with modified ATR crystal.

Solution	Equilibrium Surface Tension	Equilibrium Contact Angle	Extended Phases
Water	72.4	105º	N/A
$C_{12}E_8$/ $C_{12}E_0$ 7 cmc/2.5 mM	22.0	~15 º	Yes
$C_{12}E_6$/ $C_{12}E_0$ 7 cmc/1.3 mM	21.5	~18 º	Yes
$C_{12}E_5$/ $C_{12}E_0$ 7 cmc/0.23 mM	26.8	~33 º	Yes
$C_{14}E_8$/$C_{12}E_0$ 7 cmc/0.23 mM	23.3	~41 º	No

Table 5.1: Equilibrium contact angle for solutions showing synergistic air-liquid interfacial tension reduction.

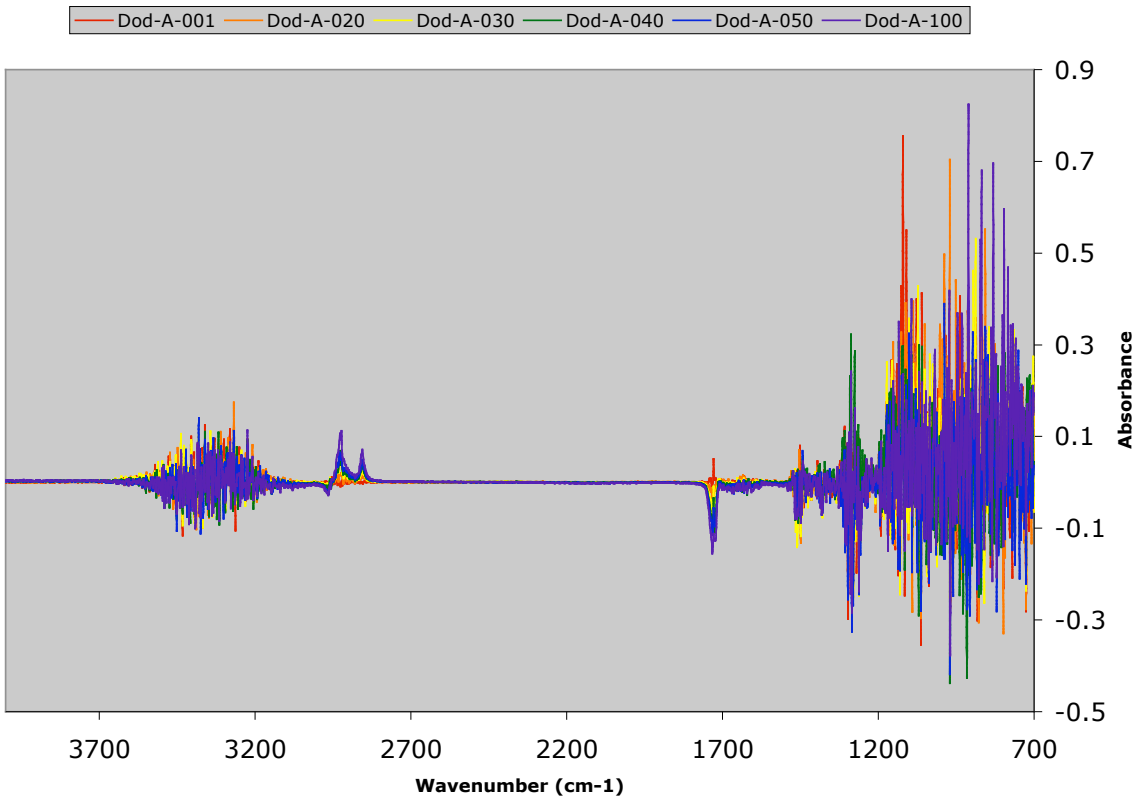

Figure 5.3: Dynamic adsorption profile via ATR/FTIR of dodecanol on an OTS monolayer

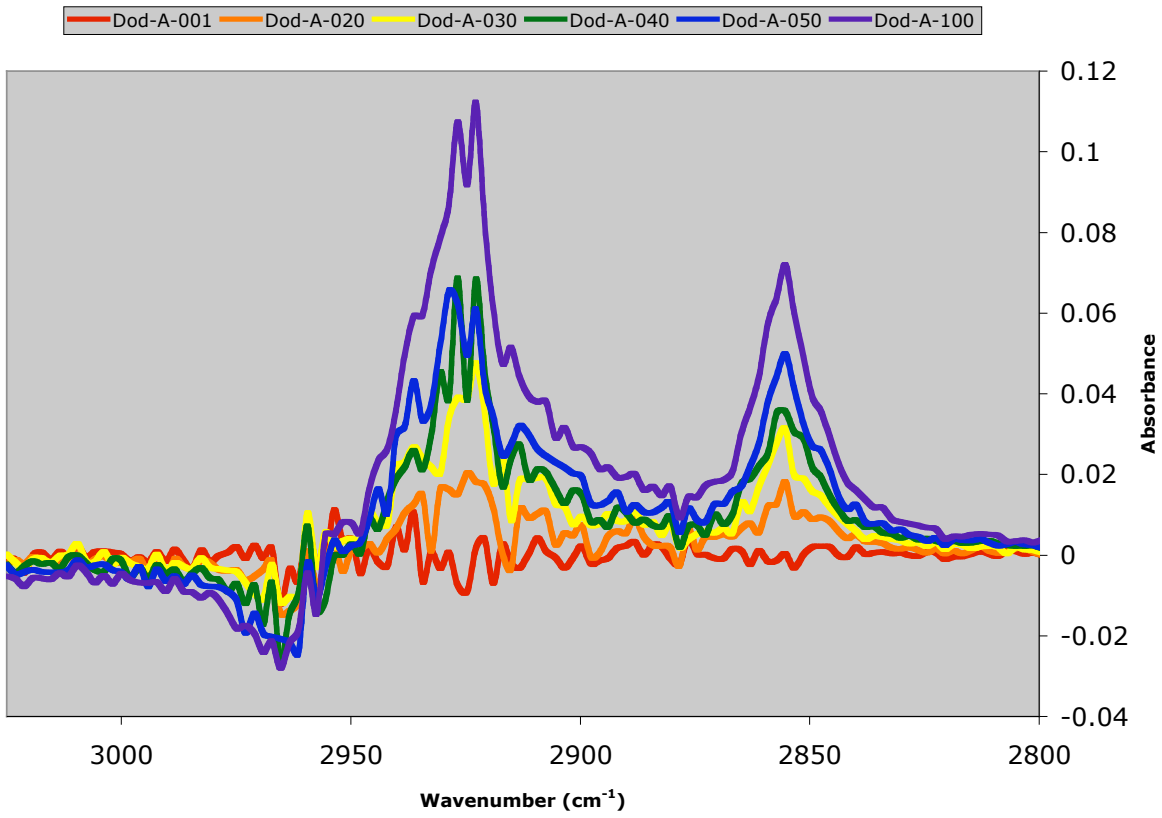

Figure 5.4: Dynamic adsorption profile via ATR/FTIR of dodecanol on an OTS monolayer. Focus on the hydrocarbon stretching modes.

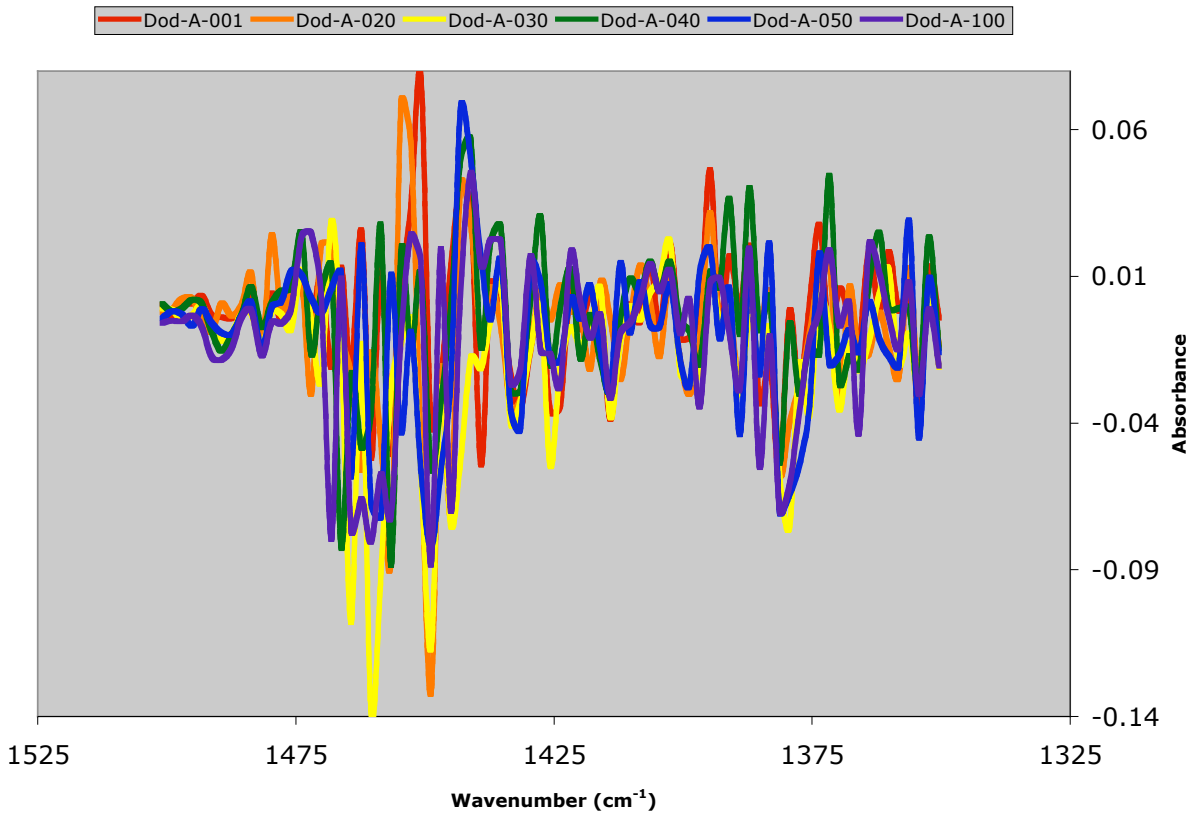

Figure 5.5: Dynamic adsorption profile via ATR/FTIR of dodecanol on an OTS monolayer. Focus on the $-CH_2$ bending modes.

Solution	Air-Liquid Interfacial Tension (mN/m)	Equilibrium Contact Angle	Calculated Solid-Liquid Interfacial Tension (mN/m)
Water	72.8	~110º	51.5
$C_{12}E_8$	34.4	~59 º	12.8
$C_{12}E_0$	28.3	~35 º	6.7
$C_{12}E_8/C_{12}E_0$	22.0	~15 º	5.2

Table 5.2: Calculated solid-liquid interfacial tensions for water, dodecanol, $C_{12}E_8$ and the dodecanol/$C_{12}E_8$ mixture.

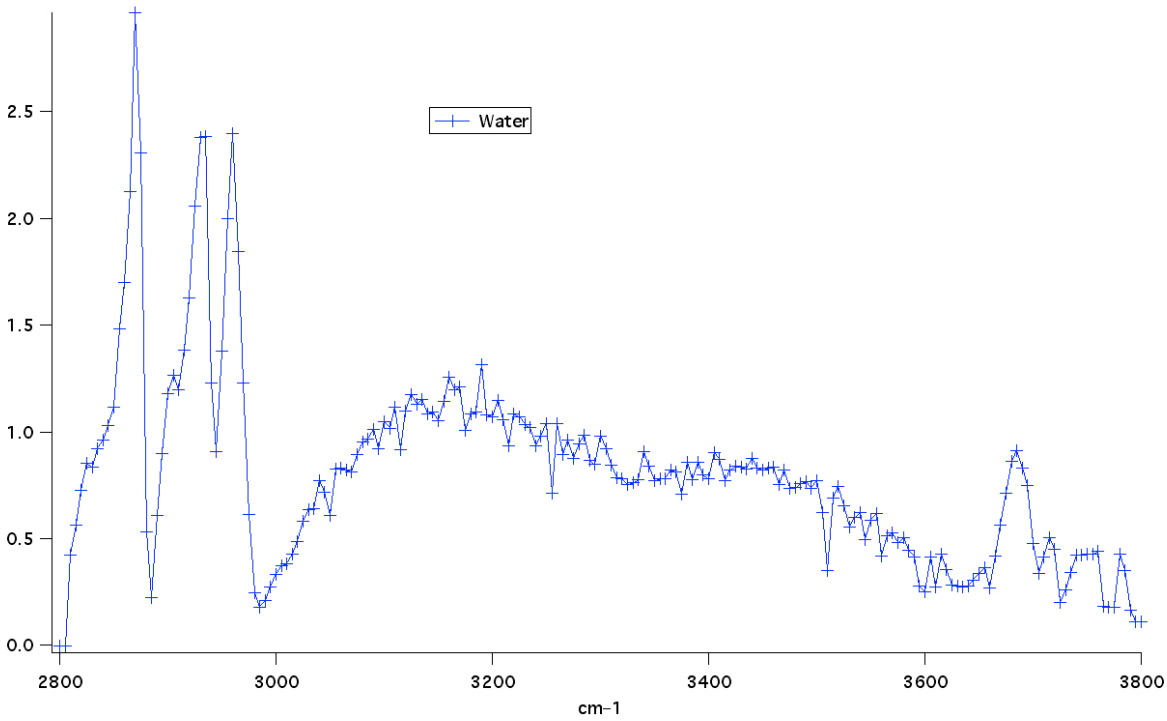

Figure 5.6: SFG spectrum of pure water on an OTS modified quartz interface.

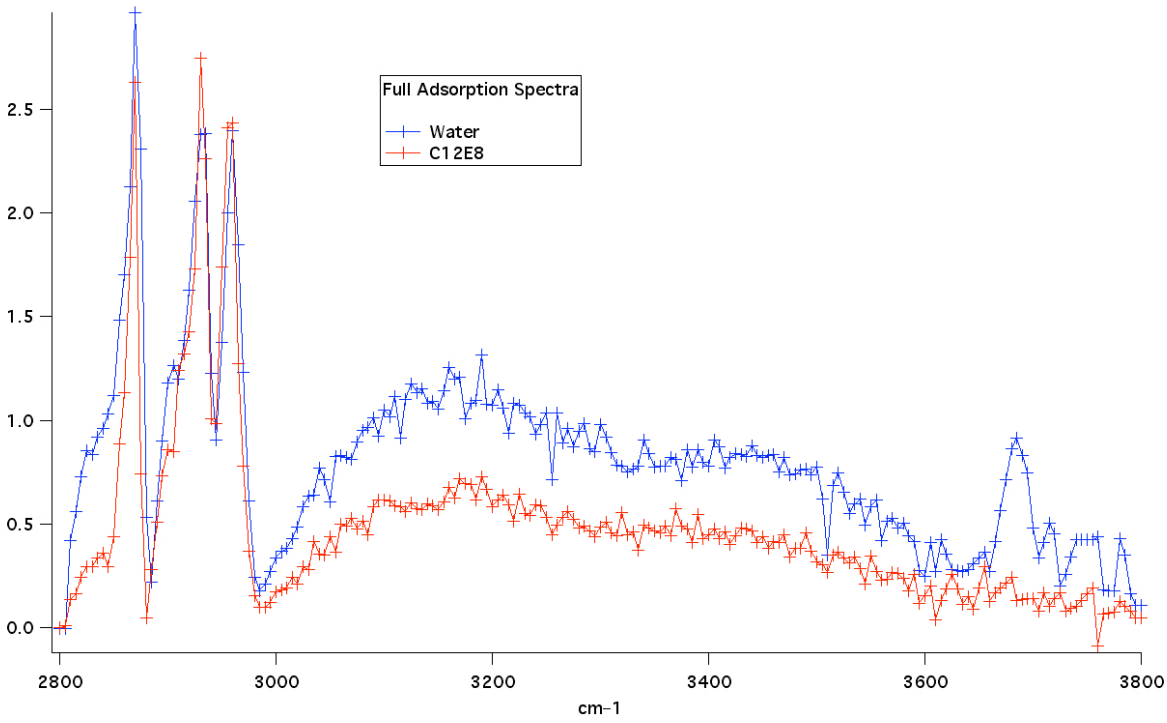

Figure 5.7: SFG spectra comparing the adsorption behavior of pure water to that of a 7CMC $C_{12}E_8$ surfactant solution.

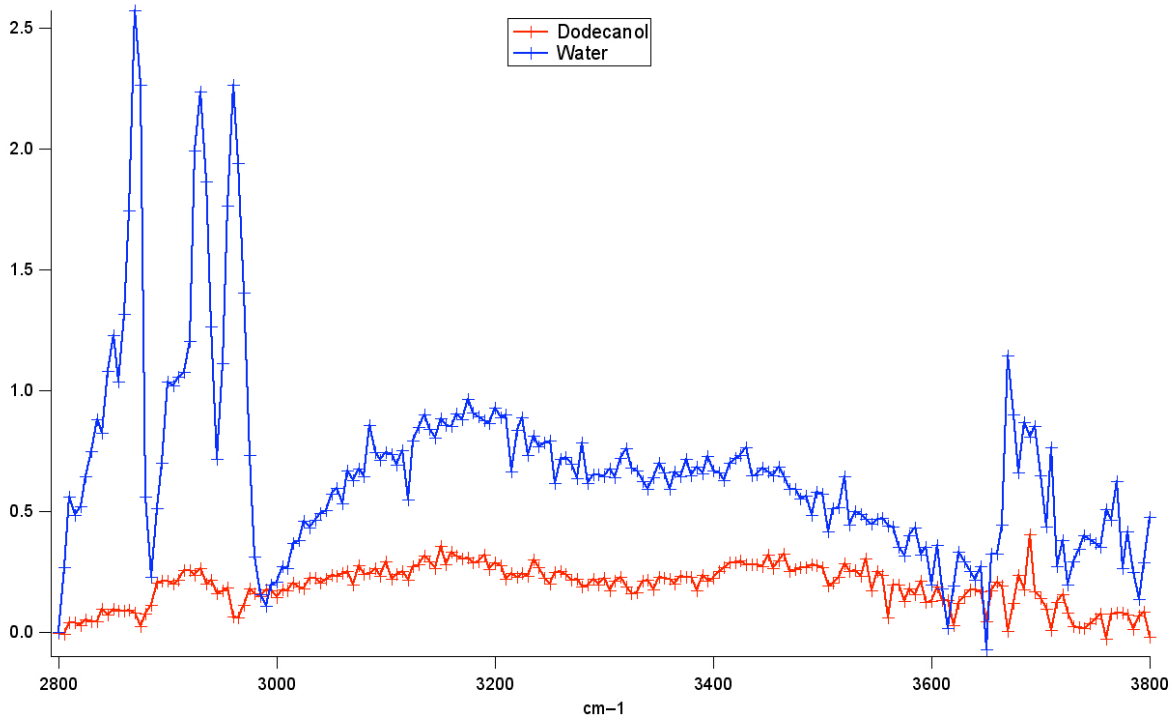

Figure 5.8: SFG spectra comparing the adsorption behavior of pure water to that of a saturated solution of dodecanol.

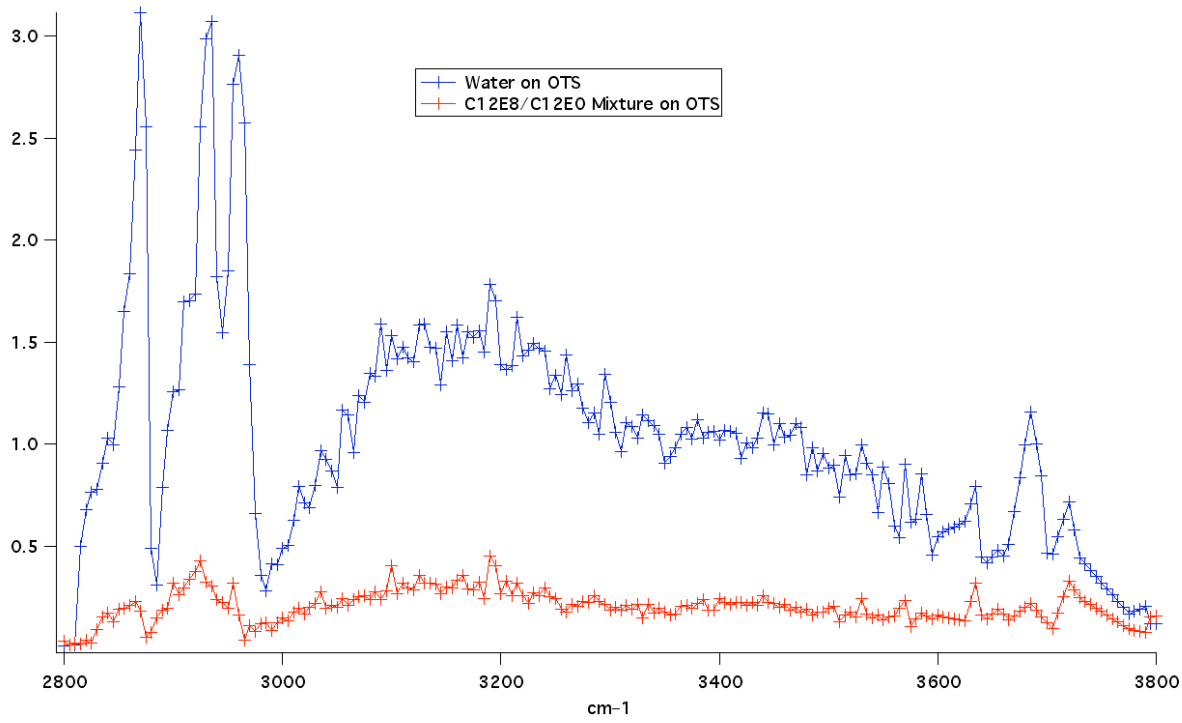

Figure 5.9: SFG spectra comparing the adsorption behavior of pure water to that of a dodecanol/$C_{12}E_8$ binary surfactant solution.

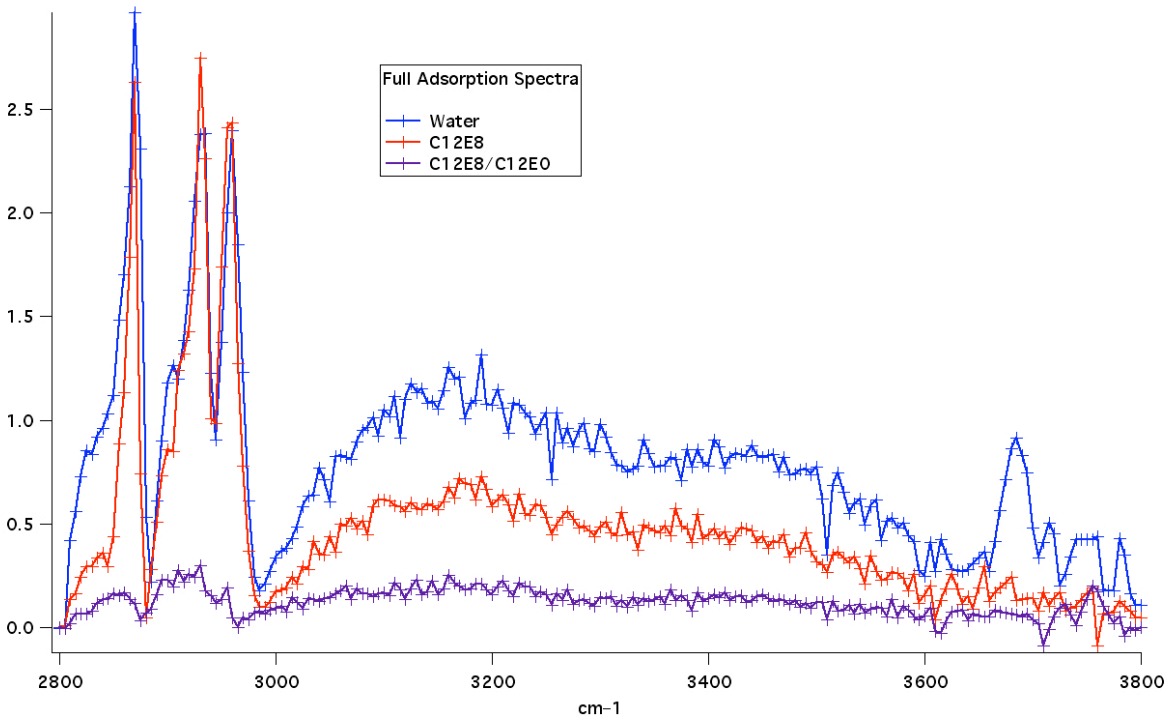

Figure 5.10: SFG spectra comparing the adsorption behavior of pure water to that of a 7CMC $C_{12}E_8$ surfactant solution and the corresponding mixture containing dodecanol. The water removal is enhanced by using dodecanol with $C_{12}E_8$.

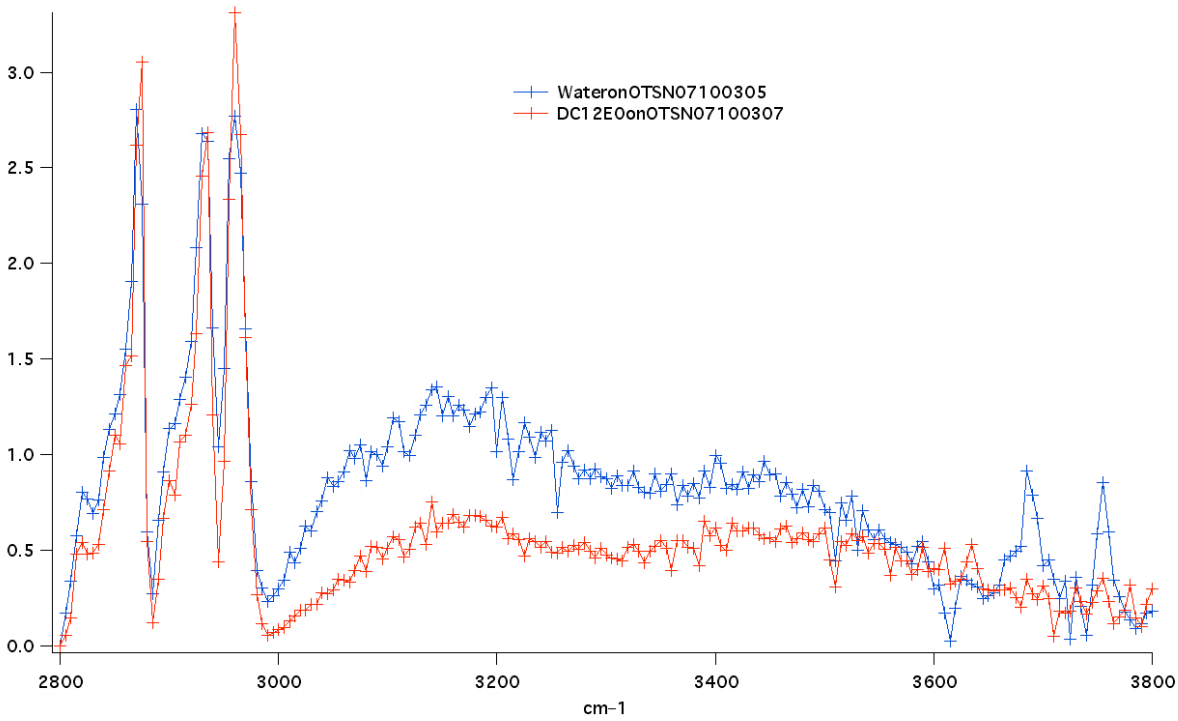

Figure 5.11: SFG spectra of a deuterated dodecanol solution compared to that of clean water.

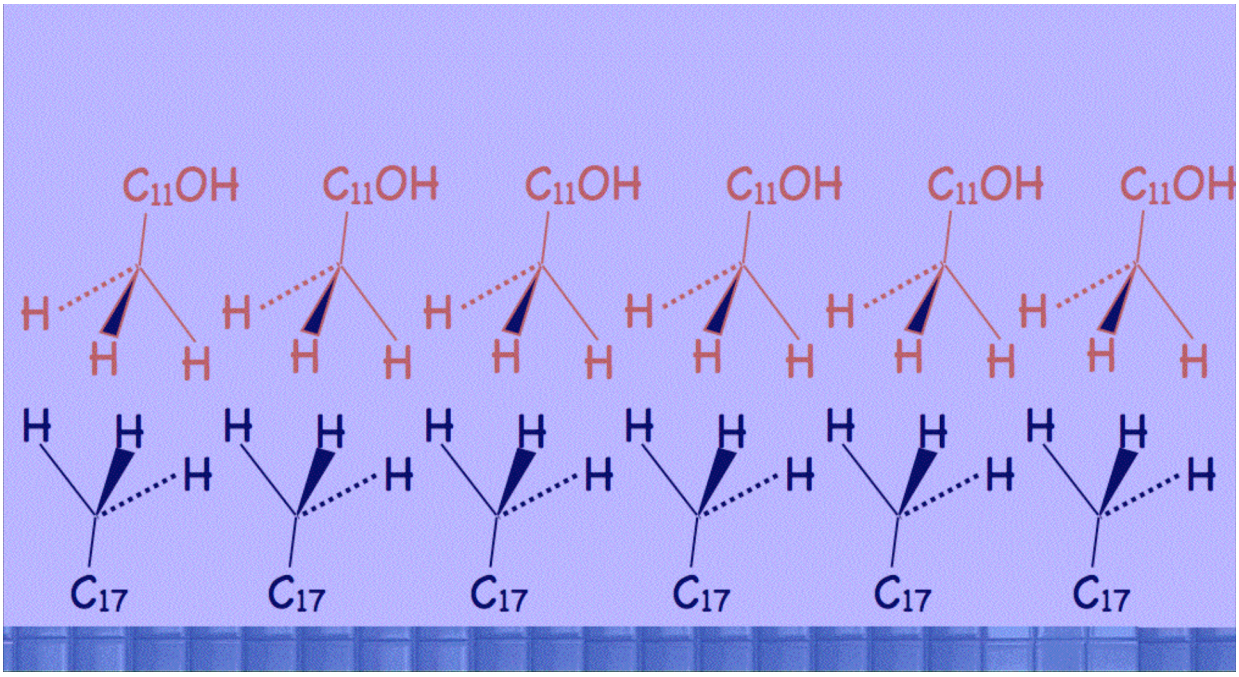

Figure 5.12: Schematic of dodecanol adsorption of onto the OTS monolayer. Symmetry is induced at the interface between the two molecules making the interface SFG invisible.

REFERENCES

(1) Chen, P.; Policova, Z.; Pace-Asciak, C. R.; Neumann, A. W. *Colloids and Surfaces B: Biointerfaces* **1999**, *15*, 313-324.

(2) Park, S. Y.; Hannemann, R. E.; Franses, E. I. *Colloids and Surfaces B: Biointerfaces* **1999**, *15*, 325-338.

(3) Sch¸rch, S.; Geiser, M.; Lee, M. M.; Gehr, P. *Colloids and Surfaces B: Biointerfaces* **1999**, *15*, 339-353.

(4) Mack, D. R.; Sherman, P. M. *Colloids and Surfaces B: Biointerfaces* **1999**, *15*, 355-363.

(5) Adams, J. W. *In Surface Phenomena and Additives in Water-Based Coatings and Printing Technology*; Plenum Press: New York, 1991.
(6) Stevens, P. J. G. *Pestic. Sci.* **1993**, *38*.

(7) Svitova, T.; Hill, R. M.; Smirnova, Y.; Stuermer, A.; Yakubov, G. *Langmuir* **1998**, *14*, 5023-5031.

(8) Svitova, T.; Hoffmann, H.; Hill, R. M. *Langmuir* **1996**, *12*, 1712-1721.

(9) He, M.; Hill, R. M.; Lin, Z.; Scrivens, L. E.; Davis, H. T. *Journal of Physical Chemistry* **1993**, *97*, 8820 - 8834.

(10) Dong, J.; Mao, G.; Hil, R. M. *Langmuir* **2004**, *20*, 2695-2700.

(11) Kunieda, H.; Taoka, H.; Iwanaga, T.; Harashima, A. *Langmuir* **1998**, *14*, 5113-5120.

(12) Churaev, N. V.; Esipova, N. E.; Hill, R. M.; Sobolev, V. D.; Starov, V. M.; Zorin, Z. M. *Langmuir* **2001**, *17*, 1338-1348.

(13) Hill, R. M.; He, M.; Davis, H. T.; Scriven, L. E. *Langmuir* **1994**, *10*, 1724-1734.

(14) Bain, C. D.; Davies, P. B.; Ward, R. N. *Langmuir* **1994**, *10*, 2060 - 2063.

(15) Bain, C. D.; Ward, R. N.; Davies, P. B. *J. Phys. Chem. B* **1997**, *101*, 1594-1601.

(16) Rosen, M. J. *Langmuir* **1991**, *7*, 885 - 888.

(17) Rosen, M. J.; Zhou, Q. *Langmuir* **2001**, *17*, 3532 - 3537.

(18) Rosen, M. J. *Langmuir*, *7*, 885-888.
(19) Vollhardt, D.; Czichocki, G. *Langmuir* **1990**, *6*, 317 - 322.

(20) Stoebe, T.; Lin, Z.; Hill, R. M.; Ward, M. D.; Davis, H. T. *Langmuir* **1996**, *12*, 337-344.

(21) Svitova, T.; Hoffmann, H.; Hill, R. M. *Langmuir* **1996**, *12*, 1712-1721.

(22) Israelachvili, J. *Intermolecular and Surface Forces*; Second ed.; Academic Press Limited: San Diego, CA, 1991.

(23) Mitchell, D. J.; Tiddy, G. J. T.; Waring, L.; Bostock, T.; Malcolm P, M. *J. Chem. Soc. Faraday Transactions* **1983**, *79*, 975 - 1000.

(24) Rosen, M. J. *Surfactants and Interfacial Phenomena*; 2nd ed.; Wiley-Interscience: New York, 1989.

(25) Schick, M. J. *Nonionic Surfactants*; Marcel Dekker, Inc.: New York, 1987; Vol. 23.

(26) Laughlin, R. G. *The Aqueous Phase Behavior of Surfactants*; Academic Press - Harcourt Brace & Company: Cincinatti, 1994.

(27) Strey, R.; Schomaker, R. *J. Chem. Soc. Faraday Transactions* **1990**, *86*, 2253 - 2261.

(28) Danino, D.; Talmon, Y.; Zana, R. *Journal of Colloid and Interface Science* **1997**, *186*, 170-179.

(29) Jahns, E.; Finkelmann, H. *Colloid & Polymer Science* **1987**, *265*, 304-311.

(30) Ning, H.; Wiegand, S.; Kita, R. In *Smart Colloidal Materials* 2006, p 111-115.

(31) Ward, R. N.; Davies, P. B.; Bain, C. D. *Journal of Physical Chemistry B* **1997**, *101*, 1594 - 1601.

(32) Penders, M. H. G. M.; Strey, R. *Journal of Physical Chemistry* **1995**, *99*, 6091 - 6095.

(33) Myrick, S. H.; Franses, E. I. *Langmuir* **1999**, *15*, 1556 - 1561.

(34) Jonstromer, M.; Strey, R. *Journal of Physical Chemistry* **1992**, *96*, 5993 - 6000.

(35) He, M.; Hill, R. M.; Lin, Z.; Scriven, L. E.; Davis, H. T. *Journal of Physical Chemistry* **1993**, *97*, 8820-8834.
(36) Matsumoto, T.; Zenkoh, H. *Colloid & Polymer Science* **1990**, *268*, 536-543.

(37) Tanford, C.; Nozeki, Y.; Rohde, M. F. *The Journal of Physical Chemistry* **1977**, *81*, 1555.

(38) Trlolo, R.; Magld, L. J.; J. S. Johnson, J.; Chlld, H. R. *The Journal of Physlcal Chemistry* **1982**, *86*.

(39) Nllsson, P.-G.; Wennerstrom, H.; Llndman, B. *The Journal of Physlcal Chemistry* **1983**, *87*.

(40) Kreuzery, H. J.; Wangy, R. L. C.; Grunzez, M. *New Journal of Pyhsics* **1999**, *1*, 1-16.

(41) Tanaka, M.; Rehfeldt, F.; Schneider, M. F.; Gege, C.; Schmidt, R. R.; Funari, S. S. *ChemPhysChem* **2005**, *6*, 101-109.

(42) Danino, D.; Talmon, Y.; Zana, R. *Journal of Colloid and Interface Science* **1997**, *186*, 170-179 **1997**, *186*, 170.

(43) Shen, Y. R. *Surface Science* **1994**, *299/300*, 551 - 562.

(44) Shen, Y. R. *Nature* **1989**, *337*, 519 - 524.

(45) Du, Q.; Superfine, R.; Freyesz, E.; Shen, Y. R. *Physical Review Letters* **1993**, *70*, 2313 - 2316.

(46) Shen, Y. R.; Du, Q.; Superfine, R.; Freyesz, E. *Physical Review Letters* **1993**, *70*, 2313 - 2316.

(47) Gragson, D. E.; Richmond, G. L. *The Journal of Physical Chemistry B* **1998**, *102*, 3847 - 3861.

(48) Gragson, D. E.; Richmond, G. L. *J. Phys. Chem. B* **1998**, *102*, 3847 - 3861.

(49) McQuarrie, D. A. *Statistical Mechanics*; 1 ed.; University Science Books: Sausalito, CA, 2000.

(50) Kumar, N.; Maldarelli, C.; Couzis, A. *Colloids and Surfaces A: Physicochemical and Engineering Aspects* **2006**, *277*, 98-106.

(51) Hiemenz, P. C.; Rajagopalan, R. *Principles of Colloid and Surface Chemistry*; 3rd ed.; Marcel Dekker, Inc: New York, 1997.

(52) Casson, B. D.; Braun, R.; Bain, C. D. *Faraday Discussions* **1996**, *104*, 209 - 229.

(53) Richmond, G. L. *Chem. Rev.* **2002**, *102*, 2693 - 2724.

(54) Casson, B. D.; Bain, C. D. *Journal of Physical Chemistry B* **1999**, *103*, 4678 - 4686.

(55) Goates, S. R.; Schofield, D. A.; Bain, C. D. *Langmuir* **1999**, *15*, 1400 - 1409.

(56) Lu, J. R.; Lee, E. M.; Thomas, R. K.; Penfold, J.; Flitach, S. L. *Langmuir* **1993**, *9*, 1352 - 1360.

(57) Lu, J. R.; Li, Z. X.; Su, T. J.; Thomas, R. K. *Langmuir* **1993**, *9*, 2408 - 2416.

(58) Zhou, Q.; Rosen, M. J. *Langmuir* **2003**, *19*, 4555 - 4562.

(59) Zhou, Q.; Wu, Y.; Rosen, M. J. *Langmuir* **2003**, *19*, 7955 - 7962.

(60) Penfold, J.; Staples, E.; Tucker, I.; Thomas, R. K. *Journal of Colloid and Interface Science* **1998**, *201*, 223 - 232.

(61) Penfold, J.; Staples, E.; Tucker, I.; Thomas, R. K.; Woodling, R.; Dong, C. C. *Journal of Colloid and Interface Science* **2003**, *262*, 235 - 242.

(62) Penfold, J.; Staples, E. J.; Tucker, I.; Thomas, R. K. *Colloids and Surfaces A: Physicochemical and Engineering Aspects* **1999**, *155*, 11 - 26.

(63) Subramanyam, R. Ph.D., City University of New York, 1999.

(64) Kumar, N. Ph.D., City University of New York, 2001.

(65) Lin, S.-Y.; chen, L.-J.; Xyu, J.-W.; Wang, W.-J. *Langmuir* **1995**, *11*, 4159 - 4166.

(66) B.P., B.; Fletcher, P. D. I.; Paunov, V. N.; D., S. *Langmuir* **2000**, *16*, 8926 - 8931.

(67) Casson, B. D.; Bain, C. D. *Journal of the American Chemical Society* **1999**, *121*, 2615 - 2616.

(68) Hsu, C.-T.; Chang, C.-H.; Lin, S.-Y. *Langmuir* **2000**, *16*, 1211 - 1215.

(69) Hsu, C.-T.; Shao, M.-J.; Lin, S.-Y. *Langmuir* **2000**, *16*, 3187 - 3194.

(70) Lee, Y.-C.; Liu, H.-S.; Lin, S.-Y. *Colloids and Surfaces A: Physicochemical and Engineering Aspects* **2003**, *212*, 123 - 134.

(71) Pollard, M. L.; Pan, R.; Steiner, C.; Maldarelli, C. *Langmuir* **1998**, *14*, 7222 - 7234.

(72) Raymond, E. A.; Tarbuck, T. L.; Brown, M. G.; Richmond, G. L. *J. Phys. Chem. B* **2003**, *107*, 546 - 556.

(73) Raymond, E. A.; Tarbuck, T. L.; Brown, M. G.; Richmond, G. L. *J. Phys. Chem. B* **2003**, *107*, 546 - 556.

(74) Vollhardt, D.; Fainerman, V. B.; Emrich, G. *J. Phys. Chem. B* **2000**, *104*, 8536 - 8543.

(75) Zhmud, B. V.; Tiberg, F.; Kizling, J. *Langmuir* **2000**, *16*, 2557 - 2565.

(76) Huibers, P. D. T.; Lobanov, V. S.; Katritzky, A. R.; Shah, D. O.; Karelson, M. *Langmuir* **1996**, *12*, 1462 - 1470.

(77) Song, Q.; Couzis, A.; Somasundaran, P.; Maldarelli, C. *Colloids and Surfaces A: Physicochem. Eng. Aspects* **2006**, *282-283*, 162 - 182.

(78) Lu, J. R.; Li, Z. X.; Thomas, R. K.; Binks, B. P.; Crichton, D.; Fletcher, P. D. I.; McNab, J. R.; Penfold, J. *J. Phys. Chem. B* **1998**, *102*, 5785 - 5793.

(79) Kumar, N.; Couzis, A.; Maldarelli, C. *Journal of Colloid and Interface Science* **2003**, *267*, 272 - 285.

(80) Goates, S. R.; Schofield, D. A.; Bain, C. D. Langmuir **1999**, 15, 1400-1409.

(81) Matsubsara, H.; Nakano, T.; Matsuda, T.; T.Takiue; M.Aratono *Langmuir* **2006**, *22*.

(82) Zhou, Q.; Rosen, M. J. *Langmuir*, *19*, 4555-4562.

(83) Du, Q.; Freysz, E.; Shen, Y. R. *Physical Review Letters* **1994**, *72*, 238 - 241.

(84) Scatena, L. F.; Brown, M. G.; Richmond, G. L. *Science* **2001**, *292*, 908 - 912.

(85) Wolgemuth, J. L.; Workman, R. K.; Manne, S. *Langmuir* **2000**, *16*, 3077-3081.

(86) Grant, L. M.; Tiberg, F.; Ducker, W. A. *J. Phys. Chem. B.* **1998**, *102*, 4288-4294.

(87) Liu, J.-F.; Ducker, W. A. *Langmuir* **2000**, *16*, 3467-3473.

(88) Zhou, Q.; Wu, Y.; Rosen, M. J. *Langmuir* **2003**, *19*, 7955 - 7962.

(89) Gautam, K. S.; Schwab, A. D.; Dhinojwala, A.; Zhang, D.; Dougal, S. M.; Yeganeh, M. S. *Physical Review Letters* **2000**, *85*, 3854-3857.

(90) Kumar, N.; Maldarelli, C.; Couzis, A. *Colloids and Surfaces A: Physicochem. Eng. Aspects* **2006**, *277*, 98 - 106.

(91) Harrick, N. J. *Internal Reflection Spectroscopy*; John Wiley & Sons Inc, 1967.

(92) Bell, G. R.; Bain, C. D.; Ward, R. N. *J. Chem. Soc. Faraday Transactions* **1996**, *92*, 515 - 523.

(93) Brown, M. G.; Raymond, E. A.; Allen, H. C.; Scatena, L. F.; Richmond, G. L. *Journal of Physical Chemistry A* **2000**, *104*, 10220 - 10226.

(94) Gragson, D. E.; McCarty, B. M.; Richmond, G. L. *J. Phys. Chem.* **1996**, *100*, 14272-14275.

(95) Kumar, N.; Maldarelli, C.; Couzis, A. *Langmuir*, *TBD*, TBD.

(96) Wang, M.; Liechti, K. M.; Wang, Q.; White, J. M. *Langmuir* **2005**, *21*, 1848-1857.

(97) Frochtenicht, R.; Kaloudis, M.; Koch, M.; Huisken, F. *J. Chem. Phys.* **1996**, *105*.

(98) Israelachvili, J. *Intermolecular and Surface Forces, Second Edition: With Applications to Colloidal and Biological Systems*; Academic Press, 1985.

CHAPTER 6

SUMMARY AND FUTURE WORK

6.1 Summary

By taking advantage of synergistic interactions between the series C_iE_j surfactant and dodecanol, we have demonstrated that aggregate structures can be formed at overall surfactant concentrations much lower than is possible when using a neat aqueous surfactant solution. In particular, the 7CMC $C_{12}E_8$, 2.5 mM dodecanol mixuture has proven to be particularly effective at forming and maintaining lamellar structures in aqueous solution. The formation of lamellae has lead to the mixture's ability to synergistically reduce the air liquid interfacial tension to values on the order of 21 mN/m, values unreachable by single surfactant solutions of $C_{12}E_8$ or dodecanol. An additional consequence is the ability for the surfactant mixture to enhance wetting on a hydrophobic surface.

6.2 Future Work

We have attempted to begin examining the trisiloxane surfactants at the solid-liquid interface via contact angle and SFG because ultimately we would like to develop a surfactant system that mimics the superwetting capability of the trisiloxane surfactants. Trisiloxane surfactants, previously described in Chapter 1, have the abbreviated structure $M(DE_jR)M$, where M is $(CH_3)_3SiO$, D is - $CH_3Si\ (CH_2)_3$-, and E_j is $(CH_2CH_2O)_j$, the same as the E_j in the C_iE_j surfactants, used in this work. The R group can be any of the following: -H, -OH, $-CH_3$ or -C(O)CH, however the for the particular surfactant we have used, Silwet L77® from Momentive Performance Materials is R = $–CH_3$. The trisiloxanes are also colloquially known as TE_j due to the unique T-shaped structure of the surfactant molecule, consequently we will refer to the molecule as TE_8 (Silwet L77 contains the 8 ethylene glycol unit moiety as the major component). Initial SFG spectra of 0.01 wt % (a superwetting concentration) TE8 indicates that it is not as effective at removing water from the solid-liquid interface. This is somewhat perplexing as it is assumed that a reorganization or removal of the water at the solid liquid interface in compulsory in order to completely wet the surface. Initial air-liquid interfacial tension measurements of the same solution indicate that the tension is approximately 19 mN/m; it does a better job at the air-liquid interface than does the $C_{12}E_8$/dodecanol mixture. A possible consequence of this is that although TE_8 does not do as well at the solid liquid interface, its performance is superior at the air-liquid interface, thus superwetting is still

possible according to Young's equation. This idea needs to be investigated further in order to full understand whether not this is indeed the case.

Anecdotally, when trying to rinse the TE_8 surfactant solution from the SFG cell, the original water signal could not be recovered without completely dismantling the cell assembly and putting the quartz crystal through the rigorous cleaning procedure outlined in SFG section in the experimental methods of Chapter 5. This was not the case for the dodecanol, $C_{12}E_8$ or dodecanol/$C_{12}E_8$ solutions used in the same experimental setup as the surfactant systems were easily removed from the cell by flushing several times with water. Based on this, it is possible that TE_8 has a stronger interaction with the OTS monolayer on the cryatal or the silicon atoms of the surfactant can interact with the silicon of the quartz substrate in a way that the hydrocarbon-based surfactants cannot. Surface for measurements on surfaces of varying chemistries may help to elucidate this part of the picture and help to shed some light on what role surface interaction plays on a surfactant's ability to superwet a hydrophobic surface.

Given the demonstrated ability for the dodecanol/$C_{12}E_8$ mixture to synergistically wet a hydrophobic solid liquid interface in is of interest to get an understanding of how the surfactants are distributed in the monolayer. Having this understanding has the potential to allow one to tune the wettability of the surface, which would have technological impact. Isotopic labeling of one or both of the molecules in the monolayer and using

techniques such as specular neutron reflection can aid determination of the population density of the surfactants.

Ultimately, the data obtained from any of these experiments provides insight into the mechanism for superspreading, but does not point to an accurate picture of it. In order to get the most accurate picture of the phenomenon, molecular dynamics simulations using real interaction potentials is necessary.